

**DIFFUSION IN NANOMATERIALS AND NANOSIZE EFFECTS ON
MASS TRANSPORT: EXPERIMENTS AND SIMULATIONS**

CO-DIRECTED PHD THESIS
FRANCE-HUNGARY

by

Zoltán ERDÉLYI

for the degree of

DOCTOR OF PHILOSOPHY

In the subject of:
MATERIALS SCIENCE

Approved 12 October 2001 in presence of committee

Dezső BEKE
Jean BERNARDINI
István SZABÓ
Christophe GIRARDEAUX
Géza TICHY (Referee)
Vassilis PONTIKIS (Referee)

"The principles of physics, as far as I can see, do not speak against the possibility of maneuvering things atom by atom."

(Richard Feynman)

To my parents and my fiancée ...

This work summarizes three years of work performed in the frame of a co -directed thesis within Laboratoire Matériaux et Microélectronique de Provence (Université Aix-Marseille III, France) and Department of Solid State Physics (University of Debrecen, Hungary). It could have never been done without the continuous help of the Cultural Service of the French Embassy in Hungary that cannot be forgotten in this acknowledgement.

It is a great pleasure for me to give thanks to professor D.L. Beke, head of Department of Solid State Physics, University of Debrecen and professor J. Bernardini, Directeur de Recherche au CNRS, Université Aix-Marseille III, for providing the co -direction of my thesis.

I would like to express my gratitude to professor V. Pontikis, professor at the Laboratoire des Solides Irradiés - Ecole Polytechnique à Palaiseau, and to professor G. Tichy, professor at the Eötvös University in Budapest, for accepting to be referees of this work and devote a small of their precious time to judge this thesis.

I would like to express my sincere thanks to A. Rolland, professor at the University of Aix-Marseille III, for her precious advice and her help during the experiments made by Auger Electron Spectroscopy and in the interpretation of the results.

Thanks to Ch. Girardeaux, Chargé de Recherche au CNRS, who introduced me to the world of Auger Electron Spectroscopy. Without his support, I could have never realised the Auger measurements. Furthermore, I would like to express my heartfelt thanks to him for assuring me of his friendship.

I could not forget to thank to I.A. Szabó and C. Cserháti, professors at the University of Debrecen, for the numerous discussions and help of which I could take advantage to carry out the theoretical aspects and simulations.

I express my thanks to G.A. Langer, professor at the University of Debrecen, and A. Csik, PhD student at the University of Debrecen, for preparation of multilayer and bilayer samples.

I am grateful to the persons who performed the supplementary experiments permitting me to verify my theoretical results and prognostics of my simulations: L. Daróczy (Transmission Electron Microscopy, University of Debrecen); M. Menyhárd, A. Sulyok (Auger Depth Profiling, Research Institute for Technical Physics and Materials Sciences in Budapest); A. Simon (Rutherford Backscattering, Institute of Nuclear Research in Debrecen).

The realisation of Auger experiments was greatly facilitated by G. Clugnet. I give thank to him for his availability and technical contribution.

I would like to express my thanks to M. Teyssier, M. Decorps and E. Szabadosné for their kindness and help to solve administrative problems.

Finally, I would like to thank to my fellow PhD student friends and all the person who has made my stays agreeable and effective by keeping good spirits in the two laboratories.

CONTENTS

CHAPTER I	17
I.1 VOLUME DIFFUSION	17
I.1.1 Fick's equations	17
I.1.2 Atomic aspects of volume diffusion	18
I.1.3 Interdiffusion	20
I.1.3.1 ATOMIC FLUXES	20
I.1.3.2 INTERDIFFUSION COEFFICIENT	21
I.1.3.3 EFFECT OF STEEP CONCENTRATION GRADIENT	23
a) <i>Gradient energy: Cahn-Hilliard model</i>	23
b) <i>Interdiffusion on atomic scale: Martin's model</i>	25
I.1.3.4 EFFECT OF INTERNAL STRESSES	28
a) <i>Cahn's model</i>	28
b) <i>Stephenson's model</i>	29
I.1.3.5 NONLINEAR EFFECTS	32
a) <i>Concentration dependent D_0</i>	33
b) <i>Concentration dependent mobility/diffusion coefficient</i>	33
I.2 SURFACE SEGREGATION	36
I.2.1 Thermodynamical aspects	36
I.2.2 Kinetic aspects	37
I.2.2.1 APPLICATION OF THE MARTIN MODEL	37
I.3 GRAIN-BOUNDARY DIFFUSION	37
I.3.1 Fisher's model	38
I.3.2 Diffusion regimes in polycrystals	39
I.3.3 Hwang-Balluffi model	40
CHAPTER II	47
II.1 SYSTEMS	47
II.1.1 Si-Ge system	47
II.1.2 Cu-Ni system	48
II.1.3 Ag-Cu system	48
II.2 SAMPLE PREPARATION AND HEAT TREATMENTS	49
II.3 ANALYTICAL TECHNIQUES	51
II.3.1 Small Angle X-Ray Diffraction	51
II.3.1.1 GENERAL DESCRIPTION OF THE METHOD	51
II.3.2 Auger Electron Spectroscopy	51
II.3.2.1 GENERAL DESCRIPTION OF THE METHOD	51
II.3.2.2 AUGER DEPTH PROFILING	52
II.3.2.3 TRADITIONAL AUGER APPARATUS	52
CHAPTER III	59

III.1	VALIDITY OF THE CONTINUUM APPROXIMATION IN MULTILAYERS	59
III.1.1	Theor	59
III.1.1.1	CONTINUUM MODE	59
III.1.1.2	DISCRETE MODE	61
III.1.1.3	CALCULATION OF INTENSITIES OF SMALL ANGLE X-RAY DIFFRACTION	62
III.1.2	Results and Discussion	62
III.1.3	Conclusio	70
III.2	CONSEQUENCES OF THE DIFFUSIONAL ASYMMETRY	70
III.2.1	Introduction	70
III.2.1.1	STRUCTURAL RELAXATION AND NONLINEARITY	71
III.2.2	Direct experimental evidences on the diffusional asymmetry and its consequences	72
III.2.2.1	RUTHERFORD BACKSCATTERING	72
III.2.2.2	AUGER DEPTH PROFILING	73
III.2.3	Calculations on the combined effects of nonlinear diffusion and stresses	75
III.2.3.1	INPUT PARAMETER SET	75
III.2.4	Conclusions	77
III.3	INTERPLAY OF NONLINER DIFFUSION AND SURFACE SEGREGATION	78
III.3.1	Method for the evaluation of dissolution kinetics	78
III.3.1.1	TIME EVOLUTION OF CONCENTRATION PROFILES IN A DISCRETE LATTICE	78
III.3.1.2	DECAY OF THE AUGER CURVE	83
III.3.1.3	DETERMINATION OF THE DIFFUSIVITY	86
III.3.2	Analysis of experimental data	87
III.3.3	Discussio	90
III.3.4	Conclusions	92
CHAPTER IV		101
IV.1	THEORY	101
IV.1.1	Surface accumulation parameter	101
IV.2	RESULT	103
IV.3	DISCUSSION	105
IV.4	CONCLUSION	107

INTRODUCTION

The dawn of nano-scale science can be traced to the classic talk of Richard Feynman gave on December 29th, 1959 at the annual meeting of the American Physical Society at the California Institute of Technology. In this lecture, Feynman suggested that there exists no fundamental reason to prevent the controlled manipulation of matter at the scale of individual atoms and molecules. Twenty-one years later, Eigler [1] and co-workers constructed the first man-made object atom-by-atom with the aid of a scanning tunnelling microscope. This was just 7000 years after Democritus postulated atoms to be the fundamental building blocks of the visible world. The field derives its name from the SI-prefix *nano*, meaning 1/1,000,000,000 of something. A nanometre is thus 1/1,000,000,000 of a metre, which is around 1/50,000 of the diameter of a human hair or the space occupied by 3-4 atoms placed end-to-end.

Recent fundamental investigations and the applied research in materials science concentrate in many aspects on the physics and technology of nanostructures. The new properties of materials at nano-scale dimensions manifest itself in peculiar mechanical, chemical, magnetic, optic and biological characteristics. The possible applications cover a wide range from the construction of materials for micro- and nanoelectronics to biomedical applications. Applications of these require, however, the knowledge of parameters and physical laws valid at nano-scale.

Grain boundaries are, generally, diffusion short circuits; consequently, the major part of material transport will occur by grain-boundary diffusion in nanomaterials where a large amount of atoms can lie on grain or interphase boundaries (50% for a grain size equal to 5 nm; 20% for a grain size equal to 10 nm). An interesting question arose during the interpretation of the already existing data on grain-boundary diffusion in nanocrystalline materials: whether the grain-boundary diffusion coefficients measured in these alloys are identical to those obtained in microcrystalline state or not? An answer to this question would solve a fundamental problem concerning to the structure of GB in these materials whether it is a well defined and more or less ordered one as in coarse grained materials or a disordered like frozen-gas structure. In Chapter IV we try to answer this question by comparing the temperature dependence of Ag grain-boundary diffusion in Cu measured by Auger electron spectroscopy in C-kinetics regime with triple products determined previously using radio tracer technique in B-kinetics regime. Furthermore the temperature dependence of the surface segregation factor will be also extracted.

We will see in Chapter III that diffusion in nanostructures has other challenging features even if the role of structural defects (dislocations, phase- or grain-boundaries) can be neglected. This can be the case for diffusion in amorphous materials, in epitaxially grown highly ideal thin films or multilayers where diffusion along short circuits can be ignored and “only” principal difficulties, related to nanoscale effects, raise. For example, one of the most important differences for diffusion in such crystalline materials – as compared to diffusion for long distances (orders of magnitude longer than the atomic spacing) – is that the continuum approach cannot be automatically applied. Furthermore, at short diffusion distances in case of interdiffusion, due to the composition dependence of the diffusion coefficients, the shape of the interface can be also different from the well-known interfaces obtained in bulk samples. Moreover, in these materials, at short diffusi

times, when the gradient of concentration is large, the usual parabolic law of diffusion can be violated, leading to a linear law even if there is no reaction control at all. These different situations will be investigated both experimentally and by simulation in different A/B couples.

REFERENCES

- 1 D.M. Eigler, E.K. Schweizer, *Nature*, **344**, 524-526 (1990)

Chapter I

Theoretical Aspects

In this chapter phenomena of diffusion and segregation will be summarized



Chapter I

THEORETICAL ASPECTS

I.1 VOLUME DIFFUSION

I.1.1 Fick's equations

Diffusion of atoms in solids can be described by the Fick's equations. The first equation relates the flux (\vec{j} : number of atoms crossing a unit area per unit time) to the gradient of the concentration (ρ : number of atoms per unit volume) via the diffusion coefficient tensor \hat{D} :

$$\vec{j} = -\hat{D} \text{grad} \rho . \quad (\text{I.1})$$

This equation permits to determine the diffusion coefficient in cases, where the concentration gradient is time independent (steady state regime).

In non steady state regime, the diffusion flux and concentration are function of time and position. In order to be able to determine the diffusion coefficient, it is necessary to take into account the conservation of matter. For not interacting particles (no chemical reaction, no reactions between different types of sites in a crystal, etc.), this is the continuity equation:

$$\frac{\partial \rho}{\partial t} + \text{div} \vec{j} = 0 . \quad (\text{I.2})$$

Combining equations (I.1) and (I.2), one obtains the second Fick's law:

$$\frac{\partial \rho}{\partial t} = \text{div} (\hat{D} \text{grad} \rho) . \quad (\text{I.3})$$

For cubic crystals and isotropic media, the diffusion coefficient tensor reduces to a scalar D , thus the first Fick's law is:

$$\vec{j} = -D \text{grad} \rho . \quad (\text{I.4})$$

Moreover, if the concentration varies only in the x direction, equation (I.3) reduces to:

$$\frac{\partial \rho}{\partial t} = \frac{\partial}{\partial x} \left(D \frac{\partial \rho}{\partial x} \right) . \quad (\text{I.5})$$

If, additionally, the diffusion coefficient is independent of the concentration, equation (I.5) can be written in the following form:

$$\frac{\partial \rho}{\partial t} = D \frac{\partial^2 \rho}{\partial x^2}. \quad (\text{I.6})$$

From mathematical point of view, equation (I.6) is a second order, linear partial differential equation. Initial and boundary conditions are necessary to solve it [1].

I.1.2 Atomic aspects of volume diffusion

Let us consider a system of migrating particles. The paths of particles belonging to time t are represented by vectors $\vec{R}(t)$. The projection on the Ox axis is denoted by X and is equal to the sum of the projections x_i of the elementary jump vectors denoted by \vec{r}_i . Since the average value of x_i is:

$$\langle x_i \rangle = \lim_{N \rightarrow \infty} \frac{1}{N} \left[\sum_{i=1}^N x_i \right], \quad (\text{I.7})$$

considering a particle making n jumps (on average) during the time t , it can be written [2,3]:

$$\langle X \rangle = n \lim_{N \rightarrow \infty} \frac{1}{N} \left[\sum_{i=1}^N x_i \right]. \quad (\text{I.8})$$

In the same way, the quadratic mean free path can be given by [2] :

$$\langle X^2 \rangle = n \lim_{N \rightarrow \infty} \frac{1}{N} \left[\sum_{i=1}^N x_i^2 + 2 \sum_{i=1}^N \sum_{\substack{j=1 \\ j \neq i}}^N (x_i x_j) \right]. \quad (\text{I.9})$$

If the migration of particles is random (Brownian migration or random walk [4,5]), the first Fick's equation is [2]:

$$j_x = - \frac{\langle X^2 \rangle}{2t} \frac{\partial c}{\partial x}, \quad (\text{I.10})$$

if the Brownian diffusion coefficient in the direction x is defined by the relation:

$$D_x = \frac{\langle X^2 \rangle}{2t}. \quad (\text{I.11})$$

Replacing the quadratic mean free path by its expression (I.9) and neglecting the second term with double summation (the double product terms of this relation compensate each other for a random walk, since jumps in opposite directions have the same probability), one obtains:

$$D_x = \frac{n}{2t} \lim_{N \rightarrow \infty} \frac{1}{N} \left[\sum_{i=1}^N x_i^2 \right] = \frac{\Gamma}{2} \langle x_i^2 \rangle, \quad (\text{I.12})$$

where $\Gamma = n/t$ is the total jump frequency of atoms. Note that the Brownian diffusion coefficient is often approached by the diffusion coefficient of an isotope (or tracer) D_x^* . We recall that, theoretically, $D_x^* = D_x f$, where f is a correlation factor [6]. Its presence is necessary because the migration of the marked (or tracer) atoms is not always completely random [7], *i.e.* the second term with double summation in (I.9) cannot be neglected. In the case of self-diffusion $f (\leq 1)$ is usually a numerical factor depending on the crystal structure and diffusion mechanism. For impurity or heterodiffusion (the tracer atoms are different from the atoms of the matrix), this factor can depend on the temperature as well.

In a crystal, the migration of atoms takes place by site -by-site. The positions of these sites are perfectly defined by the structure. If Γ_s denotes the frequency along direction s and Z is the number of neighbouring sites, one can write:

$$\Gamma = \sum_{s=1}^Z \Gamma_s . \quad (\text{I.13})$$

Since the proportion of jumps in a given direction is equal to Γ_s/Γ ,

$$D_x = \frac{\Gamma}{2} \langle x^2 \rangle = \frac{\Gamma}{2} \lim_{N \rightarrow \infty} \frac{1}{N} \sum_{s=1}^Z N \frac{\Gamma_s}{\Gamma} x_s^2 = \frac{1}{2} \sum_{s=1}^Z \Gamma_s x_s^2 . \quad (\text{I.14})$$

According to this expression, in the case of selfdiffusion by vacancy mechanism, it is possible to determine the diffusion coefficient along Ox if the lattice parameter is known.

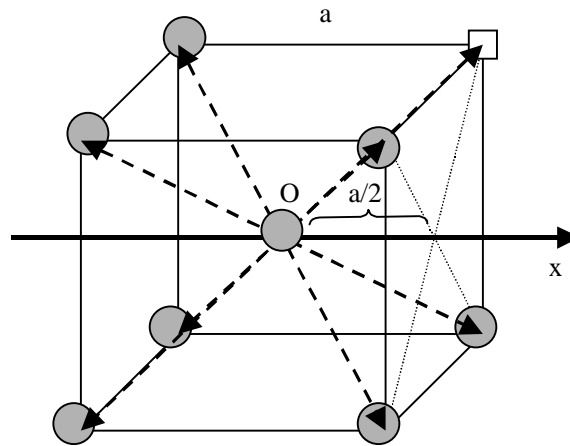


Figure I.1 Elementary jump for vacancy mechanism in a BCC structure (\square : vacancy ; \bullet : atoms).

In an isotrop crystal with body centred cubic (BCC) structure (or face centred cubic – FCC), the jumping lengths and frequencies are the same for the 8 (FCC: 12) directions [see Figure I.1 and Figure I.2]. Applying relation (I.14) for the direction Ox, one can write for both of the structure types:

$$D_x = \frac{1}{2} 8 \left(\frac{a}{2} \right)^2 \Gamma_s = \Gamma_s a^2 . \quad (\text{I.15})$$

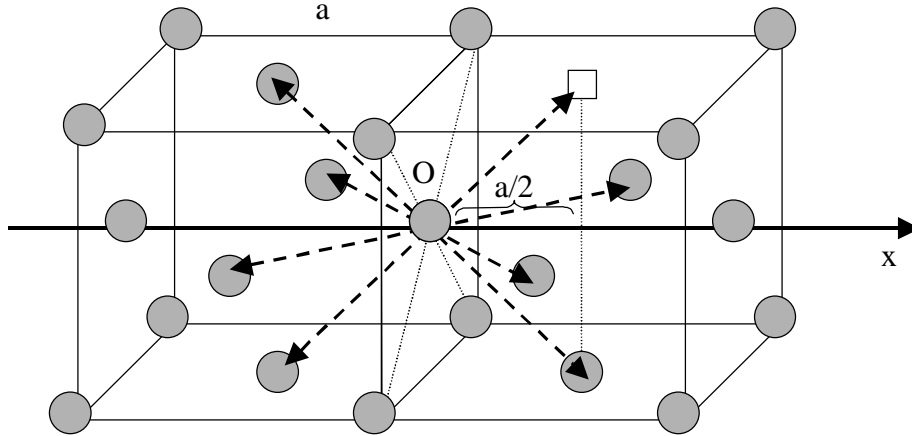


Figure I.2 Elementary jumps for vacancy mechanism in a FCC structure. Only the elementary jumps that have the projection on the axis Ox different from zero are marked by arrows (□ : vacancy ; ● : atoms).

I.1.3 Interdiffusion

I.1.3.1 ATOMIC FLUXES

According to the Onsager's theorem [3,6,8], in an A/B binary system, if the only driving force is the gradient of the chemical potential (μ_i), the flux of i (A,B) atoms relative to the lattice planes can be given as:

$$\vec{j}_i = -L_{ii} \text{grad } \mu_i, \quad (\text{I.16})$$

where L_{ii} is the 'Onsager coefficient'. The chemical potential can be expressed in the following way [9]:

$$\mu_i = \mu_0 + k_B T \ln \gamma_i c_i, \quad (\text{I.17})$$

where k_B is the Boltzmann-constant and T the absolute temperature. Moreover, c_i and γ_i are the atomic fraction and the thermodynamic activity coefficient, respectively. Combining equations (I.16) and (I.17) and using that $\rho_i \partial c_i / \partial \rho_i = c_i$ and $\rho_A + \rho_B = \rho = \text{const}$, one obtains:

$$\vec{j}_i = -\frac{k_B T L_{ii}}{\rho_i} \left[1 + \frac{\partial \ln \gamma_i}{\partial \ln c_i} \right] \text{grad } \rho_i = -\frac{k_B T L_{ii}}{\rho_i} \Theta \text{grad } \rho_i = -D_i \text{grad } \rho_i, \quad (\text{I.18})$$

where Θ is the thermodynamic factor. D_i is the *intrinsic* diffusion coefficient which relates to the Brownian diffusion coefficient [see I.1.2] D^i by Θ :

$$D_i = \Theta D^i. \quad (\text{I.19})$$

I.1.3.2 INTERDIFFUSION COEFFICIENT

When two species of atoms intermingle, their rate of mixing depends on the diffusion rates of both species. For diffusion in an isolated system, an *interdiffusion coefficient* (or mutual diffusion coefficient or chemical diffusion coefficient) can be defined, which gives the rate at which the original concentration gradient disappears.

When the two species in an interdiffusion experiment have unequal intrinsic diffusion coefficients, there is a net atom flux across any plane in the diffusion zone. Thus, more atoms will be on one side of the interface after diffusion which results a net volume transport. This is equivalent to the creation of a non-uniform stress-free strain [10]: on one side of the diffusion zone contractions, while on the other side extractions will arise. The stress field related to this stress-free strain contributes to the atomic fluxes across the driving force $-\Omega \text{grad } p$, and could cause a plastic deformation (by creep or by dislocation glide) as well. The plastic flow obviously relaxes the stress developed and results in a complex feed-back effect [11]. The description of the interdiffusion process then depends on the ratio of the relaxation time of plastic flow, τ , and the time of diffusion t .

If $t \gg \tau$ the relaxation of stress can be considered to be fast and almost complete. In this case the stress gradient as a driving force can be neglected. However, the relaxation of stresses is equivalent to a convective transport in the diffusion zone: *e.g.* for vacancy mechanism, expansion as well as contractions on different sides of the diffusion zone can be realized by annihilation and creation of vacancies at edge dislocations. From experimental point of view, if there is no change in the lateral dimensions of the specimens, a marker wire introduced originally at the interface appears to move toward one end of the diffusion couple. This effect, which was first observed by Kirkendall [12,13], is called the Kirkendall shift (see Figure I.3).

The marker wire is assumed to identify a given lattice plane. The flux \vec{j}_i of i (A, B) species with respect to a given lattice plane (or in the *lattice frame*) can be expressed in terms of intrinsic diffusion coefficients as in equation (I.18). If the plane is moving with velocity \vec{v} with respect to the ends of the diffusion couple (or in the *laboratory frame* of reference), the flux \vec{j}'_i of i (A, B) species with respect to the ends of the diffusion couple is:

$$\vec{j}'_i(\vec{r}, t) = \vec{j}_i(\vec{r}, t) + \rho_i(\vec{r}, t)\vec{v}(\vec{r}, t). \quad (\text{I.20})$$

In a two component crystal of constant dimensions and atom density (the number of lattice sites is conserved [14], *i.e.* $\partial(\rho_A + \rho_B)/\partial t = 0$), it is necessarily true that $\vec{j}'_A = -\vec{j}'_B$ and $\partial c_A/\partial x = -\partial c_B/\partial x$. Thus the total atom flux \vec{j}'_t with respect to the ends of the couple is:

$$\vec{j}'_t = \vec{j}'_A + \vec{j}'_B = -(D_A - D_B)\text{grad}\rho_A + \rho\vec{v} = 0. \quad (\text{I.21})$$

The Kirkendall velocity can then be written in the following form:

$$\vec{v} = \frac{1}{\rho}(D_A - D_B)\text{grad}\rho_A. \quad (\text{I.22})$$

Therefore, using equations (I.4), (I.20) and (I.21) the fluxes of A and B atoms can be expressed by:

$$\vec{j}'_A = -\vec{j}'_B = -\frac{1}{\rho}(\rho_B D_A + \rho_A D_B) \text{grad } \rho_A. \quad (\text{I.23})$$

Consequently, the interdiffusion can be characterised by only one diffusion coefficient defined in the following way:

$$\tilde{D} := \frac{1}{\rho}(\rho_B D_A + \rho_A D_B) = c_B D_A + c_A D_B, \quad (\text{I.24})$$

where $c_i = \rho_i/\rho$ ($i = A, B$) is the atomic fraction. Equation (I.24) is called as Darken's formula [6].

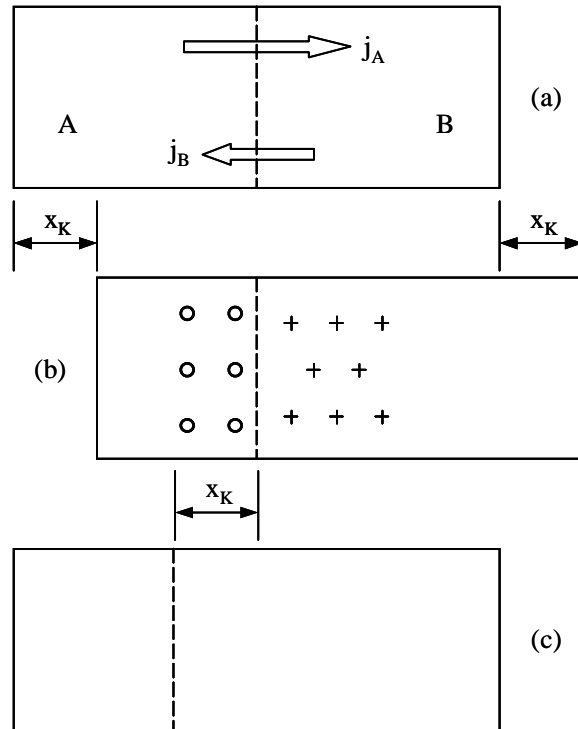


Figure I.3 Kirkendall shift. (a) During the diffusion, A atoms diffuse to the right across the marker plane (designed by the dashed line) while B atoms diffuse to the left. (b) If A diffuses faster than B, more atoms are on the right of the markers after diffusion than before. Also fewer atoms are on the left. This expands the crystal volume on the right and shrinks that on the left. If the plane containing the markers is held in a fixed position, the crystal moves to the right by a distance x_K . The hollow circles indicate the region with a surplus of vacancies, where porosity may be found. The plus signs indicate the region where extra planes are added. (c) If the crystal is then moved into alignment with diagram (a), it appears that the wires have moved to the left a distance x_K .

On the other hand, if $t \ll \tau$ (but t is long enough for the development of the stress gradient) then we can be in a second limit, when practically there is no stress relaxation at all ($\bar{v} \cong 0$). An additional term proportional to the stress (pressure) gradient should be added to the right hand side of equation (I.4) and it can be shown [15,14] that the mixing process is controlled by:

$$\tilde{D}_{NP} := \frac{D_A D_B}{c_A D_A + c_B D_B}, \quad (\text{I.25})$$

Here the index NP indicates that this is the so-called Nernst-Planck limit. After an initial transient period the pressure gradient developed makes the two fluxes equal, *i.e.* the volume transport will be determined by the slower intrinsic diffusion coefficient (series coupling of currents) in contrast to the Darken's limit (parallel coupling), where the chemical diffusion coefficient is determined by the faster one.

I.1.3.3 EFFECT OF STEEP CONCENTRATION GRADIENT

The first analysis of diffusion taking into account a steep concentration gradient as well was given by Hillert [16] in 1956. He used a regular solid solution model considering only nearest-neighbour interactions between the atoms to calculate the free energy of a binary solid solution with composition variations in one dimension. Adopting an analysis of Becker [17], Hillert showed that the excess local free energy due to a concentration gradient is proportional to the square of the gradient. Accordingly, equation (I.6) will contain an extra term proportional to $\partial^4 \rho / \partial x^4$. Considering discrete atomic planes and solving the equations numerically, Hillert determined the equilibrium distribution [16], afterwards he calculated the kinetics of the process [18].

In contrast to Hillert, Cahn and Hilliard (1958) [19] considered a continuum approximation in which three-dimensional composition variations might arise. Expressing the local free energy as the sum of Taylor series of local composition derivatives and taking just a few terms, Cahn and Hilliard also found that the local free energy depends on the square of the local composition gradient [see I.1.3.3 a)]. Furthermore, Cahn (1961, 1968) [20,21] gave the continuum diffusion equation in this approximation and determined its analytic solutions for small departures from homogeneity.

In 1969, Cook *et al.* [22,23] combined the two previous models. They considered three-dimensional composition variations on a discrete lattice and did not make any assumptions about the thermodynamics of the binary solution. Furthermore, they showed that the continuum and discrete approximations give the same results only for $\Lambda > 6d$, where Λ is the wavelength of the composition variation and d is the interatomic distance in the direction of diffusion.

More recently (1990), Martin [24] constructed a one-dimensional discrete model [see I.1.3.3 b)] in which the cohesive energy and the activation barrier for interatomic exchanges can be calculated *e.g.* from pair interaction energies. Based on this kinetic model, equations for the atomic fluxes are given. It was also shown that these equations drive the system to a correct (local) equilibrium. Furthermore, it was also illustrated that in the framework of the Bragg-Williams approximation used, the gradient energy effects were already naturally included into this model.

a) Gradient energy: Cahn-Hilliard model

Cahn and Hilliard supposed that the local free energy depends not only on the local composition, but also on the composition of the surrounding volume. It is convenient to express the local free energy in Taylor series form. Neglecting the higher order terms and considering one-dimensional composition variations, Cahn and Hilliard showed that the free energy of a solid solution consisting of A and B atoms can be expressed in the following way [19]:

$$F = A \int \left[f_0(c) + \kappa \left(\frac{\partial c}{\partial x} \right)^2 \right] dx, \quad (\text{I.26})$$

where \mathcal{A} is the cross-sectional area of the system normal to the x direction, c the atomic fraction of A atoms, $f_0(c)$ the local free energy per unit volume in a homogeneous system, and κ the gradient energy coefficient which is a combination of the Taylor coefficients. Note that κ can be calculated from a regular solid solution model and it is proportional to the ordering energy ($\kappa \propto V$) [25].

In the following, the influence of the gradient energy term will be studied. For this purpose, we will write the diffusion equation containing this term. It is always possible to choose a frame of reference such that the flux of B atoms is equal and opposite to the flux of A atoms [see I.1.3.2]. Using the mobility (always positive, M_i) and the partial free energies per unit volume (chemical potentials per unit volume, μ_i) instead of D_i and ρ_i in equation (I.4), and supposing that $\rho_A = \rho_B = \rho = 1/\Omega$ ($\Omega_A = \Omega_B$) and $M_A = M_B = M$, the interdiffusion flux can be then expressed by:

$$-\tilde{J} = M \frac{\partial}{\partial x} (\mu_A - \mu_B). \quad (\text{I.27})$$

The quantity $(\mu_A - \mu_B)$ corresponds to the exchange in free energy on reversibly replacing a unit volume of B atoms with A atoms. If the volume density of atoms is constant, it is given by:

$$\mu_A - \mu_B = \frac{\delta}{\delta c} \left[f_0(c) + \kappa \left(\frac{\partial c}{\partial x} \right)^2 \right] = f_0' - 2\kappa \frac{\partial^2 c}{\partial x^2}, \quad (\text{I.28})$$

where $f_0' = \partial f_0 / \partial c$. Therefore, the interdiffusion flux is:

$$-\tilde{J} = M f_0'' \frac{\partial c}{\partial x} - 2M\kappa \frac{\partial^3 c}{\partial x^3}, \quad (\text{I.29})$$

where $f_0'' = \partial^2 f_0 / \partial c^2$. Supposing that M , f_0'' and κ are composition independent (which is reasonable when the deviations from homogeneity are small), and taking the divergence of the flux, the following linearized diffusion equation is obtained:

$$\frac{\partial c}{\partial t} = \tilde{D} \frac{\partial^2 c}{\partial x^2} - \frac{2\tilde{D}}{f_0''} \kappa \frac{\partial^4 c}{\partial x^4}, \quad (\text{I.30})$$

where \tilde{D} is the interdiffusion coefficient and $\tilde{D} = M f_0''$. Considering a periodical concentration modulation, a particular solution of equation (I.30) is:

$$c - c_0 = \exp \left[-\tilde{D} h^2 \left(1 + \frac{2\kappa h^2}{f_0''} \right) t \right] \cosh h x. \quad (\text{I.31})$$

where c_0 is the average atomic fraction of the A component and h ($h=2\pi/\Lambda$, Λ the wavelength of the composition modulation) the wave number of the composition modulation. The amplitude A of this harmonic wave may decay or growth in the function of the sign of the amplification factor R :

$$\frac{d}{dt}(\ln A) = R = -\tilde{D} \left(1 + \frac{2\kappa h^2}{f_0''} \right) h^2 = -\tilde{D}_\Lambda h^2. \quad (\text{I.32})$$

In the presence of a steep concentration gradient, therefore, there is an effective interdiffusion coefficient \tilde{D}_Λ , which depends on the wavelength of the modulation. If there were no gradient energy effects ($\kappa = 0$), the interdiffusion coefficient would be independent of Λ .

Equation (I.31) describes the evolution of one harmonic composition wave only. In artificially modulated materials, the periodic composition variation can be described by the sum of such types of waves. The advantage of the linearized equation (I.30) is that this sum is also a solution and its components can be considered independently. The equations (I.30) and (I.32) are, therefore, very useful in the analysis of the behaviour of compositionally modulated materials. On the other hand, the linearity has a disadvantage: it is valid only for small amplitude modulations.

Moreover, even considering κ and f_0'' in the frame of the regular solid solution model [25], the behavior of materials can be classified in three categories: when $\kappa > 0$ and $f_0'' < 0$, we are in the case of a spinodal decomposition; when $\kappa > 0$ and $f_0'' > 0$, we have a phase separation; and when $\kappa < 0$ and $f_0'' > 0$, we have an ordering tendency. The fourth case is unlikely and impossible for a regular solution where only nearest neighbour interactions are taken into account. The detailed analysis of these cases can be found in reference [25].

b) Interdiffusion on atomic scale: Martin's model

In this part, we will consider only one dimensional diffusion in a discrete lattice. The model described is based on Martin's work [24].

Statistical description

We consider N lattice planes normal to the X axis (Figure I.4): there are Ω atomic sites on each lattice plane. Each site has z_l nearest neighbours on the same plane and z_v on the neighbour planes. For example for BCC[100] $z_l=0$, $z_v=4$; for FCC[111] $z_l=6$, $z_v=3$. The coordination number is $Z=z_l+2z_v$. Besides, we suppose that there are no vacancies, *i.e.* in a binary system, the A and B atoms occupy every $N \times \Omega$ atomic site. Be $\{A_1; \dots; A_i; \dots; A_N\}$ the number of A atoms on the planes 1, ..., i , ..., N , and $c_i = A_i / \Omega$ atomic fraction; $c(x)$ gives the concentration profile [here $x = (i-1)d$, where d is the distance between the planes s in the X direction].

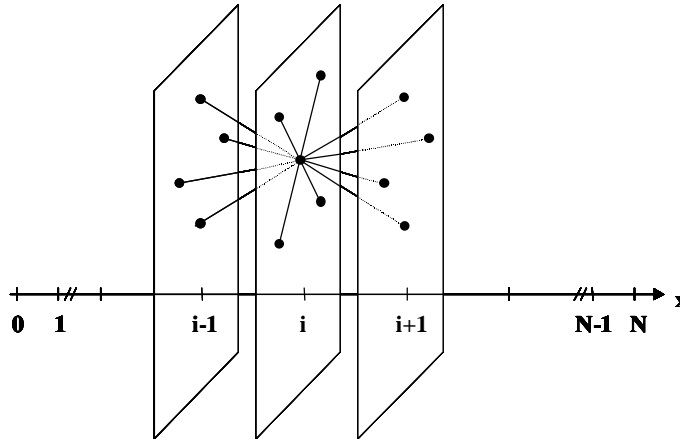


Figure I.4 One atom in plane i has z_l nearest neighbours in the same plane and z_v in plans $(i-1)$ and $(i+1)$. The coordination number is $Z=z_l+2z_v$, there are Ω lattice sites in each plane. The number of A atoms in plane i is A_i . In the figure $z_l=4$, $z_v=4$ and $Z=z_l+2z_v=12$.

We can create an N dimensional vector \vec{A} from the $\{A_i\}$ quantities. In this way, it is possible to define an internal energy $E(\vec{A})$ for each atomic configuration. At equilibrium, the probability for a given configuration to occur is:

$$P(\vec{A}) = Z^{-1} W(\vec{A}) \exp[-\beta E(\vec{A})], \quad (\text{I.33})$$

where $\beta=1/k_B T$, Z is the normalisation factor (partition function), and $W(\vec{A})$ is the number of microscopic states of the configuration \vec{A} :

$$Z = \sum_{\vec{A}} \exp[-\beta E(\vec{A})] \quad (\text{I.34})$$

Here the summation is performed over all possible arrangements of the A and B atoms that keep the overall composition constant.

Equation (I.33) may be rewritten:

$$P(\vec{A}) = Z^{-1} \exp[-\beta \mathcal{F}(\vec{A})], \quad (\text{I.35})$$

where

$$\mathcal{F}(\vec{A}) = E(\vec{A}) - TS(\vec{A}), \quad (\text{I.36})$$

$$S(\vec{A}) = k_B \ln W(\vec{A}). \quad (\text{I.37})$$

$\mathcal{F}(\vec{A})$ and $S(\vec{A})$ are the Helmholtz energy and configurational entropy.

According to the equation (I.35), the most possible configuration is which has the minimal free energy. Therefore, one has to calculate the *free energy* of the binary system, then to find its minimum with the condition that the number of particles is constant (extreme value problem).

For interior planes ($i=2, \dots, N-1$), the result (Bragg-Williams description, taking into account nearest neighbour interactions) is:

$$-\frac{2V}{k_B T} [Zc_i + z_v (c_{i+1} + c_{i-1} - 2c_i)] + \ln \frac{c_i}{1-c_i} = \mu \quad (\text{I.38})$$

where $V = V_{AB} - (V_{AA} + V_{BB})/2$ is the ordering energy and μ the chemical potential. In principle, it is possible to determine the configuration of equilibrium from these equations, but it is not an easy problem. {Note that in equation (I.38), the term $2V(c_{i+1} + c_{i-1} - 2c_i)$ presents the naturally involved gradient energy ($2\kappa \partial^2 c / \partial x^2$) [see equation (I.28)].} Instead, Martin [24] constructed a procedure allowing not only the calculation of the equilibrium configuration but to follow the time evolution of the system as well

Deterministic kinetic description

Let us introduce the exchange frequency (jump frequency) $\Gamma_{i,i+1}$ with which an A atom in plane i exchanges with a B atom in plane ($i+1$), and $\Gamma_{i,i-1}$ denotes the exchange frequency with which an A atom in plane i exchanges with a B atom in plane ($i-1$). The variation in the concentration in plane i is given by the following equation:

$$\frac{dc_i}{dt} = J_{i-1,i} - J_{i,i+1} \quad (\text{I.39})$$

where $J_{i,i+1}$ is the net flux [24] (the atomic flux is $j_{i,i+1} = J_{i,i+1}/A$, where A is the area of the specimen perpendicular to the direction of the diffusion) of A atoms between the planes i and ($i+1$):

$$J_{i,i+1} = z_v [c_i (1 - c_{i+1}) \Gamma_{i,i+1} - c_{i+1} (1 - c_i) \Gamma_{i+1,i}]. \quad (\text{I.40})$$

For $J_{i-1,i}$ a similar expression can be written. c_i is the probability that a site in plane i is occupied by an A atom and $z_v(1-c_{i+1})$ gives the probability that one site in plane ($i+1$) is occupied by a B atom. Thus, equation (I.39) can be given by:

$$\frac{dc_i}{dt} = -z_v [c_i (1 - c_{i-1}) \Gamma_{i,i-1} - (1 - c_i) c_{i-1} \Gamma_{i-1,i} + c_i (1 - c_{i+1}) \Gamma_{i,i+1} - (1 - c_i) c_{i+1} \Gamma_{i+1,i}]. \quad (\text{I.41})$$

From this equation, the steady-state condition is:

$$\frac{c_i (1 - c_{i+1})}{c_{i+1} (1 - c_i)} = \frac{\Gamma_{i+1,i}}{\Gamma_{i,i+1}}. \quad (\text{I.42})$$

This condition should coincide with (I.38). In this case it would be possible to find the same equilibrium state by equations (I.41) and (I.38). Additionally, such a way we could also calculate the transition states.

Martin [24] showed that adequate choices for jumping frequencies exist. Assuming Arrhenius-type temperature dependence:

$$\Gamma_{i,i+1} = \nu \exp\left(-\frac{E_{i,i+1}}{k_B T}\right), \quad (\text{I.43})$$

where ν denotes the attempt frequency and $E_{i,i+1}$ is the activation barrier of diffusion, for instance, the following choice [26]:

$$\begin{aligned}
 E_{i,i+1} = E^0 & - [z_\nu (c_i + c_{i+2}) + z_l c_{i+1}] (V_{AB} - V_{BB}) \\
 & + [z_\nu (c_{i-1} + c_{i+1}) + z_l c_i] (V_{AB} - V_{AA}) \\
 & - Z(V_{AB} + V_{BB}) \quad i = 2, \dots, N-1
 \end{aligned}
 \tag{I.44}$$

satisfies (I.42).

I.1.3.4 EFFECT OF INTERNAL STRESSES

Diffusion induced deformation can be due to three effects [27] : i) the sizes and/or ii) the difference of diffusivity of atoms and/or iii) a reaction between the components. Even if there is no reaction during the diffusing process, in most real cases, the difference of size or/and diffusivity exists. Consequently, there is a resultant current of volume, which builds up strain and stress field. In this part, we will treat this phenomenon in details.

a) Cahn's model

The first treatment of strain effects on the free energy of a compositionally modulated solid was given by Cahn (1961) [20]. He considered a three-dimensional isotropic solid with no long-range elastic strain fields. Furthermore, there were no dislocations (*e.g.* no sinks and sources of defects and/or vehicle of stress relaxations) in the sample. Moreover, coherency strains will arise during diffusion if the molar volume is a function of composition. Taking into account only small composition variations, he obtained for the free energy of the system:

$$F = A \int \left[f_0(c) + \kappa \left(\frac{\partial c}{\partial x} \right)^2 + \frac{\eta^2 E}{1-\nu} (c - c_0)^2 \right] dx,
 \tag{I.45}$$

where $\eta = (1/a)(da/dc)$, a is the lattice parameter, E and ν the Young's modulus and the Poisson's ratio, and c_0 the average atomic fraction of one of the two components. From this expression, following a similar procedure as in I.1.3.3a), it is possible to determine the amplification factor:

$$R = -\tilde{D} \left(1 + \frac{2\kappa h^2}{f_0''} + \frac{2\eta^2 E}{f_0''(1-\nu)} \right) h^2.
 \tag{I.46}$$

Subsequently, Cahn (1962) [21] extended his continuum model to the case of cubic crystals in which the elastic deformation is anisotropic. He showed that in this case the amplification factor is:

$$R = -\tilde{D} \left(1 + \frac{2\kappa h^2}{f_0''} + \frac{2\eta^2}{f_0''} Y_{\langle uvw \rangle} \right) h^2,
 \tag{I.47}$$

where the modulus $Y_{\langle UVW \rangle}$ is the function of the wave vector of the composition modulation. In an isotropic material, the value of $Y_{\langle UVW \rangle}$ is equal to $E/(1-\nu)$ [see equation (I.46)].

As was mentioned in I.1.3.3, the continuum model became imprecise when the wavelength of the composition modulation and the interatomic distances are comparable. Consequently, we have to use a discrete model. Cook and de Fontaine (1969, 1971) [28,29] used the microscopic theory of elasticity formulated by Born and Huang (1954) to derive the elastic free energy. In contrast to the continuum model, it was found that the excess free energy, in the case of a harmonic composition modulation, depends not only on the direction, but also on the magnitude of the wave vector of the modulation. Therefore, $Y_{\langle UVW \rangle}$ has to be replaced in the equation (I.47) by a wavelength dependent effective modulus $M_{\langle UVW \rangle}$.

On the basis of the above results, Speapen (1996) [30] showed that if stress develops during the diffusion itself the process can be characterised by an effective coefficient. For example for an ideal system ($\kappa = 0$):

$$\tilde{D}_{eff} = \tilde{D} \left[1 + \frac{2\eta^2 E}{f_0''(1-\nu)} \left(1 - \frac{A_0}{A} \right) \right], \quad (I.48)$$

where A_0 is the initial amplitude of the wave. As the expression shows, \tilde{D}_{eff} depends on the time [$A = A(t)$] and it decays gradually with time. It becomes zero when the increase of the stress energy can stop the diffusion. At this time, A/A_0 reaches its terminal value: $[1 + f_0''(1-\nu)/2\eta^2 E]^{-1}$. Therefore, the expression (I.48) shows clearly that this model does not contain the relaxation of stress.

b) Stephenson's model

Stephenson presented a general theory of stress and deformation effects during interdiffusion which unifies the analysis of the Kirkendall effect by Darken, and the treatment of the interaction between stress and deformation proposed by Cahn *et al.* [20,31,32,33,34].

The idea, which will be presented here, is based rather on the work of Daruka *et al.* (1996) [35] than that of Stephenson (1988) [10].

Material transport

According to the classical treatment of Darken, the continuity equation for component i in the fixed laboratory frame of reference is:

$$\frac{\partial \rho_i}{\partial t} + \text{div} (\tilde{j}_i + \rho_i \tilde{v}) = 0 \quad (I.49)$$

Where ρ_i is the volume density, \tilde{v} the Kirkendall velocity due to convective transport and \tilde{j}_i the flux in the *lattice frame*. The substantial derivative, $D\rho_i/Dt$ gives the rate of change of ρ_i seen at the actual (moving) lattice point and can be expressed by partial derivatives as:

$$\frac{D\rho_i}{Dt} = \frac{\partial \rho_i}{\partial t} + \tilde{v} \text{grad} \rho_i. \quad (I.50)$$

From equations (I.49) and (I.50), one can easily obtain:

$$\frac{D\rho_i}{Dt} + \operatorname{div} \vec{j}_i + \rho_i \operatorname{div} \vec{v} = 0. \quad (\text{I.51})$$

According to Stephenson [10], in the case of isotropic stress field, the diffusion potential (generalized chemical potential) is the sum of the chemical potential in an unstressed system (μ_i^{SF}) and the product $p\Omega_i$, where p and Ω_i are the pressure and the atomic volume, respectively:

$$\mu_i = \mu_i^{SF} + p\Omega_i. \quad (\text{I.52})$$

Note that the equation (I.52) is applicable only in the case when the number and efficiency of sources and sinks are high enough to establish the local equilibrium of the defects at any time (local equilibrium hypothesis). Thus the expressions of the fluxes are given by:

$$\vec{j}_i = -M_i \rho_i \nabla (\mu_i^{SF} + \Omega_i p), \quad (\text{I.53})$$

where M_i is the mobility. Formally, the flux can be also written in the following way:

$$\vec{j}_i = -D_i \operatorname{grad} \rho_i - L_i \rho_i \operatorname{grad} p, \quad i = 1, 2 \quad (\text{I.54})$$

where D_i is the intrinsic diffusion coefficient and L_i the cross coefficient. The relation between the thermodynamic factor (Θ) and the chemical potential is:

$$RT\Theta \nabla c = c \nabla \mu_1^{SF} = -(1-c) \nabla \mu_2^{SF}, \quad (\text{I.55})$$

where $c = \rho_1/\rho$ ($1-c = \rho_2/\rho$) and $\rho = 1/\Omega$ the average density of the solid solution. Comparing equations (I.53) and (I.55) and using the Vegard-law:

$$\Omega_1 \rho_1 + \Omega_2 \rho_2 = 1, \quad (\text{I.56})$$

one obtains a relation between the mobility and the intrinsic diffusion coefficient

$$D_1 = M_1 RT\Theta / \rho \Omega_2, \quad (\text{I.57})$$

where R is the molar gas constant and T the absolute temperature. Moreover, from the equations (I.54), (I.53) and (I.57):

$$L_1 = M_1 \Omega_1 = D_1 \rho \Omega_1 \Omega_2 / RT\Theta. \quad (\text{I.58})$$

Strains and stresses

The total strain tensor is taken to be the sum of elastic, plastic and stress -free strain tensors [10], that is:

$$\boldsymbol{\varepsilon}_{ij}^T = \boldsymbol{\varepsilon}_{ij}^E + \boldsymbol{\varepsilon}_{ij}^P + \boldsymbol{\varepsilon}_{ij}^{SF}, \quad (\text{I.59})$$

the stress-free strain is related to the volume transport and we will suppose that this deformation is isotropic, *i.e.* on the length scales of interest there is a dense, isotropic distribution of sources and sinks of lattice sites. The rate of the stress-free deformation can be given by the expression:

$$\frac{De^{SF}}{Dt} = -\frac{1}{3} \left(\Omega_1 \operatorname{div} \vec{j}_1 + \Omega_2 \operatorname{div} \vec{j}_2 \right), \quad (\text{I.60})$$

where $e^{SF} = \operatorname{trace}(\boldsymbol{\varepsilon}^{SF}/3)$ [10].

If the stress developed it can relax by creep. The resultant macroscopic deformation relaxes the stress level without changing the total volume. Consequently, one can use the simple viscous creep model (Newtonian flow; see also equation (24) in [10]):

$$\frac{D\boldsymbol{\varepsilon}_{ij}^P}{Dt} = \frac{1}{\eta} \left(\sigma_{ij} - \sigma_{ij} \delta_{ij} / 3 \right), \quad (\text{I.61})$$

where η is the shear viscosity.

The stress relaxation can also take place by dislocation gliding mechanism, if the stress exceeds the critical shear stress level. Using the Tresca-flow model, this effect can be taken into account introducing a cut-off stress level; the value of the shear stress cannot exceed this level.

The internal stress can also be related to the elastic deformation. According to Hook's law:

$$\sigma_{ij} = \frac{E}{(1+\nu)(1-2\nu)} \left[(1-2\nu) \boldsymbol{\varepsilon}_{ij}^E + \nu \boldsymbol{\varepsilon}_{kk}^E \delta_{ij} \right] \quad (\text{I.62a})$$

or

$$\boldsymbol{\varepsilon}_{ij}^E = \frac{1}{E} \left[(1+\nu) \sigma_{ij} - \nu \sigma_{kk} \delta_{ij} \right] \quad (\text{I.62b})$$

where E and ν are the Young modulus and the Poisson ratio.

It is worth mentioning that there is a relation between \vec{V} and the strain rate:

$$\frac{De^T}{Dt} = \frac{1}{3} \operatorname{div} \vec{V}, \quad (\text{I.63})$$

where $e^T = \operatorname{trace}(\boldsymbol{\varepsilon}^T/3)$ and $e^P = 0$. Moreover, for isotropic case equation (I.62b) has the following form:

$$e^E = -\frac{1-2\nu}{E} p \quad (\text{I.64})$$

and

$$\operatorname{div} \vec{V} = -\left(\Omega_1 \operatorname{div} \vec{j}_1 + \Omega_2 \operatorname{div} \vec{j}_2 \right) - \frac{3(1-2\nu)}{E} \frac{Dp}{Dt}. \quad (\text{I.65})$$

Thus, from equations (I.51) and (I.65), the continuity equation can be written into the form:

$$\frac{D\rho_1}{Dt} = \Omega_2 (\rho_1 \operatorname{div} \vec{j}_2 - \rho_2 \operatorname{div} \vec{j}_1) + \rho_1 \frac{3(1-2\nu)}{E} \frac{Dp}{Dt}, \quad (\text{I.66})$$

where the Vegard-law was used [equation (I.56)].

The stress distribution will be governed by the condition of local mechanical equilibrium [10]

$$\operatorname{div} \sigma = 0, \quad (\text{I.67})$$

and by nonlocal boundary conditions and constraints. The final form of the coupled equations of system and thus their solutions can be different for different boundary conditions.

For example Stephenson (1993) [36], in the case of an amorphous, isotropic, one-dimensional system, obtained the following equations:

$$\frac{Dp}{Dt} = -\frac{2E}{9(1-\nu)} \left[\sum_{i=1}^2 (\Omega_i \nabla j_i) + \frac{3}{4\eta} p \right], \quad (\text{I.68})$$

$$\nabla v = -\sum_{i=1}^2 (\Omega_i \nabla j_i) - \frac{3(1-2\nu)}{E} \frac{Dp}{Dt}, \quad (\text{I.69})$$

$$\frac{Dc}{Dt} = -\frac{1}{\rho} [(1-c) \nabla j_1 - c \nabla j_2]. \quad (\text{I.70})$$

Note that, considering that $c = \rho_1/\rho$, equations (I.66) and (I.70) are equivalent and:

$$\frac{Dc}{Dt} = \frac{1}{\rho} \frac{D\rho_1}{Dt} - \frac{\rho_1}{\rho^2} \frac{D\rho}{Dt}. \quad (\text{I.71})$$

Equations (I.70) and (I.68) determine the evolution of concentration and pressure in the function of time. Since the system of equations is strongly coupled and contains nonlinear terms, it is impossible to solve it analytically. It can be solved only numerically. Linearizing the equations, the analytical solution is possible [10].

I.1.3.5 NONLINEAR EFFECTS

In the previous paragraphs, linearized equations were used to describe the diffusion phenomena. In this case, the Fourier components of a concentration profile evolve independently in time and there can be characterized by the amplification factor R . It implies that the parameters M , f_0'' , κ and the parameters characterizing the stress effect η , $Y_{\langle UVW \rangle}$ are independent of the concentration. It is evident that these assumptions are not justified in the case of composition modulations with large amplitudes (there exist during spinodal decomposition or at the beginning of the heat treatment of artificial multilayers). Thus nonlinear analysis is necessary. Let us consider an initially homogeneous spinodal system. The beginning of the reaction can be written satisfactorily by a linear analysis putting the average concentration in the parameters. If we keep this average value to describe the continuation of the phenomena, we will have an exponential growth of the

fluctuations. In reality, they slow down in time, principally because the parameter f_0'' is not constant, especially when we approach the total decomposition.

a) Concentration dependent f_0''

The first possibility to solve the problem can be to consider a concentration dependent f_0'' .

One of the earliest treatment of nonlinear diffusion in compositionally modulated materials was given by Hillert (1956, 1961) [16,18]. He assumed a system with composition modulations in one dimension in which he calculated the free energy from a regular solid solution model considering only nearest-neighbour interactions, and no restrictive assumptions were made about f_0'' . He ignored, however, the strain effects as well as $M/c(1-c)$ and κ were taken to be constant. He demonstrated that the growth slowed down as equilibrium compositions were approached and that "stationary states" would be reached at infinite time. He also showed that the stationary states are the minimum energy configurations for a given modulation wavelength. Fluctuations of large wavelength exhibited an appreciable amount of "squaring" during growth, and in the resulting stationary states the composition profiles were not harmonic.

Tsakalacos (1977) [37] derived analytical expressions describing the stationary states, which are in excellent agreement with Hillert's numerical solutions.

Cahn (1961) [20] considered modulations only of a single wavelength in $\langle 100 \rangle$ directions in a three-dimensional system. Solving the nonlinear diffusion equation, he showed that after the initial stages, harmonics of the original wavelength appear and the odd harmonics cause squaring of the modulation.

The coarsening demonstrated by Hillert is relevant for one-dimensional composition modulations such as are found in artificially modulated structures. Because of the assumption of a single initial wavelength, the Cahn's approach may also be appropriate only for these cases.

b) Concentration dependent mobility/diffusion coefficient

The second possibility to solve the problem can be to consider a concentration dependent mobility/diffusion coefficient.

De Fontaine (1967) [38] studied the evolution of a one-dimensional modulated system. The gradient energy term κ was assumed to be zero and the interdiffusivity \tilde{D} was a quadratic function of composition. Figure I.5 shows the evolution of the first three Fourier components of an A-Au-layered structure. The first Fourier component decays almost exponentially; the effect of the nonlinearity on this component is small. The second and third Fourier components, however, are strongly affected by nonlinearity. The most striking feature is the emergence of the second component, which is not present at all in the original rectangular profile. This reflects the developing asymmetry in the composition profile, due to the faster diffusion in the Au-rich than in the Ag-rich region. Tsakalacos [37] has given an approximate analytical solution to the nonlinear diffusion equation, which is in good agreement with de Fontaine's numerical results.

Later on (1992), Menon and de Fontaine [39], from numerical solutions of the diffusion equation for a quadratic concentration dependence of the diffusion coefficient, postulated the following conjecture: '... the n th amplitude of the Fourier spectrum of the solution of the diffusion equation with nonlinear diffusivity changes its sign $(n-1)$ times

before decaying exponentially with time.' This behaviour can be seen in Figure I.6. for Ag-50at% Au system.

De Fontaine [38] and Hilliard (1970) [40] have taken into account the composition dependence of both parameters. They used the parameters for the Al -Zn system. They described the variation of the free energy with composition by a fourth-degree polynomial. The interdiffusion coefficient was described by a quadratic function of composition. The results for asymmetric alloy Al-22.5at%Zn obtained by numerical solution of the nonlinear diffusion equation are shown in Figure I.7. This shows the development of a regular structure followed by coarsening.

The higher-order terms in the expression of the free energy of a nonhomogeneous solution lead to deviations in the wavelength -dependence of the interdiffusivity \tilde{D}_A , as given by equations (I.32), (I.45) and (I.47) [41].

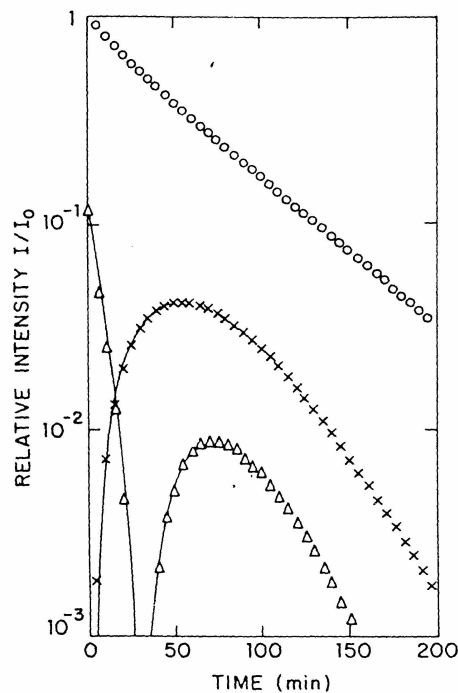


Figure I.5 First three Fourier components of an Ag-Au-layered structure. [38]

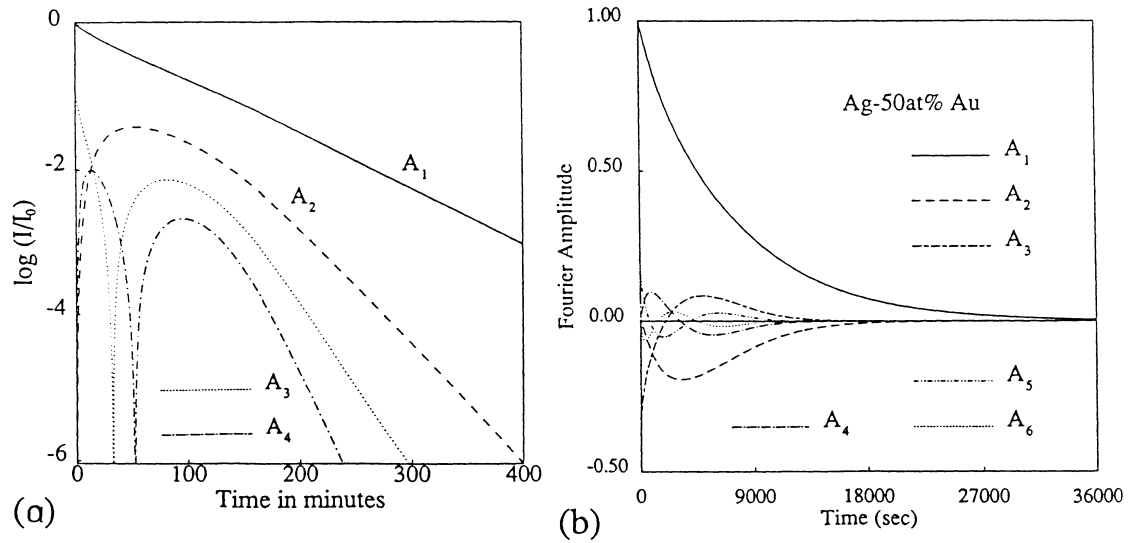


Figure I.6 (a) Logarithm of the normalized intensities vs. time (the first four order) for the Ag-50at% Au system. (b) The first six harmonics vs. time. [I_0 and A_0 are the initial first order intensity and amplitude] [39]

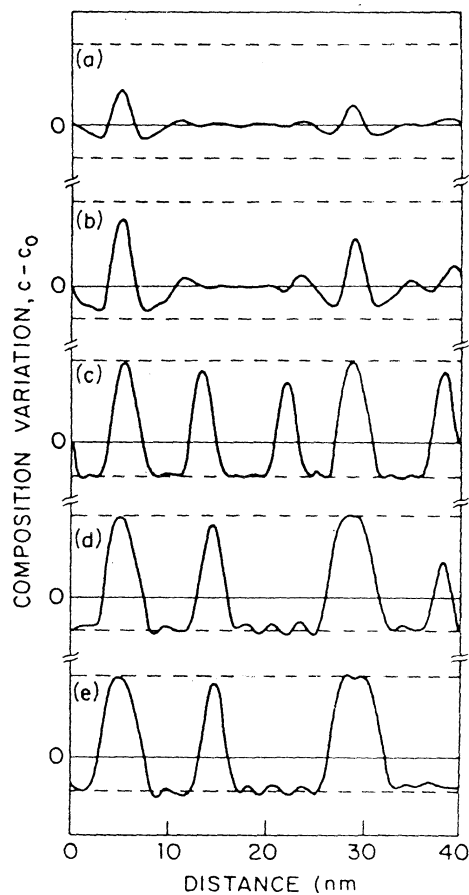


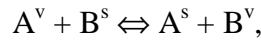
Figure I.7 Evolution of the composition profile vs. time in an Al-22.5%Zn alloy at 100°C. (a) 10, (b) 13.3, (c) 60, (d) 400 and (e) 416 min. The horizontal dashed-lines denote the equilibrium composition. [38,40]

I.2 SURFACE SEGREGATION

I.2.1 Thermodynamical aspects

In a binary alloy, the concentration close to the surface can be different from its bulk value. This phenomenon is called surface segregation. Although it was treated already at the end of the nineteenth century by J.W. Gibbs [42], a sophisticated statistical thermodynamical treatment can be very difficult, and many experimental and theoretical aspects of the problem are still actively studied in the literature [43].

Theoretically, the segregation must affect the properties of several atomic planes. Nevertheless, the most used model, since it is the simplest, is the monolayer one [44]. The surface is defined as a two-dimensional homogeneous phase of the same structure as the volume. The equilibrium of surface segregation in an AB binary system corresponds to the following relation:



where the superscripts s and v correspond to the surface and volume, respectively.

Determining the chemical potentials of A (μ_A) and B (μ_B) atoms both in the surface layer and in the volume, and using that chemical potentials are equal in the surface layer and in the volume ($\mu_A^s - \mu_B^s = \mu_A^v - \mu_B^v$), one obtains the well-known relation:

$$\frac{c_A^s}{1-c_A^s} = \frac{c_A^v}{1-c_A^v} \exp\left[-\frac{\Delta H}{RT}\right]. \quad (\text{I.72})$$

c^i ($i = s, v$) are the surface and volume atomic fractions of A and B atoms and ΔH is the segregation energy. Formally, the expression of ΔH can be divided into three parts:

$$\Delta H = \Delta H_{tens} + \Delta H_{chem} + \Delta H_{size}. \quad (\text{I.73})$$

The first term represents the effect of surface tension (ΔH_{tens}) [42], which tends to segregate the element having the smaller surface tension, the second one corresponds to the chemical effect (ΔH_{chem}) [42], which takes into consideration the nature and the number of interactions between atoms at the surface and the last one (ΔH_{size}) takes into account the elastic energy of relaxation [45, 46].

Sometimes, the size effect is negligible as compared to the two other terms. However, if the sign of these two terms are different, they can compensate each other and the size effect can be dominant.

Of course, the concept mentioned above cannot be applied in all cases. For example, if the segregation extends more than one surface layer, a multilayer model can be used (with different approaches for the energy terms in (I.73), see *e.g.* estimates based on pair interactions [47,48,49] or, in transition and noble metal alloys, on the electronic structure: Tight Binding Ising Model [50]).

I.2.2 Kinetic aspects

In practice, the determination of segregation data is difficult since the equilibrium distribution of composition has to be reached.

Application of the “local equilibrium” hypothesis [51,52] permits, however, to obtain these data from kinetic studies. During the segregation process, two phenomena have to be taken into account: exchange of atoms close to the surface and the volume diffusion.

Most of the models describing the kinetics of surface segregation (e.g. [53,54]) are based on the simplified concept that only the surface (terminal, first) layer is distinct from the volume (monolayer model). A multilayer approach is far more appropriate than the monolayer one. The starting point can be the Ising model with nearest neighbour interactions and the Bragg-Williams approximation [55], and e.g. Cserhádi *et al.* applied Martin’s model [see I.1.3.3b)] to calculate the kinetics of surface segregation in ordered alloys [26].

I.2.2.1 APPLICATION OF THE MARTIN MODE

Since Martin have not written explicitly the expression of the chemical potentials and diffusion activation barriers for the terminal layers, Cserhádi *et al.* [26] gave it ($i = 1$):

$$-\frac{2V}{k_B T} \left[Zc_1 + z_v \left(\frac{P}{2V} + c_2 - 2c_1 \right) \right] + \ln \frac{c_1}{1-c_1} = \mu \quad (\text{I.74})$$

where $P = (V_{AA} - V_{BB})/2 + V$ (for the N -th plane, a similar relation can be created) and

$$E_{1,2} = E^0 - [z_v(c_1 + c_3) + z_l c_2](V_{AB} - V_{BB}) + [z_v c_2 + z_l c_1](V_{AB} - V_{AA}) - ZV_{BB} - (z_l + z_v)V_{AB} \quad (\text{I.75})$$

For the plane $i = N$, similar expressions can be written. As input parameters in [26] pair interaction energies were used, but of course, in the literature, there are other models for more appropriate description of the energetics taking into account e.g. structural relaxation, size effect, electronic structure, etc. (embedded-atom [56], Kinetic Tight Binding Ising Model [57]).

I.3 GRAIN-BOUNDARY DIFFUSION

Up to this point, we treated only monocrystalline or amorphous materials. In these systems, the material transport occurs by volume diffusion only. Whereas, in polycrystalline materials, grain boundaries are, generally, diffusion short circuits, consequently, the major part of material transports occurs by grain-boundary diffusion.

I.3.1 Fisher's model

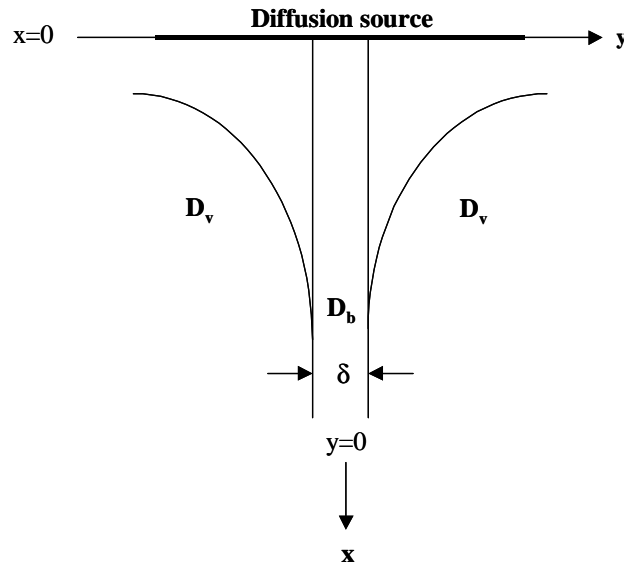


Figure I.8 Illustration of Fisher's model

As it can be seen in Figure I.8, grain boundaries, with thickness δ are perpendicular to the surface where the diffusion source is deposited, are considered as an isotropic medium, semi-infinite, uniform characterized by a higher diffusivity as compared to the bulk [58,59]. With these assumptions, and considering the case, when there is also diffusion into the grains (type B-regime), the Fisher model is based on the following statements:

1. Volume and grain-boundary diffusion coefficients (D_v and D_b) are isotropic, concentration, position and time independent.
2. The concentration and the flux are continuous at the boundary/volum interface.
3. The grain-boundary thickness is so small that the concentration variation in the boundary is negligible in the y direction.

Then

$$\begin{aligned} \frac{\partial c_v}{\partial t} &= D_v \left(\frac{\partial^2 c_v}{\partial x^2} + \frac{\partial^2 c_v}{\partial y^2} \right) \text{ pour } |y| \geq \frac{\delta}{2} \\ \frac{\partial c_b}{\partial t} &= D_j \frac{\partial^2 c_b}{\partial x^2} + \frac{2D_v}{\delta} \frac{\partial c_v}{\partial y} \Big|_{|y|=\frac{\delta}{2}}, \end{aligned} \quad (\text{I.76})$$

where c_v and c_b are the concentrations of the diffusing species in the bulk and in the boundary, respectively, and t the time.

One can find several solutions of equations (I.76) in the literature. For example Suzuoka [60,61] gave the solution for the case of a thin -film source. Whipple's solution [62] applies when the surface concentration is maintained constant on the surface of the sample. Le Claire formulated a simple relationship between δD_b , D_v , t and the slope of the

experimental penetration curve ($\partial \ln \bar{c} / \partial x^{6/5}$, where \bar{c} is the value of the concentration in the yz plane) [58,7]. These expressions are used, in general, for the interpretation of experimental penetration curves. Plotting the logarithm of the concentration versus $x^{6/5}$, at penetrations larger than $5\sqrt{D_v t}$, a straight line is obtained, the slope of which can be used for evaluation of δD_b .

However, the solutions of equations (I.76) concern only diffusion in bicrystals. Levine and MacCallum treated the case of grain-boundary self-diffusion for polycrystals in the most general way [63]. They considered that the crystal contains randomly oriented grain boundaries and that the grain size distribution is also random. Supposing that concentration gradients are uniquely oriented along the grain boundaries, it is possible to show that Le Claire's equations can be used, provided that the mean inclination of boundaries is taken into account. Therefore, these equations give the basis of the mathematical analysis of grain-boundary diffusion in polycrystals.

I.3.2 Diffusion regimes in polycrystals

Bulk materials are, generally, polycrystalline. In polycrystals, three diffusion regimes are distinguished by Harrison [64]: type A, B and C regimes (Figure I.9).

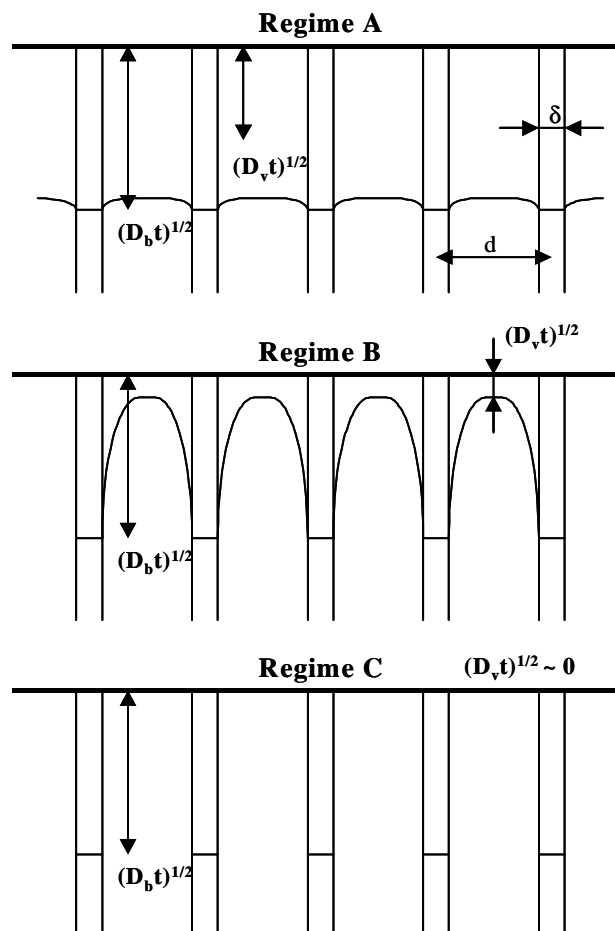


Figure I.9 Schematic illustration of Harrison's diffusion regimes

Regime A: If the diffusion annealing time is sufficiently long and/or the grain boundary size d is small ($\sqrt{D_v t} \gg d$), the diffusion fields related to the diffusion into the grains are

not isolated from each other. Macroscopically, the crystal behaves like a homogeneous medium, characterised by one effective diffusion coefficient D_{eff} . This effective diffusion coefficient can be related to volume and grain-boundary diffusivities by the fraction f of the atomic sites in grain boundaries: $D_{eff} = fD_b + (1-f)D_v$.

Regime B: In this case the different grains are isolated from each other with a non negligible contribution of volume diffusion from the surface and from the boundaries. This regime was already treated in I.3.1.

Regime C: If $1 \ll k_b \delta / 2(D_v t)^{1/2}$, the diffusion process takes place only in grain boundaries, since the direct volume diffusion contribution and lateral leakage from grain boundaries are negligible. Therefore, the process is characterized by one diffusion coefficient (D_b) in a homogeneous medium. The advantage of this regime is that the grain-boundary diffusion coefficient can directly be measured without any supposition on the grain-boundary width. However, it is generally extremely difficult to attain the necessary experimental conditions using the tracer technique [65].

I.3.3 Hwang-Balluffi model

Hwang *et al.* [66] analysed the problem of diffusion in an array of uniformly spaced parallel grain boundaries in a thin-film system under the conditions of C kinetics. In this regime, volume diffusion is essentially frozen out so that the material transport takes place only within the grain boundaries without any leakage into the adjoining grains. The geometry and the notations of the thin-film system analyzed are illustrated in Figure I.10.

Hwang and Balluffi developed a mathematical analysis for interpretation of the accumulation kinetics measurements. They assumed that the atoms arriving from the grain boundaries spread out on the surface.

They determined a relation, which links the grain-boundary diffusion coefficient D_b with the average concentration c_s of the accumulation surface. This Hwang-Balluffi relation is given by:

$$(k''/k')c_s/c_0 = 1 - \exp(-\omega t'), \quad (I.77)$$

$$\omega = \delta D_b \lambda / \delta_s h k'. \quad (I.78)$$

Here λ is the grain-boundary density (*e.g.* for a polycrystal having cubic grains with d , $\lambda = 2/d$). Moreover, k' is the segregation coefficient at the accumulation surface/grain-boundary interface and k'' the segregation coefficient at the grain-boundary/source interface. They are defined by the proportions c_s/c_b and c_b/c_0 , respectively. We note that the form given here is not exactly that written in [66], but it's a little bit generalised version [58,67]. The t' quantity is a "corrected time" of the form:

$$t' = t - t_0, \quad (I.79)$$

where t_0 is a constant, taking into account that a transient phenomenon occurs in each diffusion measurement before a quasi-steady-state is reached and t is the real time. The Hwang-Balluffi equation can be applied under the following conditions: i) a quasi-steady-state grain-boundary diffusion current to the accumulation surface has been established; ii) the surface diffusion rate is sufficiently rapid so that the segregated atoms are uniformly

distributed laterally in the surface region; iii) a constant concentration of diffusing source atoms is maintained in the grain-boundary/source interface.

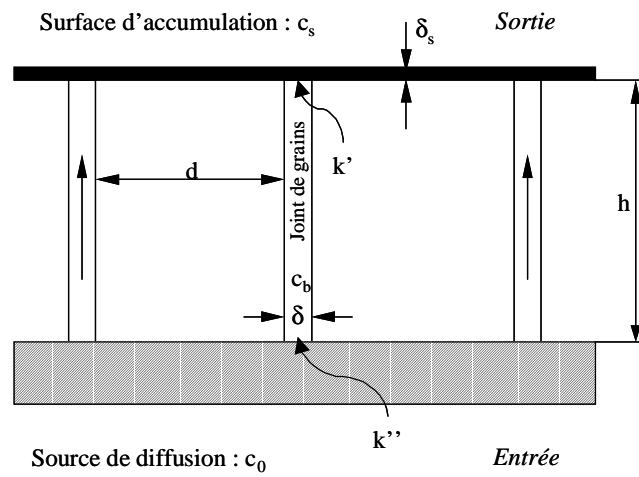


Figure I.10 Geometry of the thin film system used in the Hwang-Balluffi method


REFERENCES

- 1 Y. Adda et J. Philibert, *La diffusion dans les solides*, Presses Universitaires de France, Paris (1966)
- 2 C.J.A. Monty, Théorie atomique statistique de la diffusion, *Difusão em Materiais*, Editado por J. Philibert, A.C.S. Sabioni, F. Dymont, Ouro Preto: Editora REM-Revista Escola de Minas, 51 (1996)
- 3 J. Philibert, *Atom Movements – Diffusion and Mass Transport in Solids*, Les Editions de Physique (1991)
- 4 A. Einstein, *Ann. Physik.*, **17**, 549 (1905)
- 5 M.V. Smoluchowski, *Z. Physik. Chemie*, **92**, 129 (1917)
- 6 Diffusion in Semiconductors and Nano-Metallic Solids, Beke, D.L. (ed.), Landolt-Börnstein, New Series, Vol. 33 -B1, Berlin: Springer-Verlag, 1999
- 7 A.D. Le Claire, *Brit. J. Appl. Phys.*, **44**, 351 (1963)
- 8 A.R. Allnatt and A.B. Lidiard, *Atomic Transport in Solid* (University Press, Cambridge), 170 (1993)
- 9 C.P. Flynn, *Point Defects and Diffusion*, Oxford, Clarendon Press, (1972)
- 10 G.B. Stephenson, *Acta Metall.*, **36**, 2663 (1988)
- 11 D.L. Beke, *Defect and Diffusion Forum*, **129-130**, 9 (1996)
- 12 E.O. Kirkendall, *Trans. A.I.M.E.*, **147**, 104 (1942)
- 13 A.D. Smigelskas and E.O. Kirkendall, *Trans. A.I.M.E.*, **171**, 130 (1947)
- 14 D.L. Beke, *Key Eng. Mater.*, **103**, 51 (1995)
- 15 B.S. Bokstein, Z.S. Zsukhovicki *Thermodynamics and kinetics of diffusion in solids*, Moscow: Metallurgya, 1974
- 16 M. Hillert, *Sc. D. Thesis*, Massachusetts Institute of Technology, Cambridge, Massachusetts (1956)
- 17 R. Becker, *Ann. Physik*, **32**, 128 (1938)
- 18 M. Hillert, *Acta Metall.*, **5**, 29 (1961)
- 19 J.W. Cahn and J.E. Hilliard, *J. Chem. Phys.*, **28**, 258 (1958)
- 20 J.W. Cahn, *Acta Metall.*, **9**, 795 (1961)
- 21 J.W. Cahn, *Trans. Metall. Soc. AIME*, **242**, 166 (1968)
- 22 H.E. Cook and D. de Fontaine, *Acta Metall.*, **17**, 915 (1969)
- 23 H.E. Cook, D. de Fontaine and J.E. Hilliard, *Acta Metall.*, **17**, 765 (1969)
- 24 G. Martin, *Phys. Rev. B*, **41**, 2279 (1990)
- 25 A.L. Greer and F. Spaepen, *Synthetic Modulated Structure Materials* (L. Chang and B.C Giessen, eds.), New York: Academic Press (1985)
- 26 Cs. Cserhádi, H. Bakker, D.L. Beke, *Surf. Sci.*, **290**, 345 (1993)
- 27 D.L. Beke, I.A. Szabó, *Def. and Diff. Forum*, **95-98**, 537 (1993)
- 28 H.E. Cook and D. de Fontaine, *Acta Metall.*, **17**, 915 (1969)
- 29 H.E. Cook and D. de Fontaine, *Acta Metall.*, **19**, 607 (1971)
- 30 F. Spaepen, *J of Magn. Magn. Mat.*, **156**, 407 (1996)
- 31 F.C. Larché and J.W. Cahn, *Acta Metall.*, **30**, 1835 (1982)
- 32 F.C. Larché and J.W. Cahn, *Acta Metall.*, **33**, 331 (1985)
- 33 F.C. Larché and J.W. Cahn, *Acta Metall.*, **21**, 1051 (1973)
- 34 F.C. Larché and J.W. Cahn, *Acta Metall.*, **26**, 53 (1978)
- 35 I. Daruka, I.A. Szabó, D.L. Beke, Cs. Cserhádi, and A. Kodentsov, F.J.J. van Loo, *Acta mater.*, **44**, 4981 (1996)
- 36 G.B. Stephenson, *Defect and Diffusion Forum*, **95-98**, 507 (1993)
- 37 T. Tsakalakos, *Ph.D. Thesis*, Northwestern University, Evanston, Illinois (1977)
- 38 D. de Fontaine, *Ph.D. Thesis*, Northwestern University, Evanston, Illinois (1967)

-
- 39 E.S.K. Menon and D. de Fontaine, *Scripta Metall.*, **27**, 395 (1992)
 - 40 J.E. Hilliard, *Phase Transform. Pap. Semin. Am. Soc. Met.*, ASM, Metals Park, Ohio, 497 (1970)
 - 41 T. Tsakalakos, *Thin Sol. Films*, **86**, 79 (1981)
 - 42 J.W. Gibbs, *The Collected Works of J.W. Gibbs*, Yale University Press, New Haven, Vol. 1 (1948)
 - 43 P.A. Dowben, A. Miller, *Surface Segregation Phenomena*, CRC press, 1990
 - 44 E.A. Guggenheim, *Trans. Faraday Soc.*, **36**, 397 (1940)
 - 45 P. Wynblatt and R.C. Ku, *Surf. Sci.*, **65**, 511 (1977)
 - 46 J. Freidel, *Advan. Phys.*, **3**, 446 (1954)
 - 47 F.L. Williams and D. Nason, *Surf. Sci.*, **45**, 377 (1974)
 - 48 M.J. Kelley and V. Ponec, *Prog. Surf. Sci.*, **11**, 139 (1981)
 - 49 M.J. Sparnaay, *Surf. Sci. Rept.*, 4, 101 (1984)
 - 50 G. Tréglia, B. Legrand et F. Ducastelle, *Europhys. Lett.*, **7**, 575 (1988)
 - 51 M. Lagües, *Philips Res. Repts. Suppl.*, 5 (1976)
 - 52 M. Lagües and J.L. Domange, *Surf. Sci.*, **47**, 77 (1975)
 - 53 P.A. Dowben and A. Miller, *Surface Segregation Phenomena*, CRC Press, Boca Raton (1990)
 - 54 J. Du Plessis, *Surface Segregation, Diffusion and Defect Data, Solid State Phenomenon, Sci. Tech.*, **11** (1990)
 - 55 T. Muto and Y. Takagi, *Theory fo Order-Disorder Transition in Alloy, Solid State Phys.*, **1**, 31, (1955)
 - 56 M. Lundberg, *Phys. Rev. B*, **36**, 4692 (1987)
 - 57 A. Senhaji, G. Tréglia, B. Legrand, N.T Barrett, C. Guillot et B. Vilette, *Surf. Sci.* , **274**, 297 (1992)
 - 58 I. Kaur, Yu Mishin and Gust, *Fundamentals of Grain and Interphase Boundary Diffusion*, Third enlarged edition, John Wiley & Sons Ltd (1995)
 - 59 J.C. Fisher, *J. Appl. Phys.*, **22**, 74 (1951)
 - 60 T. Suzuoka, *Trans. Japan Inst. Metals*, **2**, 25 (1961)
 - 61 T. Suzuoka, *J. Phys. Soc. Japan*, **19**, 839 (1964)
 - 62 R.T. Whipple, *Phil. Mag.*, **45**, 1225 (1954)
 - 63 H.S. Levine and C.J. MacCallum, *J. Appl. Phys.*, **31**, 595 (1960)
 - 64 L.G. Harrison, *Trans. Faraday Soc.*, **57**, 1191 (1961)
 - 65 D.L. Beke, I. Gődény, F.J. Kedves, *Transactions of the Jap. Inst. of Metals*, **27**, 649 (1986)
 - 66 J.C.M. Hwang, J.D. Pan, R.W. Balluffi, *J. Appl. Phys.*, **50**, 1339 (1979)
 - 67 J.C.M. Hwang, J.D. Pan, R.W. Balluffi, *J. Appl. Phys.*, **50**, 1335 (1979)

Chapter II

Systems and Techniques



In this chapter we present the systems studied experimentally, the techniques applied and the methods used for fabrication of multilayers and thin films.

Chapter II

SYSTEMS AND TECHNIQUES

II.1 SYSTEMS

In this chapter, we present the systems studied experimentally, the techniques applied and the methods used for fabrication of multilayers and thin films.

II.1.1 Si-Ge system

The Ge-Si phase diagram is shown in Figure II.1 [1]. There is a complete mutual solubility in this system. The mutual diffusion coefficients (Si in Ge and vice versa) are strongly influenced by the chemical composition of the alloy. Moreover, it is possible to prepare samples in amorphous state.

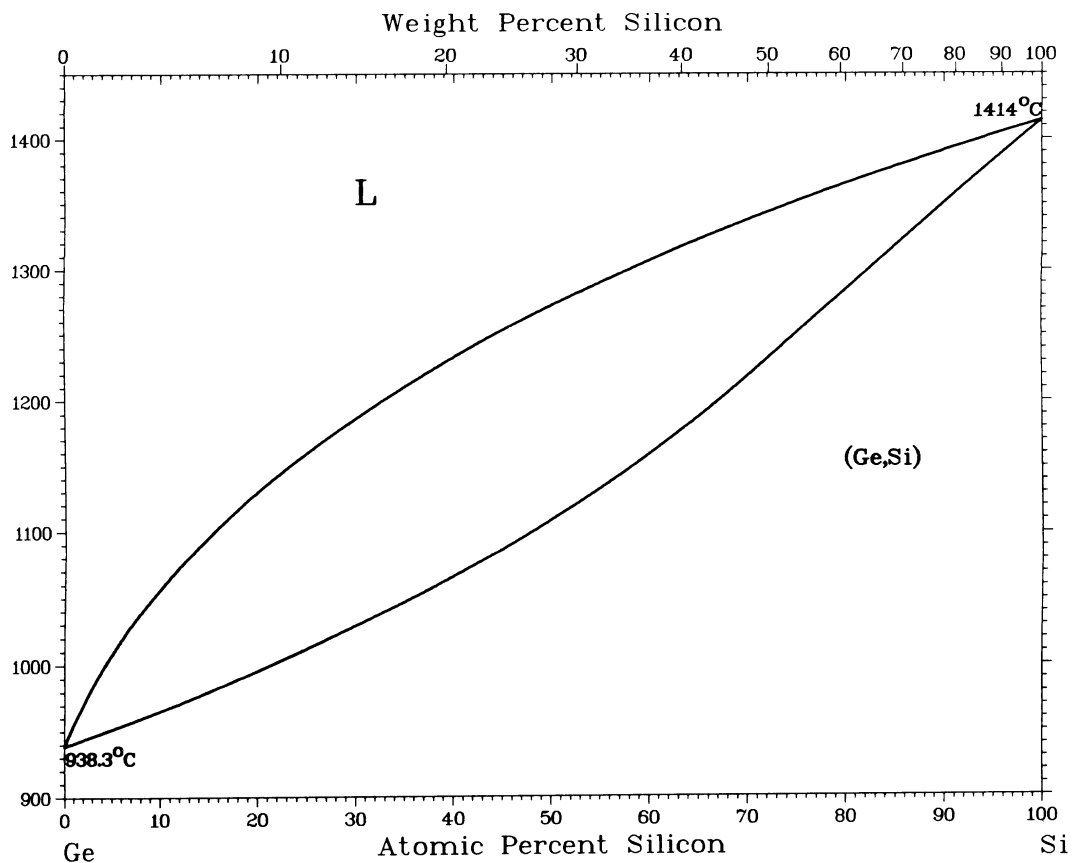


Figure II.1 Ge-Si phase diagram [1]

II.1.2 Cu-Ni system

The Cu-Ni phase diagram is shown in Figure II.2 [1]. There is a complete mutual solubility in this system. Both elements form a BCC structure. The mutual diffusion coefficients (Cu in Ni and vice versa) are strongly influenced by the chemical composition of the alloy, especially at low temperatures. According to certain authors [1,2], there exist, however, a miscibility gap at lower temperatures than we worked.

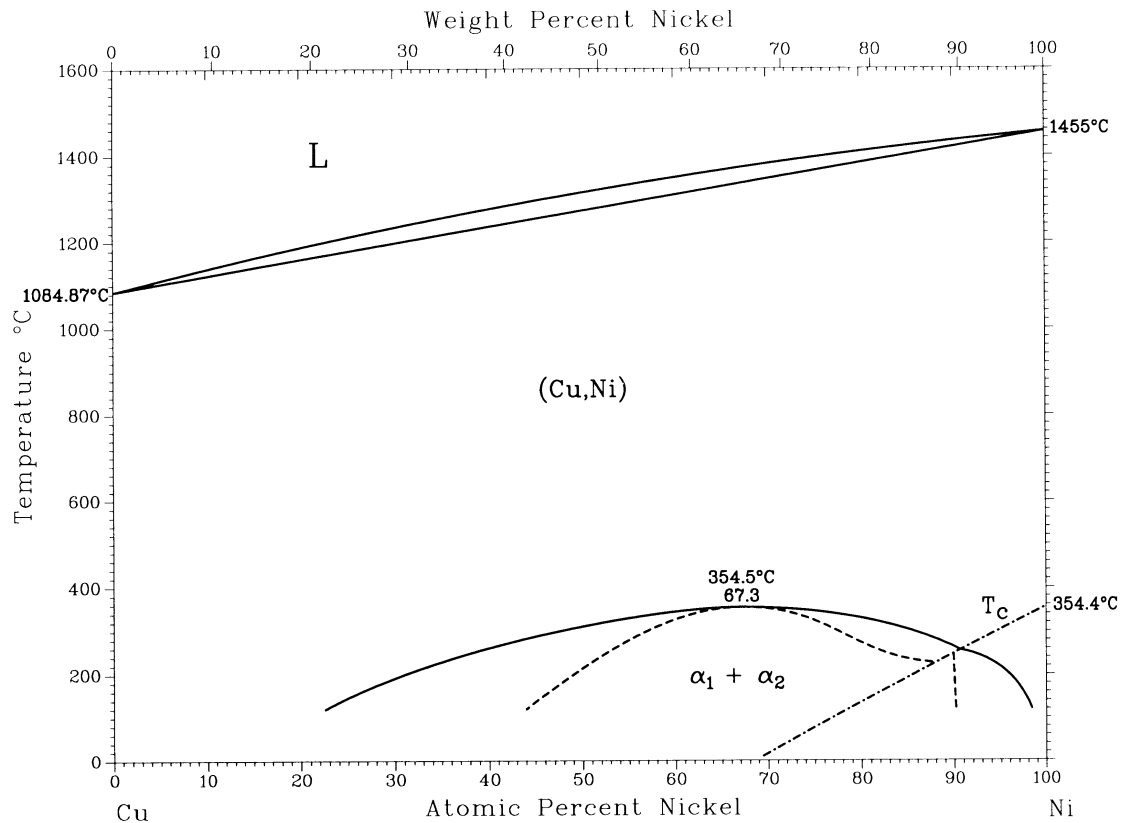


Figure II.2 Cu-Ni phase diagram [1]

II.1.3 Ag-Cu system

The Ag-Cu phase diagram is shown in Figure II.3 [1]. There is a miscibility gap in this system. Both elements form a FCC structure.

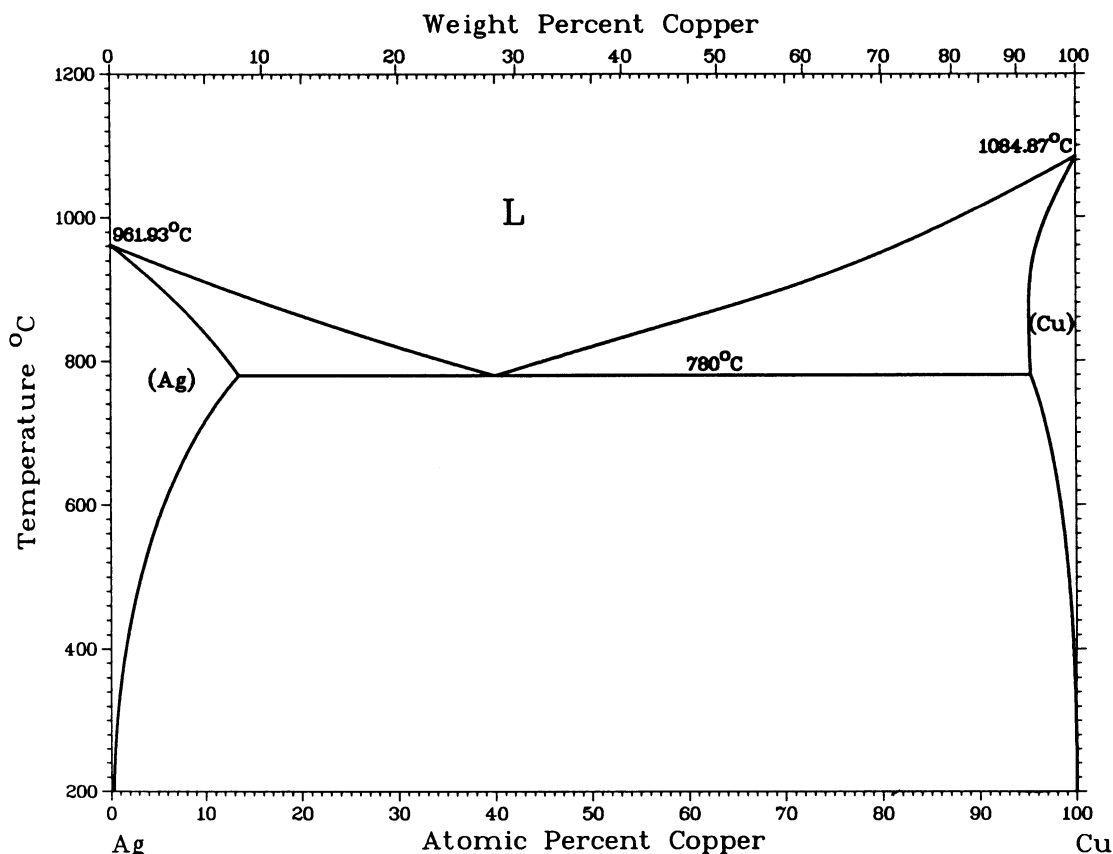


Figure II.3 Ag-Cu phase diagram [1]

II.2 SAMPLE PREPARATION AND HEAT TREATMENTS

Our samples were prepared by magnetron sputtering (Si -Ge and Cu-Ag) except for the Cu-Ni which were evaporated in-situ under ultra high vacuum.

Sputter deposition is a rapid, fairly inexpensive process, which produces dense films, often with near-bulk qualities. In the sputtering process a plasma discharge is maintained above the targets, which are sputtered onto SiO₂ substrate by Ar⁺ ion bombardment ($P = 7 \times 10^{-3}$ mbar). Our Si-Ge multilayers (5-120 nm) and Cu (21 nm)-Ag (12 nm) thin film samples were prepared from elemental targets. Thicknesses are measured by a quartz crystal monitor. Figure II.4 shows the sputtering system designed and built in our laboratory (Department of Solid States Physics, University of Debrecen) [3]. This system can be used for deposition of various metals, semi conductors, multilayered structures and alloys. The deposition chamber (of 400 mm diameter and 300 mm height) is connected to an ultra-high vacuum system pumped by a diffusion pump. Pressure of $1-5 \times 10^{-7}$ mbar is routinely obtained with liquid nitrogen trap. The sputtering chamber contains two magnetrons with shutters, instrumentation feedthroughs, viewing port, quartz crystal monitor, associated electric leads, gas management, ferrofluidics rotary feedthroughs and vacuum gauges. The magnetrons are two identical commercially available 5 cm diameter planar sources. They are positioned in the bottom plate of the stainless-steel vacuum chamber. The pneumatically driven substrate holder equipped with an option of heating the substrates during the motion is placed on the top plate of the sputtering chamber. To produce multilayers the substrates are translated between the beams from the sources and

the motion of substrate holder and the shutters of magnetrons is synchronised and controlled by computer. This system makes it possible to control the deposition time for each layer with 0.1 s. In order to decrease the interfacial intermixing between the layers, a delay of 1 s between the closing of one shutter and the opening of the other one is employed.

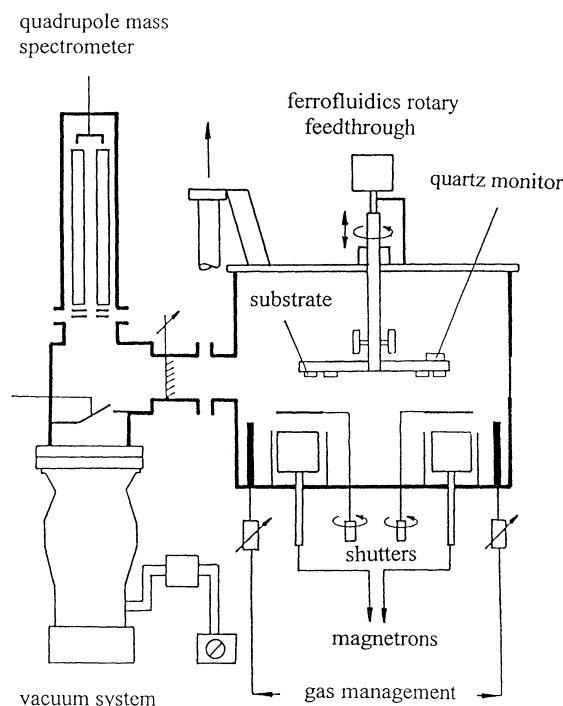


Figure II.4 Scheme of the magnetron sputtering equipment.

The characteristics of Si-Ge multilayers prepared for RBS and Auger analysis are a little bit different. In the first case the modulation lengths are between 10 and 40 nm and the total thickness is changed between 55 et 220 nm. For the second technique the modulation length are between 10 et 20 nm and the total thickness is changed between 60 and 120 nm. In both cases the thickness of the Si and Ge layers is practically equivalent.

The structure of the multilayers (amorphous for Si-Ge) and the thin films was controlled by transmission electron microscopy (Jeol 2000 FX-II). In the case of the Cu-Ag system the grain size of the Cu film, determined before and after heat treatment, was about 20 nm.

The Si-Ge multilayers were heat treated in high purity argon atmosphere (99.999%) at 683 K (RBS experiment) and 680 K (Auger experiment), *i.e.* below the re-crystallisation temperatures of Ge (700 K) and Si (900 K) [4]. The temperature was measured by a NiCr-Ni thermocouple.

Nickel dissolution into monocrystalline Cu(111) as well as silver grain-boundary diffusion in nanostructured Cu were studied *in-situ* in high vacuum in the traditional Auger equipment.

A Cu(111) single crystal was cleaned *in-situ* prior to any nickel deposition by repeated cycles of argon ion bombardment and thermal annealing at 400°C until no impurity could be detected. The Ni/Cu (111) sample was prepared *in-situ* by vapour deposition of Ni onto the Cu(111) substrate by heating a nickel wire. LEED observations were performed to confirm that epitaxial Ni layers deposited onto Cu(111) and the calibration of the as-deposited nickel quantities (3, 6, 14 eq-ML) was carried out in the same way as described in [5].

II.3 ANALYTICAL TECHNIQUES

II.3.1 Small Angle X-Ray Diffraction

II.3.1.1 GENERAL DESCRIPTION OF THE METHOD

X-ray diffractometry is a powerful, widely used technique for characterisation of multilayers. It is non-destructive and provides structural information on atomic scale. The X-ray diffraction patterns are commonly divided into small angle ($\leq 15^\circ$) and high angle ($\geq 15^\circ$) regions. At small angle the length scale is greater than the lattice spacing of the constituent layers, so the scattering of X-ray can be considered as arising from the chemical modulation of the structure and is practically independent of the particular atomic structure (and that is why amorphous multilayers can also be characterised with the help of this technique). A good quality of multilayer with a modulation length of Λ can provide many orders of intense and sharp Bragg-reflections at positions described by the modified Bragg-formula [6]:

$$\sin^2 \Theta = \left[\frac{n\lambda}{2\Lambda} \right]^2 + 2\delta, \quad (\text{II.1})$$

where Θ is the angle of the peak position, n is the order of reflection, λ is the radiation wavelength, and $1-\delta$ is the real part of the average index of reflection of the superlattice. By fitting a straight line to the $\sin^2 \Theta$ versus n^2 function the Λ and the index of reflection of the superlattice can be determined. The intensity of the small angle Bragg-peaks is strongly influenced by the sharpness of the interface. This behaviour can be used to control interdiffusion in multilayers.

II.3.2 Auger Electron Spectroscopy

In the following paragraph the Auger effect is summarised briefly (a detailed description of the technique is given in reference [7]) and the used apparatus is described.

II.3.2.1 GENERAL DESCRIPTION OF THE METHOD

The sample is irradiated by a focused monoenergetic electron beam (1-10 keV) (Figure II.5). These electrons undertake several types of perturbations. In elastic collisions the incident electrons undertake an angular deflection but conserve their initial energy. Individual inelastic collisions cause the ionisation of atoms. The incident electron loses an energy of ΔE , which is higher than that of the electron level E_1 with which it interacted. The amount of energy ($\Delta E - E_1$) is communicated with a reemitted secondary electron. In collective inelastic collisions an incident electron transmits a part of the energy to the electron gas of metals. The Auger effect is the result of the following process: after ionisation the hole of the internal level (E_1) is filled in by an electron of a more external level (E_2). Two relaxation modes are possible: i) emission of an X photon with an energy $h\nu = E_1 - E_2$ or ii) a transfer of this energy to an electron of a more external level (E_3), which is reemitted. Therefore, the kinetic energy of an Auger electron is characteristic of three electron levels of the element: $E = E_1 - E_2 - E_3$ and it makes possible to identify the emitting atom [8]. The Auger spectroscopy is a surface analysis technique, since most of the Auger

transitions are in between 40 and 1000 eV: the mean free path of these electrons varies from 2 to 10 monoatomic layers [9].

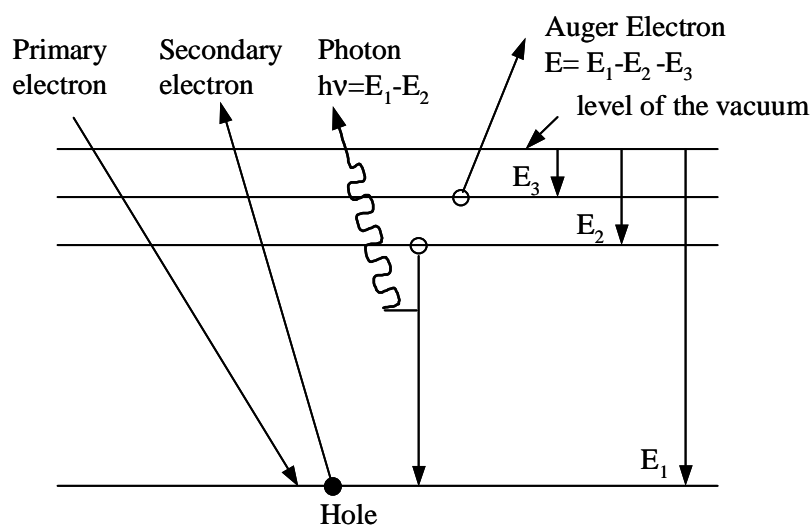


Figure II.5 Schematic illustration of the emission of Auger electron

II.3.2. AUGER DEPTH PROFILING

This equipment was used to determine experimentally the interdiffusion profiles in the Si-Ge multilayers. The profiles were measured in the following conditions [10]: ion energy 0.8 keV; angle of incidence (with respect to the surface normal) 80°; the specimen was rotated during ion sputtering. The sputtering rate of silicon and germanium using these sputtering conditions are the same [11] and thus the sputtering time can be readily transformed to sputter depth. For Auger analysis the following Auger peaks have been recorded: Ge 52 eV and Si 92 eV. The small Ge peak of 89 eV overlaps with the measured Si peak thus the latter was corrected by assuming that the alloying (mixing) of Ge and Si does not influence the peak shapes. The concentration was calculated by comparing the corrected Si peak with that measured on pure silicon substrate; correction for backscattering was made [11]. Because of the ion sputtering induced alterations, the measured depth profile is a distorted version of the original concentration distribution. A recently developed method was used to calculate the original concentration distribution from the measured depth profile [11,12]. In this method, it is supposed that the majority of the ion-induced alteration is due to ballistic mixing (which assumption is satisfied for this case, since the other important distorting process the surface roughening results in less than 1 nm rms roughness using the earlier sputtering parameters [13]), which is properly described by TRIM simulation [12,14]. The method takes also into account the intrinsic interface roughness or waviness.

II.3.2. TRADITIONAL AUGER APPARATUS

This apparatus was used for studying Ni dissolution into monocrystalline (111) copper and silver grain-boundary diffusion in nanostructured copper films. The equipment contains a conventional UHV chamber ($P < 1.10^{-9}$ torr) equipped with a three-gird LEED optics, an ion gun and a cylindrical mirror analyser (CMA). The gun operated with an electron beam of 2 keV and 60 μ A. A 4eV modulation tension was used to obtain the

derivative spectrum $dN(E)/dE$. The sample was fixed on a heater (carbon furnace encapsulated in a boron nitride ceramic), which presents 5 degrees of freedom (X, Y, Z and two rotational movements). This heater is monitored by an Eurotherm regulator (902P) and the temperature controlled by a Pt-PtRh thermocouple fixed on the surface of the sample. In the present work the surface concentrations of silver and copper were monitored by following the behavior of the 356 eV silver Auger peak and the 60 and 920 eV copper peaks as a function of annealing time. The peak heights were obtained by the usual procedure of measuring the difference of intensity from the most negative point (from where the kinetic energy is measured) to the most positive point on each peak of the derivative spectrum.

Before heat treatment, a survey spectrum of the samples was recorded to check the cleanness of surface. Since oxygen and carbon contamination were observed systematically, a rather low Ar^+ sputtering (ions being accelerated to 2 keV with current densities of $70 \mu A cm^{-2}$) of the surface was applied.

In the case of the study of Ni dissolution into copper, during annealing of the sample, Auger peak -to-peak heights variations of Cu(920eV) and Ni(848eV) versus time were recorded. The dissolution kinetics were measured at different temperatures: 635-721 K. There is an overlapping between the Ni(848eV) and Cu(849eV) Auger transitions, and thus a similar method was used than for the Si-Ge system.

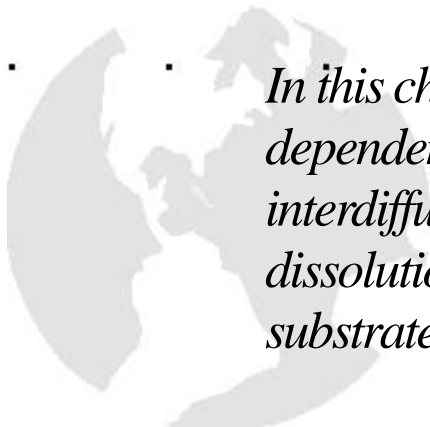
In the case of Cu-Ag system the surface concentrations of silver and copper were monitored by following the behaviour of the 356 eV silver Auger peak and the 60 and 920 eV copper peaks as a function of annealing time. The study of silver grain -boundary diffusion was made at 393-428 K.

REFERENCES

- 1 T.B. Massalski, Binary Alloys Phase Diagrams, *The materials Soc. Second Edition* (1992)
- 2 W. Wagner, R. Poerschke and A. Axmann, *Phys. Rev. B*, **21**, 3087 (1980)
- 3 D.L. Beke, G.A. Langer, M. Kiss-Varga, A. Dudas, P. Nemes, L. Daróczi, Gy. Kerekes, Z. Erdélyi, *Vacuum*, 1998, **50**, No. 3-4, 373-383
- 4 E.P. Donovan, F. Spaepen, D. Turnbull, J.M. Poate, D.C. Jacobson, *J. Appl. Phys.*, **57**, 1795 (1985)
- 5 Zs. Tôkei, D.L. Beke, J. Bernardini and A. Rolland, *Scripta Materialia*, **39**, 1127 (1998)
- 6 A.L. Greer and F. Speapen, in *Synthetic Modulated Structures*, edited by L. Chang and B.C. Giessen, Academic Press, New York (1986)
- 7 H.E. Bishop, in *Methods of Surface Analysis*, edited by J.M. Walls, Cambridge University Press, Cambridge (1989)
- 8 L.E. Davis, N.C. MacDonald, P.W. Plamberg, G.E. Riach and R.E. Weber, *Handbook of Auger Electron Spectroscopy, Second edition, Physical Electronics Industries* (1976)
- 9 M. P. Seah and W. A. Dench, *Surface and Interface analysis*, **1**, No. 1, 2 (1979)
- 10 A. Barna and M. Menyhard, *Phys. Status Solidi A*, **145**, 263 (1994)
- 11 M. Menyhard, A. Barna, J.P. Biersack, K. Järrendhal and J.-E. Sundgren, *J. Vac. Sci. Technol. A*, **13**, 1999 (1995)
- 12 M. Menyhard, *Surf. Interface Anal.*, **26**, 1001 (1998)
- 13 A. Barna, B. Pécz and M. Menyhard, *Ultramicroscopy*, **70**, 161 (1998)
- 14 J.P. Biersack, *Nucl. Instrum. Methods Phys. Res. B*, **27**, 21 (1987)

Chapter III

Nonlinear Diffusion



In this chapter the effect of concentration dependent diffusion coefficient on interdiffusion in multilayers and on dissolution of an ultra-thin film into a bulk substrate will be investigated

Chapter III

NONLINEAR DIFFUSION

III. VALIDITY OF THE CONTINUUM APPROXIMATION IN MULTILAYERS

As we have seen, the continuum model becomes imprecise on atomic scales. For example Cook *et al.* [1,2] showed that the continuum and discrete approximations give the same results only if the wavelength of the modulation Λ is at least six times longer than the interatomic distance, d , in the direction of the diffusion ($\Lambda > 6d$) [see paragraph I.1.3.2]. Furthermore, in references [3,4] it was shown that in crystalline materials the continuum description breaks down for concentration fluctuations with $\Lambda < 10d$, where Λ is the wavelength of a sinusoidal concentration profile. Cahn [5] and Yamauchi and Hilliard [6] found the similar range of validity of the continuum approach for intermixing of multilayers. These conclusions, however, are obtained in linear approximation, *i.e.* assuming that the diffusion coefficient is independent of concentration. The treatment of the effects of this type of nonlinearity is very complicated even if one neglects the stress effects [see paragraph I.1.3.5]. As is written in paragraph I.1.3.5, Tsakalakos [7,8] and Menon and de Fontaine [9] tried to treat this problem analytically, or by solving the continuum equations numerically considering a concentration dependence no stronger than a quadratic one in the diffusion coefficient, although even in ideal solutions it can be stronger and is better described by an exponential dependence [10].

In this chapter [11,12,13], the problem of the stronger concentration dependence of the diffusion coefficient is investigated in the frame of the continuum and discrete models [see I.1.3.4b) and I.1.3.3b)].

III.1.1 Theory

For the sake of simplicity, we will restrict ourselves to the case of an *ideal* binary solid solution (*i.e.* no gradient energy effects), although both of the models (continuum and discrete) can take into account the gradient energy effect [see Appendix at the end of this chapter]. Moreover, as the discrete model does not contain the Kirkendall and stress effects, the input parameters have to be chosen in such a way that these effects do not intervene and thus the two models can be compared under the same conditions.

III.1.1. CONTINUUM MODE

First of all, it is necessary to include the composition dependence of the diffusion coefficient in the continuum model. Constructing the expression of atomic flux [see I.1.3.1 and I.1.3.4b)], no restriction has been made related to the composition dependence of the diffusion coefficient, therefore, we can assume that it is exponential:

$$\ln D = mc + \ln D(0) . \quad (\text{III.1})$$

Here c is the atomic fraction of one of the two components, $D(0)$ the diffusion coefficient for $c = 0$. Note that coefficient m can be large, because in the pure constituents the values

of D can be considerably different [10].¹ Furthermore, the form of the activation energies in the Martin model [see I.1.3.3b)] also suggest that equation (III.1) gives a good description.

Since the discrete model is not able to describe the Kirkendall shift and the pressure effects, we have to assume that both of the intrinsic diffusivities and the atomic volumes are equal to each other:

$$\begin{aligned} D_1 = D_2 = D \quad \text{and} \\ \Omega_1 = \Omega_2 = \Omega . \end{aligned} \quad (\text{III.2})$$

Therefore, there is no net transport of volume, *i.e.* the absolute values of the atomic fluxes of the two components are equal to each other. Note that under these conditions, the atomic flux is given by [see equation (III.39)]:

$$j_i = -D(c)\text{grad}c/\Omega . \quad (\text{III.3})$$

The input parameters in the calculations are close to the Mo -V system. This is a nearly ideal system, and we assumed that $V = 0$. Thus, since the thermodynamic factor is unity [$\Theta = 1$, see equation (III.47)], the intrinsic diffusion coefficients are identical to the tracer diffusion coefficients [see equation (I.19) ($f = 1$)]. There are no tracer diffusion data in the literature for either Mo or V diffusion as a function of the concentration in the Mo-V system. Thus, fixing the two ends of equation (III.1), diffusion data for the V diffusion in pure Mo and V were used [10]: $D_V(c_V = 0) = 9.8 \times 10^{-28} \text{ m}^2/\text{s}$ and $D_V(c_V = 1) = 1.8 \times 10^{-20} \text{ m}^2/\text{s}$ at $T = 1053 \text{ K}$. These values determine the experimental value of m in equation (III.1): $m_{exp} = 16.7$, but as we will see later, m can be used as a parameter as well. Note that the ratio of the impurity diffusion of V in Mo and Mo self diffusion coefficient at the temperature for which our calculation was carried out is $D_V(c_V = 0)/D_{Mo}(c_V = 0) = 2$ [10]. Furthermore, the atomic volume of V was taken as Ω ($8.36 \times 10^{-6} \text{ m}^3/\text{mol}$) in the calculations.

A finite difference method was used to calculate the evolution of the concentration distribution. We started from an initially square composition profile and the only spatial coordinate axis (one-dimension) was parallel to the direction of diffusion. Since the composition profile is periodical (multilayer) and symmetrical to the middle of the one of the monolayers during the process, it is enough to consider a half -bilayer during the numerical calculations. A calculation cycle can be divided onto two subsequent steps: first the atomic fluxes of each element are calculated from the equation (III.3), then the new concentration distribution is obtained from the difference form of (I.70), and using it, the new value of the diffusion coefficient is calculated from equation (III.1). In the above calculations, the values of the compositions and diffusion coefficient are defined at the midpoint of each slab, and accordingly, $\text{grad} c$ is calculated between two neighbouring slabs, while in the expression of the atomic flux [equation (III.3)], D is calculated as the arithmetic mean of the two values.

¹ In this way, the system of equations (I.68), (I.69), (I.70) and (III.39) can be used to calculate the time evolution of the concentration distribution taking into account all the effects mentioned (Kirkendall, stress, gradient energy, concentration dependence of the diffusion coefficient).

III.1.1. DISCRETE MODE

A numerical method was used to solve the set of coupled difference equations (I.41) to obtain the time dependence of compositions in different layers. Since the composition profile is periodical and symmetrical like in the continuum case, we can use a similar half-bilayer system (consisting of N atomic planes). The boundary conditions were established in the following way: at each calculation cycle, the concentration in the atomic layers on both sides of the symmetry plane were taken to be equal (*e.g.* $c_N = c_{N+1}$) to each other. We note that the modulation length Λ is determined implicitly by the lattice spacing d in the direction of diffusion and N ($\Lambda = 2Nd$).

Since, as was mentioned, we want to compare the continuum and discrete models, we have to choose a consistent set of input parameters. It is easy to show that if $V = 0$, $E_{i,i+1} = E_{i+1,i}$ and $\Gamma_{i,i+1} = \Gamma_{i+1,i} = \Gamma$. Thus, for a bcc or fcc structure [see equation (I.15)]:

$$\Gamma = D/d^2 . \quad (\text{III.4})$$

Furthermore, taking a bcc lattice with a (100) direction of diffusion, *i.e.* $z_v = 4$, $z_l = 0$, we have [see equations (I.43) and (I.44)]:

$$\begin{aligned} \Gamma &= v \exp(-E/k_B T) \\ &= v \exp(-Q/k_B T) \\ &\quad \times \exp[-2(V_{AA} - V_{BB})(c_{i-1} + c_i + c_{i+1} + c_{i+2})] , \end{aligned} \quad (\text{III.5})$$

where $Q = E^0 + 4(V_{AA} + 3V_{BB})$. According to equation (III.1), for $c = 1$:

$$m = \ln[D(1)/D(0)] \quad (\text{III.6})$$

and thus

$$D = D_0 \exp(-Q_0/k_B T) \exp(mc) . \quad (\text{III.7})$$

Here D_0 and Q_0 are independent of concentration and, for example, Q_0 corresponds to the activation energy of V self-diffusion. Comparing equations (III.4), (III.5), (III.6) and (III.7):

$$D_0 = vd^2, \quad Q = Q_0 \quad (\text{III.8})$$

and

$$\begin{aligned} m = \ln[D(1)/D(0)] &= 2(V_{AA} - V_{BB})(c_{i-1} + c_i + c_{i+1} + c_{i-1} + c_{i+2})/ck_B T \\ &= 8(V_{AA} - V_{BB})/k_B T . \end{aligned} \quad (\text{III.9})$$

Thus all the input parameters for the discrete model are fixed. It is worth mentioning, that equation (III.9) corresponds to the result which can be obtained for the linear concentration dependence of activation energy from a continuum, mean field approximation in an ideal solid solution, *i.e.* equation (III.9) establishes the condition that the concentrati

dependence of the activation energy should be identical in the two models if the concentration distribution is homogeneous ($c_{i-1} = c_i = c_{i+1} = c_{i+2} = c$).

A calculation cycle can be divided into two subsequent steps: first the activation barrier and the jump frequency are calculated from equations (I.43) and (I.44), then the new configuration of the composition from equation (I.41).

III.1.1. CALCULATION OF INTENSITIES OF SMALL ANGLE X-RAY DIFFRACTION

In both cases, $\ln(I_n/I_0)$ vs. t curves for the different orders of the small angle X-ray diffractions (SAXRD) were always calculated from the $c(x,t)$ distributions in the following way (I_n is the n th order and I_0 the initial height of the first order SAXRD peak). The Fourier transform of the electron density ρ was made to obtain the amplitude of the wave scattered by the electrons of the atoms of the specimen $A(\vec{s})$ (scattering amplitude; \vec{s} is the scattering vector). For example, for a multilayer it is given by [14]:

$$\frac{A(s)}{A_e} = \frac{\sin(\pi s N \Lambda)}{\sin(\pi s \Lambda)} \exp[\pi i(N-1)s\Lambda] \int_0^\Lambda \rho(z) \exp(-2\pi i s z) dz, \quad (\text{III.10})$$

where s is the component of \vec{s} in the z direction (z is the direction of the modulation, i.e. $s_x = s_y = 0$, $s_z = s$), N the number of bilayers composing the multilayer, Λ the modulation length, A_e the scattering amplitude of an electron and i is the imaginary unity. The square of this quantity vs. s gives the normalized (A_e) small angle X-ray diffraction spectrum.

A multilayer can be considered as a one-dimensional superlattice with Λ lattice parameter, and the basis is one bilayer. The absolute value of the reciprocal-lattice vector (\vec{g}) of this superlattice is $1/\Lambda$. Thus, since $s = n/\Lambda$ (according to the Bragg equation), from equation (III.10) the square of the n th order normalized scattering amplitude, i.e. the n th order normalized intensity is:

$$\ln \frac{I_n}{I_0} = \ln \left[\frac{A(n/\Lambda, t)}{A(1/\Lambda, t=0)} \right]^2. \quad (\text{III.11})$$

III.1.2 Results and Discussion

First, in order to check our calculation procedure, the programs were run with a concentration independent diffusion coefficient, i.e. with $m = 0$. Figure III.1 shows that, as expected, the curves obtained from the continuum as well as discrete model coincide with each other for $\Lambda > 8d$ ($d = 0.3$ nm).

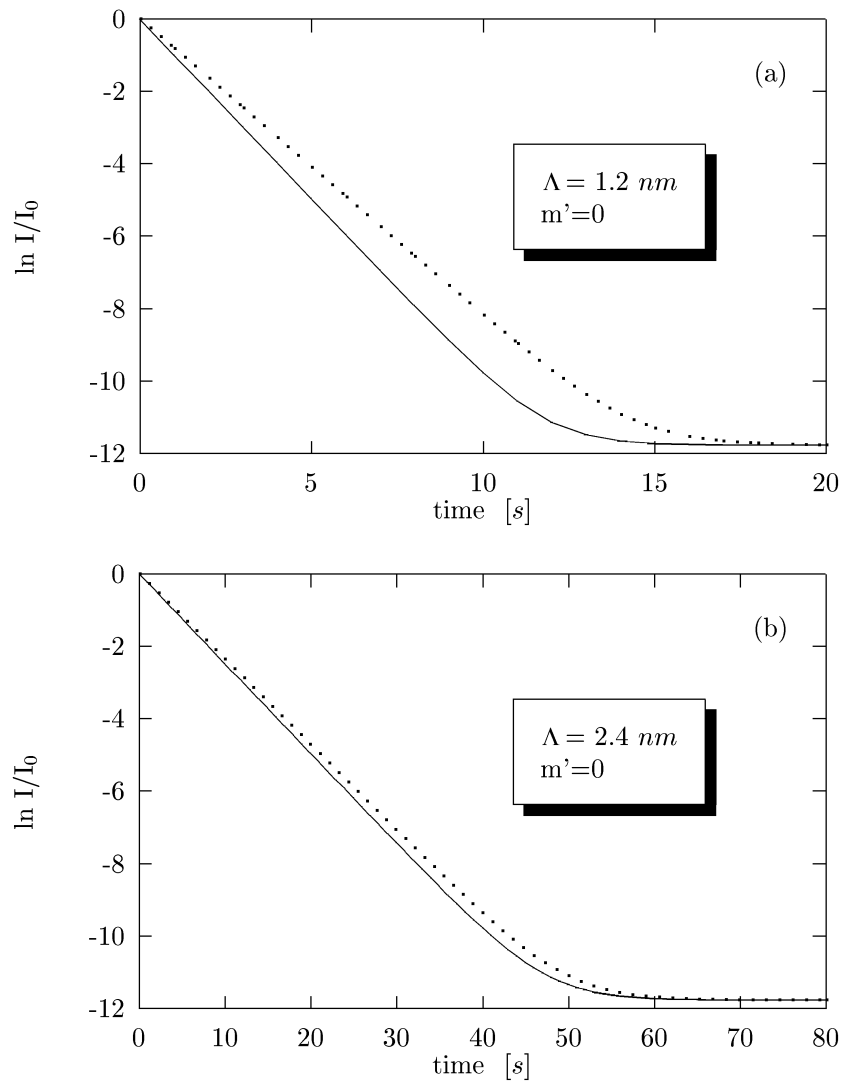


Figure III.1 Comparison of the decay of the height of the first order X-ray peaks (a) for $\Lambda = 4 = 1.2 \text{ nm}$ and (b) for $\Lambda = 8 = 2.4 \text{ nm}$ for continuum (solid line) and discrete (dotted line) models when the diffusion coefficient is concentration independent. Note that in (b) the slopes of the two curves differ by less than 5%.

For the simulation of the effect of the strong concentration dependence of D , the value of m , and accordingly the value of

$$m' = m \log e \quad (\text{III.12})$$

was changed ($0 \leq m' \leq 7.3$, m' is introduced in order to make the comparison easier with experimental data usually plotted on $\log D$ vs. $1/T$, or $\log D$ vs. c). Figure III.2 illustrates the range of the input parameters for D used in the calculations.

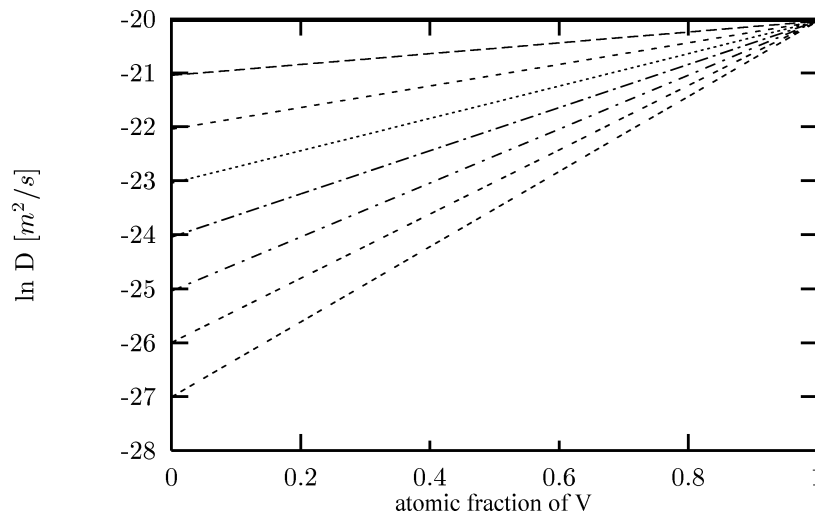


Figure III.2 The assumed concentration dependencies of the diffusion coefficients in the calculation s ; each straight line corresponds to a given m or m' value [see equations (III.1) and (III.12)]

Figure III.3 contains the concentration distributions at different times for the discrete and continuum models as well, when D strongly depends on the concentration, *i.e.* $m' = 7.3$. There are five main interesting features of the curves:

- (i) In both cases, due to the fast diffusion in vanadium, there is a fast homogenisation on the vanadium side; here the concentration profile is practically flat at each time and only the amplitude of the composition modulation decreases gradually.
- (ii) There is a shift of the boundary between the pure Mo and the V(Mo) alloy towards the Mo side. The boundary remains sharp although its height gradually decreases.
- (iii) The shape of the boundary is different in the two models: in the continuum model (Figure III.3b) it remains almost as sharp as it was at the beginning (the small sharp break on the curves at the first three times can be an artefact of the finite difference calculation). On the other hand in the discrete model a layer-by-layer dissolution of Mo can be observed (Figure III.3a). For example on the curve a $t = 5 \times 10^3$ s the sharp break illustrates that from the original (atomic flat) interface the first atomic layer partially dissolved. This dissolution continues until almost the whole layer dissolves (see the curve at the next time), and the dissolution of the new layer starts (curve a $t = 4 \times 10^4$ s). The “interface” can be also two or three atomic layers thick: the dissolution of the next layer can start before the previous one has been finished (curves at $t = 7.5 \times 10^4$ and $t = 2.5 \times 10^5$ s). This plane-by-plane dissolution mechanism is also reflected in Figure III.4, where the concentrations in different lattice planes are plotted as a function of time. This layer-by-layer dissolution behaviour is also reflected on the curve shown in Figure III.5, where, in order to emphasise the effect of above layer-by-layer dissolution, the *derivative* of the $\ln I/I_0$ vs. t function is also plotted. It can be seen that around points where a new atomic layer starts to dissolve there is a small enhancement in the homogenisation process. The minima (indicated by arrows) shown in Figure III.5b correspond to the moment when the concentration profile changes its shape from convex to concave one (on the Mo side). The last wide minimum (not indicated by arrow) indicates the beginning of the acceleration due to the consumption of the Mo layer.
- (iv) When the boundary (its height is still about 0.4 - 0.5) reaches the centre of the Mo layer the homogenisation process suddenly considerably accelerates because of the consumption of the Mo layer (which has a very low diffusivity and thus serves as a diffusion barrier) in both models. It can be seen in Figure III.6 that there is indeed

- an acceleration of the process and the slope of the $\ln I/I_0$ vs. t function visibly increases. Obviously the beginning of this effect is Λ dependent. Note that in this plots the small effects illustrated in Figure III.5 cannot be seen. Thus while the sudden acceleration caused by the elimination of the last slab of the slow diffusing component is large enough to be experimentally well detected, probably the detection of effect of the layer by layer dissolution will be a more delicate problem.
- (v) Although in the case shown in Figure III.6a $\Lambda = 16d$, there is a definite difference between the rates of the processes in the two models: the continuum model gives a faster homogenisation. This is also illustrated in Figure III.6b, where it can be seen that the validity limit of the continuum model is shifted by about one order of magnitude as compared to the case of the concentration independent (linear) problem. Figure III.7 summarises the results of our calculations carried out for different m' values by giving the values of the critical Λ_c (above which the continuum model is valid) as the function of the exponent $m' = m \lg e$. It can be seen that for the range covered here, the validity limit of the continuum model is shifted by about one order of magnitude. This means that for modulation lengths typical in experiments for *e.g.* in Mo-V system, the continuum approach cannot be used.

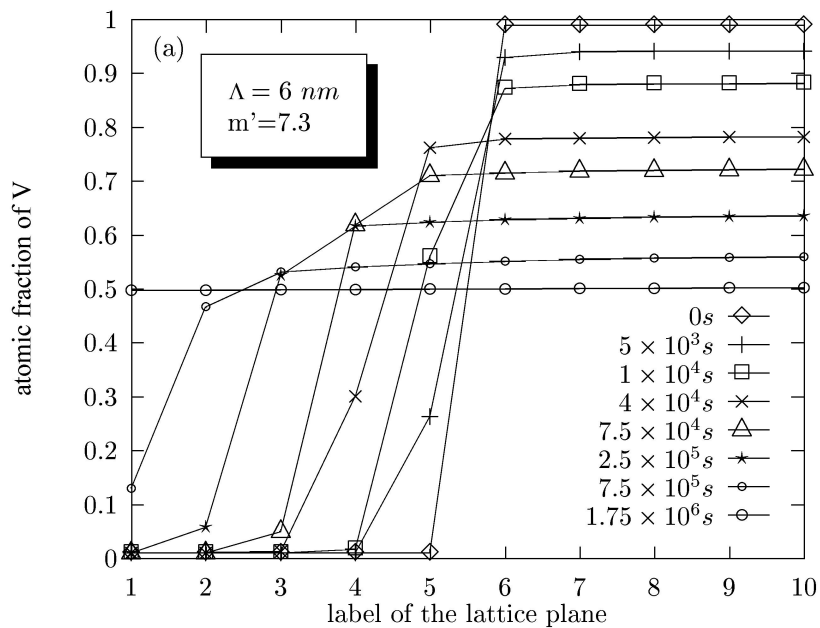


Figure III.3 Concentration distributions at different times for (a) the discrete (the solid lines drawn only to guide the eye) and (b) continuum models at $T = 1053$ K and for $\Lambda = 6$ nm and $m' = 7.3$ (see also the text)

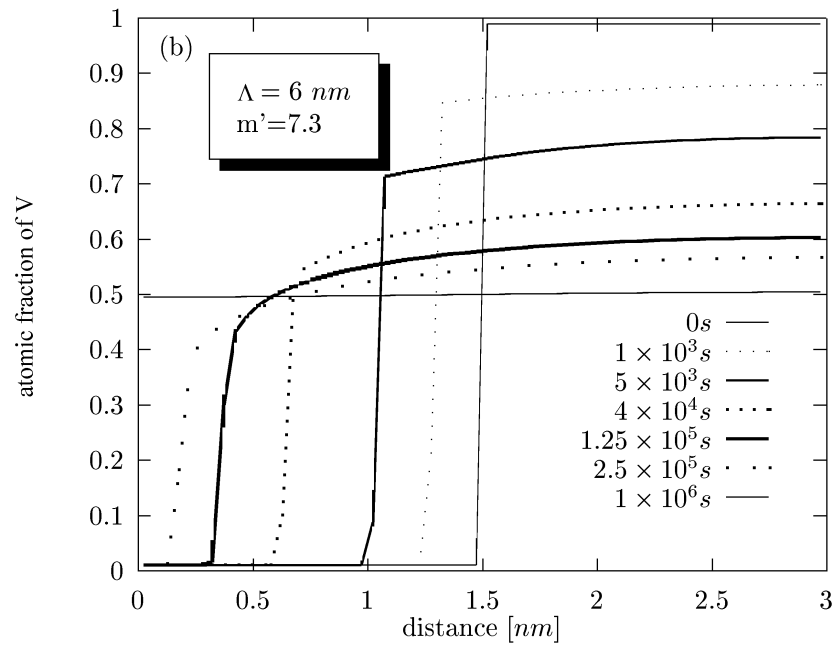


Figure III.3

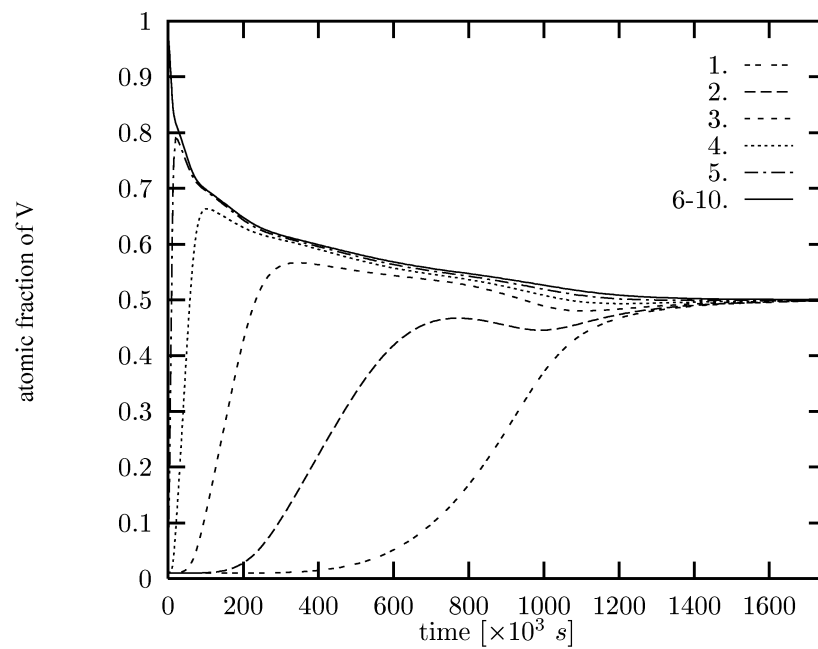


Figure III.4 Concentrations in different atomic planes as a function of time

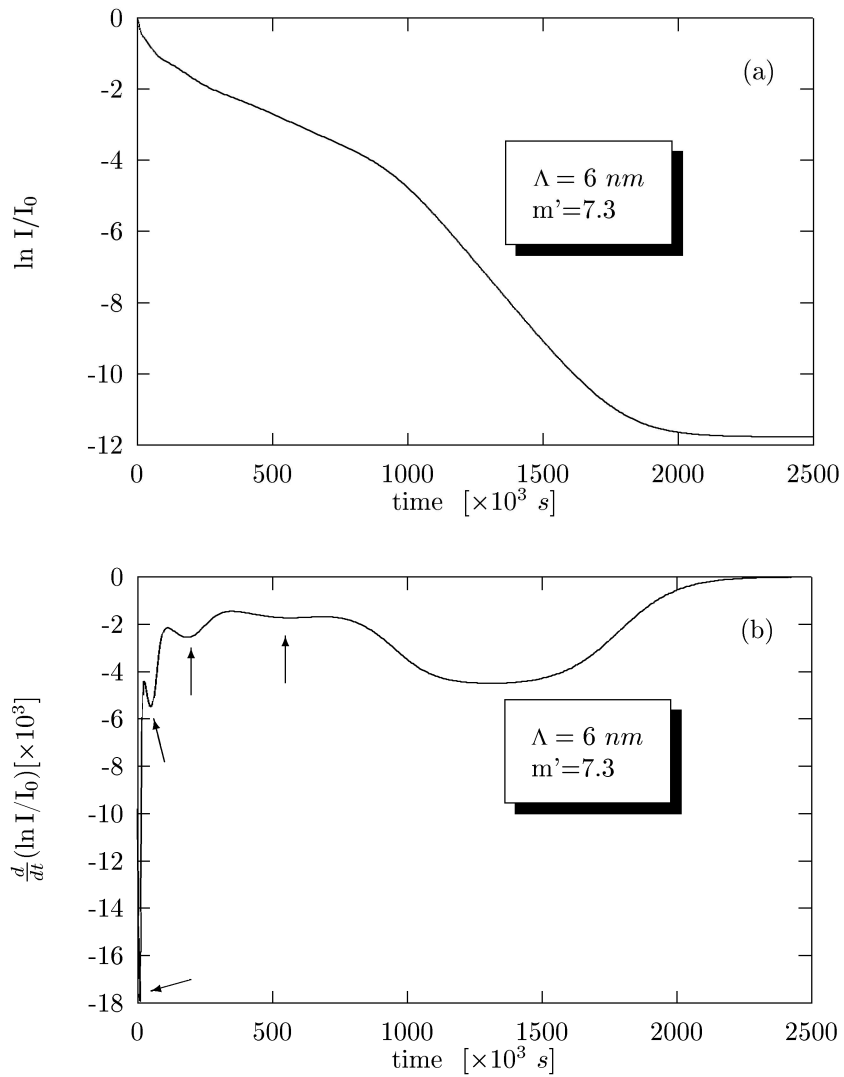
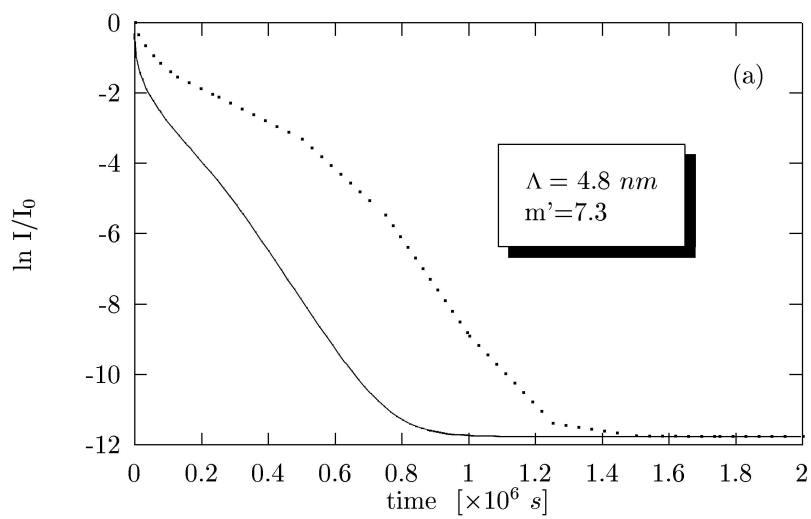


Figure III.5 Usual decay of (a) the height of the first order X-ray peak and (b) its time derivate for the discrete model, obtained from the concentration curves shown in Figure III.3a



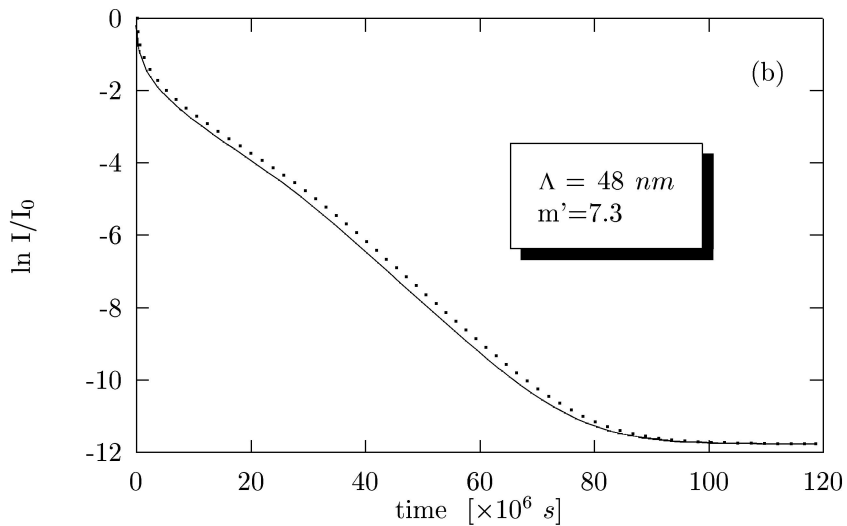


Figure III.6 Comparison of the decay of the height of the first order X -ray peaks for $\Lambda = 16d = 4.8 \text{ nm}$ (a) and for $\Lambda = 160d = 48 \text{ nm}$ (b) for the continuum (solid line) and discrete (dash-short dash line) models when the diffusion coefficient strongly depends on the concentration ($m' = 7.3$).

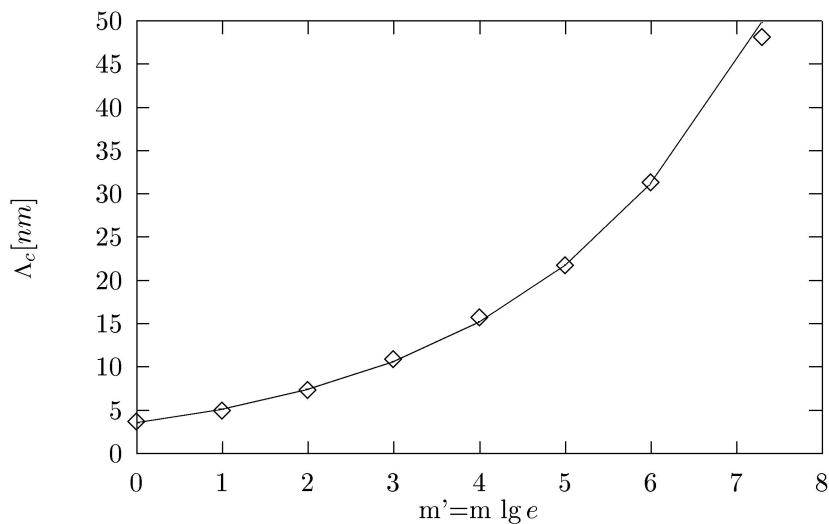


Figure III.7 Values for the critical modulation length, Λ_c , above which the continuum model is valid, as a function of the value of exponent in the concentration dependence of D [$m' = m \lg e$: see also equati (III.1)].

Finally, it is worth investigating the behaviour of the higher order peaks of the sma angle X-ray diffraction spectrum, in order to compare our results to the hypothesis o Menon and de Fontaine [9] [see I.1.3.5b)]. Figure III.8 shows that this statement is valid for both models in our case as well. In this figure $m' = 1$ corresponds to the case investigated by Menon and de Fontaine [9].

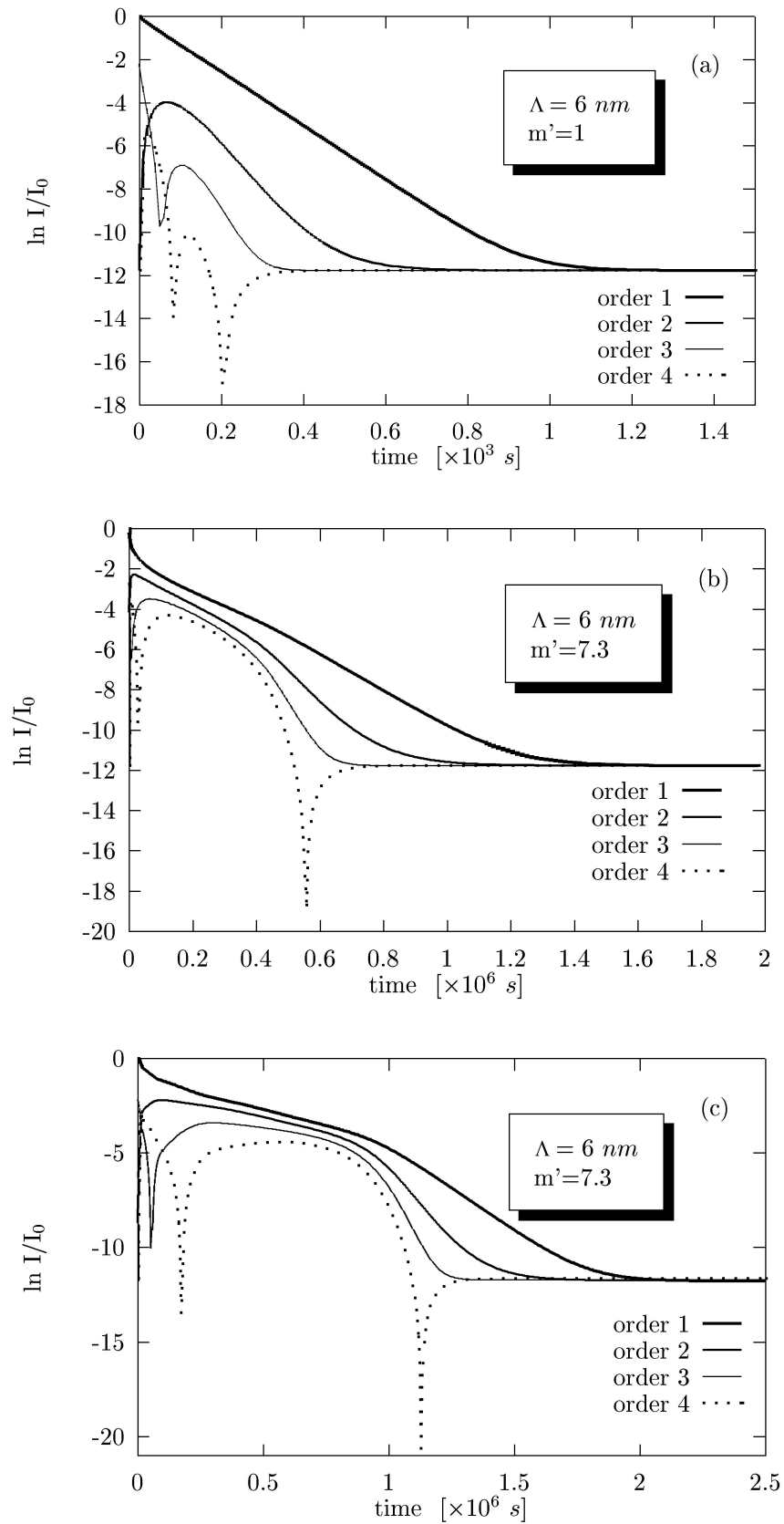


Figure III.8. Decay curves of the height of the higher order X-ray peaks for $T = 1053 \text{ K}$, $\Lambda = 20d$ for the continuum model at $m' = 1$ (a) and $m' = 7.3$ (b) as well as for the discrete model at $m' = 7.3$ (c).

III.1.3 Conclusions

We have shown that in case of strong (exponential) concentration dependence of the interdiffusion coefficient, the large asymmetry is manifested in

- (i) a fast homogenisation on the side where the diffusion is faster, and here the distribution is practically flat and only the amplitude of the composition modulation decreases with time
- (ii) a shift of a sharp boundary between the slow component and the newly formed (homogeneous) alloy; and when the slab of the slow component is used up the homogenisation process is considerably accelerated
- (iii) a difference between the results obtained from the continuum and discrete models: the shape of the moving boundary changes with time in the discrete model and it shows a layer-by-layer dissolution kinetics, while in the continuum model the interface remains atomic sharp
- (iv) a strong change in the range of the validity of the continuum model: this change depends on the strength of the concentration dependence of D , and in many real multilayer systems with typical modulation length of few nanometer, it can break down.

III. CONSEQUENCES OF THE DIFFUSIONAL ASYMMETRY

In this paragraph, experimental results obtained by SAXRD [15], Rutherford backscattering (RBS) [16] and Auger depth profiling (AESDP) [17] on Si-Ge homogenisation will be shown.

III.2.1 Introduction

In accordance with the linear approach, the $\ln I/I_0$ versus t curve ($I = I_I$) should decrease according to [see equation (I.32) and $I \propto A^{1/2}$]

$$\frac{d}{dt} \left[\ln \left(\frac{I}{I_0} \right) \right] = -\frac{8\pi^2}{\Lambda^2} \tilde{D}_\Lambda. \quad (\text{III.13})$$

Thus the decay of the first order normalized intensity is a linear function of time and its slope is proportional to the interdiffusion coefficient. This relation is obtained for sinusoidal modulations, as was mentioned in I.1.3.3a). However, it can also be used for a general periodical composition modulation because it can be described by a Fourier series and the Fourier components develop independently as a function of time. Furthermore, in linear approach, the higher harmonics in that series will decay rapidly, so that after some interdiffusion the fundamental will be the only significant term. That is, the composition modulation will become sinusoidal, only the first order SAXRD intensity will be observed, and equation (III.13) can be used directly [18].

According to recent works, however, frequently there is a significant initial curvature on the $\ln I/I_0$ vs t curve, which is many times explained by structural relaxation and stresses [19]. Nevertheless in the previous paragraph, we could already observe that in case of concentration independent diffusion coefficient the intensity decay function is linear (except for the homogenisation part, see Figure III.1), whereas when D depends on the composition, there is a significant curvature, although there are no stress effects or

structural relaxation. For that reason, in this paragraph a detailed analysis will be given regarding the strong concentration dependence of the diffusion coefficients in amorphous multilayers and its influences on the $\ln I/I_0$ vs t curve which can give another possible explication for the curvature mentioned above. Moreover, direct studies of the concentration distributions by Rutherford backscattering (RBS) and Auger depth profiling (AESDP) will also be shown.

By SAXRD, multilayers with only short modulation length can be investigated. Thus according to the results of the previous paragraph, regarding the simulation of diffusional processes, the discrete model should be used. But, there are no vacancies and stress effects, whereas they can be important from intermixing point of view of. To lift this contradiction, we wanted to choose an amorphous system where the continuum model can be also used. Furthermore, in order to study a pure intermixing, we wanted to choose an ideal or near ideal solid solution system ($V \cong 0$). The Si-Ge system is an ideal candidate for this since it has a complete mutual solubility and they can easily produced in amorphous state. Additionally, these amorphous multilayers are of considerable microelectronic interest [20].

III.2.1. STRUCTURAL RELAXATION AND NONLINEARITY

If the curvature of the $\ln I/I_0 - t$ curves at the beginning is caused by structural relaxation, the interdiffusion coefficient should depend on t [19]:

$$\tilde{D}(t) = D_0 + D_1 e^{-t/\tau}, \quad (\text{III.14})$$

where D_0 , D_1 are constants and τ is the relaxation coefficient. Therefore $\tilde{D}(t)$ is concentration independent. Considering a periodical concentration modulation [$c - c_0 = A(t) \cos(hx)$], from equation (I.30) for $\kappa = 0$:

$$\frac{d}{dt} \ln A(t) = -\tilde{D}(t) h^2, \quad (\text{III.15})$$

i.e.

$$\frac{d}{dt} \left[\ln \left(\frac{I}{I_0} \right) \right] = -2\tilde{D}(t) h^2 = -\frac{8\pi^2}{\Lambda^2} \tilde{D}(t). \quad (\text{III.16})$$

This equation can be integrated, thus the $\ln I/I_0$ versus t function is given by:

$$\ln I/I_0 = -\frac{8\pi^2}{\Lambda^2} \left[D_0 t + \tau D_1 (1 - e^{-t/\tau}) \right]. \quad (\text{III.17})$$

Consequently, in a $\Lambda^2 \ln I/I_0$ versus t plot all intensity decay curves should run together if only structural relaxation was present and caused the upward curvature at their beginnings. As it can be seen in Figure III.9, it is not satisfied.

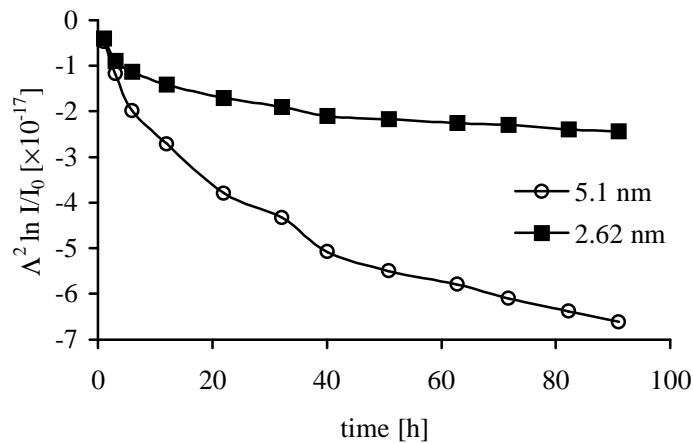


Figure III.9 Experimental $\Lambda^2 \ln I/I_0$ versus t curves for amorphous Si/Ge system ($T = 703\text{K}$) [15]

III.2.2 Direct experimental evidences on the diffusional asymmetry and its consequences

In order to check directly the validity of our theory according to which the diffusion is asymmetric, consequently the interface remains sharp and shifts, we made two experiments being able to uncover the composition distribution of our samples: Rutherford backscattering (RBS) and Auger depth profiling (AESDP). In this paragraph the results of these experiments will be presented.

III.2.2. RUTHERFORD BACKSCATTERING

The RBS analyses were performed using 1 MeV He^+ beam at the 5 MeV Van de Gra accelerator of ATOMKI in Debrecen. The backscattered particles were detected at 165° to the beam direction with a 14 keV energy resolution PIPS detector. The parameters of the measurements were optimised by calculating the depth resolution for Ge and Si at different depths. For these calculations the latest upgrade of DEPTH code, which software is generalised for multilayers, was used [21,22]. The RBS spectra were evaluated and simulated by the RBX computer code [23].

We tried to detect directly the theoretically predicted thickening of the Ge layer. Several high-resolution RBS analysis were done for this reason with a depth resolution of 2 nm for the first Ge layer being at 10-20 nm depth. However, experimental observation of the above effect was not unambiguous. By evaluating and simulating the measured spectra we got the best fit by taking into account the thickening effect [see Figure III.10 (a)-(b)]. According to the simulated layer structures the depth resolution at these experimental conditions was not enough to detect directly the thickening of the Ge layer, as it was just about 10% of the layer thickness.

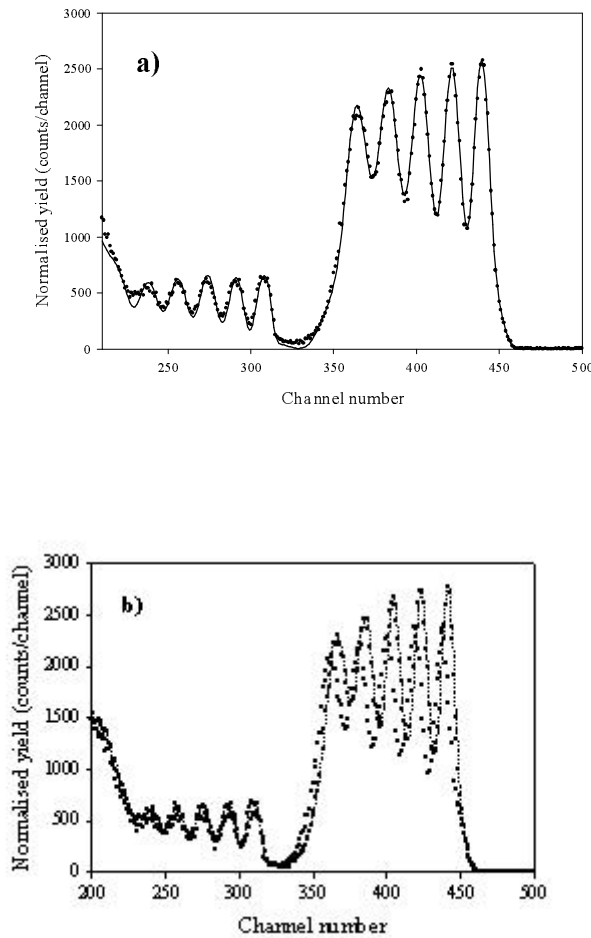


Figure III.10 RBS spectra of a Si/Ge multilayer sample with repeat length of 20 nm: (a) experimental and simulated (solid line) spectra of the as-received sample; (b) as-deposited and annealed sample (683 K, 100 h), simulated (solid line), measured before and after annealing (fill and hollow circle, respectively). [16]

III.2.2. AUGER DEPTH PROFILING

Figure III.11 shows one period of the measured depth profiles for the as-received and annealed (680 K, 100 h) specimens, respectively. It is clear that the structure of specimen changed due to the annealing; the thickness of the silicon layer decreased, and the silicon concentration in the germanium layer increased. On the other hand, no germanium could be observed in the silicon layer. It should be mentioned that silicon was also present in germanium layer of the as-received specimen. This silicon can be attributed to some contamination from the sputtering system.

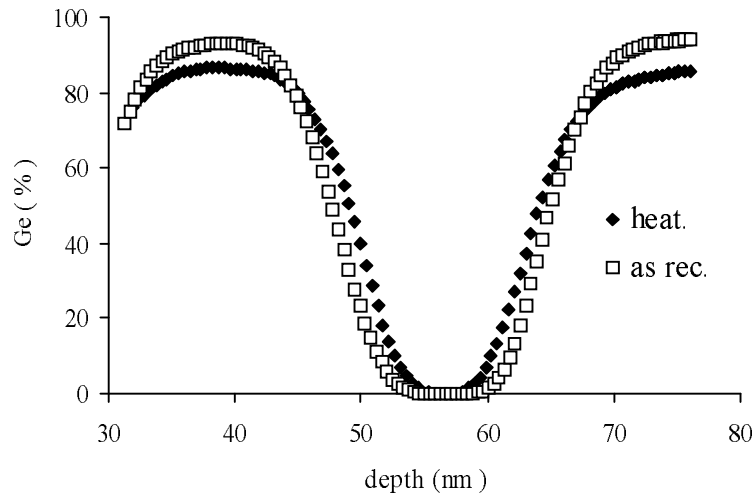


Figure III.11 One period of the measured depth profiles for the as -received and annealed specimens. [17]

In the case of the as-received specimen, the best agreement between the measured and simulated depth profiles was obtained by supposing an original structure of 19 nm Ge(94%)Si(6%) and 17 nm pure Si, and an interface waviness of 1.8 nm amplitude. Applying this method, the thickness of all layers in the specimen (supposing the same waviness) has been determined to be 18.6 ± 0.6 and 17.2 ± 0.5 nm for the Ge(94%)Si(6%) and pure Si layer, respectively. These thicknesses slightly differ from the nominal ones (18 nm Si/ 18 nm Ge).

Figure III.12 shows the measured and simulated depth profiles (assuming the same waviness) for a period of the depth profiles in the case of the heat treated specimen. In this case we have obtained, considering all the layers, the following structure: 21.3 ± 0.7 nm Ge(86%)Si(14%) and 14 ± 0.5 nm pure Si.

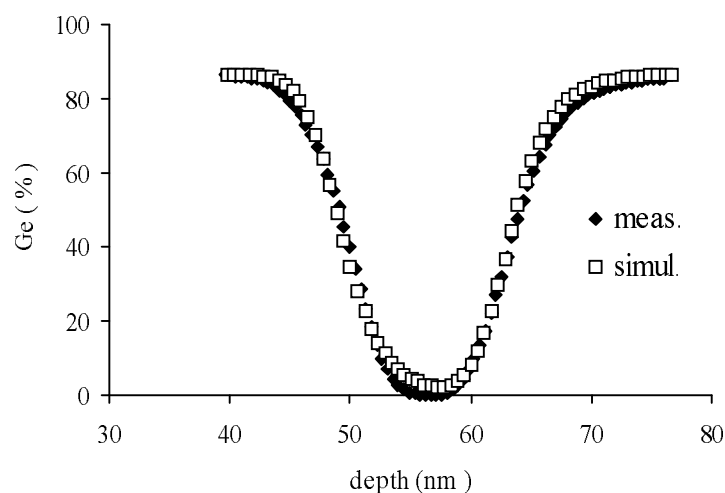


Figure III.12 Measured and simulated depth profiles for the annealed specimen. [17]

The results clearly show that the diffusion is indeed very asymmetric. In accordance with our calculations, the silicon could enter into the germanium layer but the germanium

could not diffuse into the silicon. At the same time, due to the silicon diffusion to germanium, the germanium layer became thicker and the thickness of Si decreased from 17 to 14 nm. It is also clear that during the heat treatment the sharpness of the interface remained the same, which is also in accordance with our calculations. On the other hand, our results clearly indicate that the diffusion coefficient should strongly depend on the concentration and consequently measurements based on the SAXRD of multilayers cannot be interpreted by neglecting nonlinear effects and/or relying, *e.g.*, on the effects of structural relaxations alone.

In conclusion the Auger depth profiling technique provided direct evidence on the asymmetric interdiffusion in amorphous Si-Ge system. Due to the strong concentration dependence of the interdiffusion coefficient, the silicon almost homogeneously had been distributed in the Ge layer and there was practically no Ge diffusion into the Si.

III.2.3 Calculations on the combined effects of nonlinear diffusion and stresses

III.2.3. INPUT PARAMETER SET

In order to solve the coupled equations (I.68) - (I.70) and (I.54), one has to specify the necessary input parameters. Table III.1 shows those of them which were kept constant during the calculations and correspond to the amorphous Si-Ge system [19,24].

Table III.1 Input parameters kept constant during the calculations corresponding to Si-Ge system

T [K]	Ω_{Si} [m ³ /mol]	Ω_{Ge} [m ³ /mol]	E [Pa]	ν	η [Pas]
700	1.20×10^{-5}	1.36×10^{-5}	8.40×10^{10}	0.3	2×10^{12}

Furthermore, we assumed, in accordance with the binary phase diagram [25] and Spaepen [19], that the Si-Ge system is nearly ideal, *i.e.* $V = 0$ and thus $\kappa = 0$ and $\Theta = 1$, therefore $j_i^{se} = 0$ ($i = Si$ or Ge) [see Appendix at the end of this chapter].

From compilations of diffusion data in crystalline Si-Ge alloys [26,27], it is known that the diffusion coefficient depend on the composition. In this work, in order to get more relevant estimate of the order of magnitude in amorphous state, the absolute values of D_{Si} at 700 K were fitted to experimental data for the concentration dependence published in [28,29,30]. For the ratio of D_{Si}/D_{Ge} , we supposed that it is independent of the concentration and equal to 2.4 (Figure III.13). This is in accordance with the experimental fact that $D_{Si} > D_{Ge}$ and is within the allowed range determined by the scatter of experimental data for tracer diffusion of Ge and Si in crystalline Si [19].

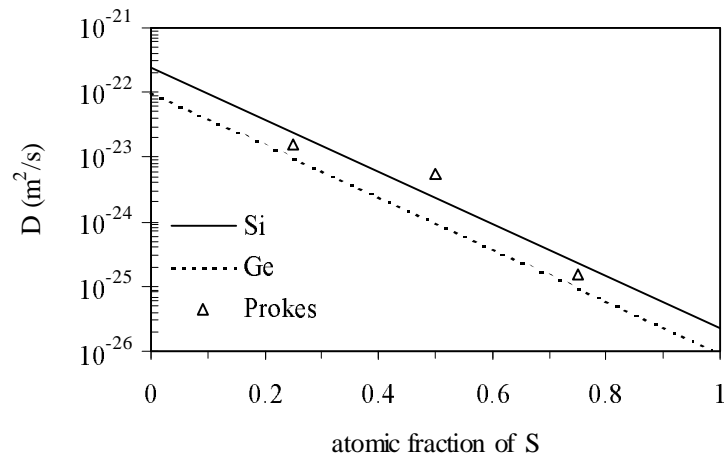
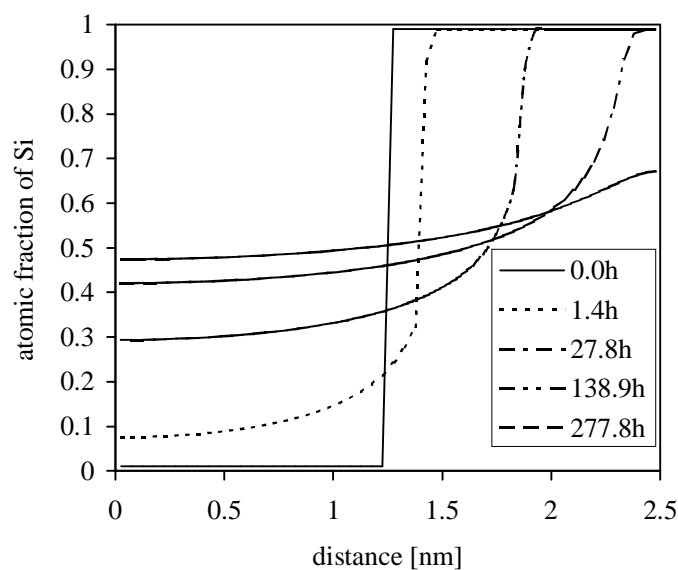
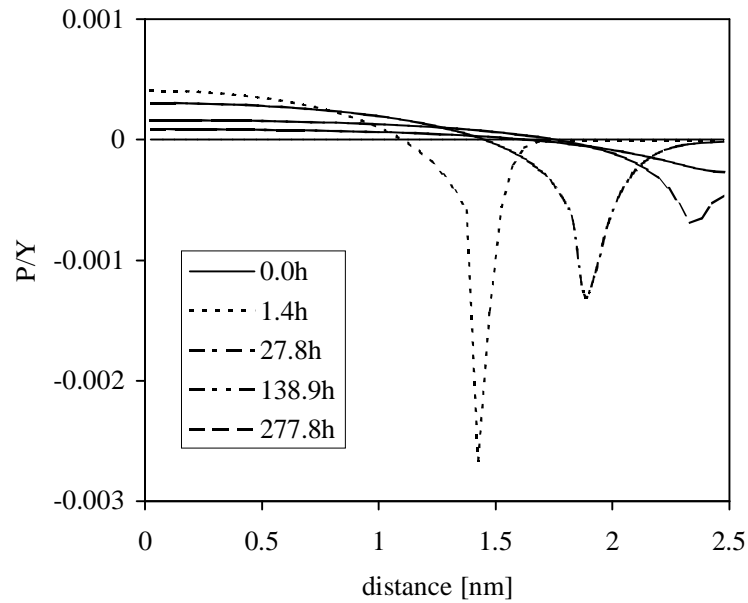


Figure III.13 Concentration dependence of the diffusion coefficients used in the simulation. Triangles denote experimental data measured in amorphous Si-Ge system by Prokes [28,29,30].

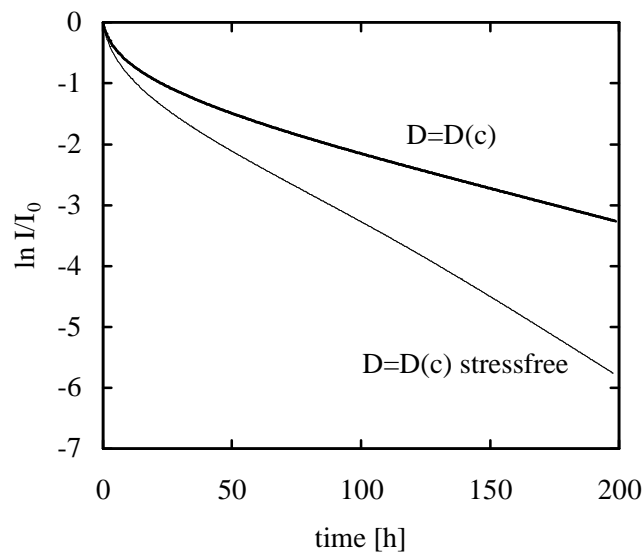
Figure III.14 shows the concentration and pressure distribution at different annealing times for $\Lambda = 5$ nm. It can be seen in Figure III.14a that, due again to the strong diffusional asymmetry, there is a similar behaviour which is shown already in Figure III.3 for the Mo-V system. The diffusion in the Ge-Si alloy is very fast and almost a flat concentration profile is observed in this part, whereas there is a shift of boundary between this alloy and the pure silicon. The pressure distribution shows a sharp tensile peak on the silicon side just at the boundary, and relaxation of this becomes intensive when the pure silicon has been consumed (Figure III.14b). Figure III.14c shows the $1/I_0$ versus t curves which presents a significant upward curvature at the beginning as it was seen and discussed in details in the previous paragraphs. It is worth noting that this calculation was repeated for stressfree case and stress effects did not modify the behaviour of the composition profile and the time evolution of the intensity curve only its 'slope'.



(a)



(b)



(c)

Figure III.14 Concentration (a) and pressure (b) distribution at different annealing times for $\Lambda = 5$ nm and the corresponding $\ln I/I_0$ decay curve (c)

III.2.4 Conclusions

Investigating the combined effects of stress and non-linearity due to the concentration dependence of the diffusion coefficients, it was shown that in the Si-Ge system not only the concentration but the pressure distribution is also very asymmetrical. Furthermore, stress effects do not modify the behaviour of the composition profile and the time evolution of the intensity but slow down the homogenisation.

III. INTERPLAY OF NONLINEAR DIFFUSION AND SURFACE SEGREGATION

The growth of nickel onto the (111) surface of a Cu single-crystal at room temperature and its dissolution kinetics were recently investigated by low energy electron diffraction (LEED) and Auger electron spectroscopy (AES) [31,32]. Measurements of the dissolution of nickel in copper were also performed by Auger spectroscopy in the temperature range of 635-721 K. For the evaluation of the Ni bulk diffusion coefficients, a simple analysis of the kinetics, using a thin film solution of the diffusion equation, has been applied. It was concluded that the values obtained are in agreement with the Ni impurity diffusion data in Cu published elsewhere [33,34,35].

The aim of this paragraph is to propose a more sophisticated method to evaluate the experimental kinetics of dissolution/segregation of thin layers of Ni into Cu(111) and to investigate the effect of surface segregation on the interdiffusion between the finite Ni layer and the semi-infinite Cu substrate. Although several studies have been devoted to surface segregation in Cu(Ni) system [36,37], kinetic effects in a discrete lattice mode have not yet been studied. Since the nickel thickness was between 3 and 14 equivalent monolayers (eq-ML), deviations from the continuum description of diffusion are expected (see III.1) and, due to the interplay between dissolution and segregation, the effective diffusion coefficient determined should depend on time. As we will see, our simulation indicates a step-wise character of the dissolution and an interesting interaction between surface segregation and nonlinear diffusion. On the basis of these calculations a procedure for the evaluation of an averaged diffusion coefficient is given.

Besides the re-evaluation of our previous results on 8 eq-ML's [31], we also carried out new measurements with 3, 6 and 14 eq-ML's in the temperature range of 600-730 K, and they have been evaluated in the same way.

III.3.1 Method for the evaluation of dissolution kinetics

The calculations can be divided into three successive steps: i) Calculations of time evolution of the concentration profiles in a discrete lattice model for an initial distribution of several atomic layers of Ni on the semi-infinite Cu slab. ii) Calculation of the intensities of the Auger signal coming from the distributions obtained in step i). iii) Determination of the diffusion coefficient from the time evolution of the Auger signal. Note that in the simulations - in accordance with [25,38] - it was supposed that there is a complete mutual solubility in this system.

III.3.1. TIME EVOLUTION OF CONCENTRATION PROFILES IN A DISCRETE LATTICE

The model used in our calculations concerning to the time evolution of concentration profiles is based on Martin's deterministic kinetic equations [39] described in I.1.3.3b), I.2.2.1 and III.1.1.2.

To compare the theoretical results with the experimental ones, the calculations were conducted for the following initial distributions:

- I) 3ML of nickel
- II) 8ML of nickel

on the top of a Cu(111) monocrystal containing 51 lattice planes (*i.e.* $N = 54$ and $N = 59$ for I and II, respectively) and

- III) 100ML of nickel

on the top of a semi-infinite Cu(111) monocrystal. The following input parameters were chosen: $T = 1000$ K, $V_{NiNi} = -0.74$ eV, $V_{NiCu} = -0.66$ eV, $V_{CuCu} = -0.58$ eV (these values

were calculated from the cohesive energies of pure metals [40]). Note that, since it was supposed that the system is ideal, $(V_{NiNi} + V_{CuCu})/2 = V_{NiCu}$. Thus, not regarding the concentration independent terms in equations (I.44) and (I.75), the activation energies are determined by $(V_{NiNi} - V_{CuCu})$.

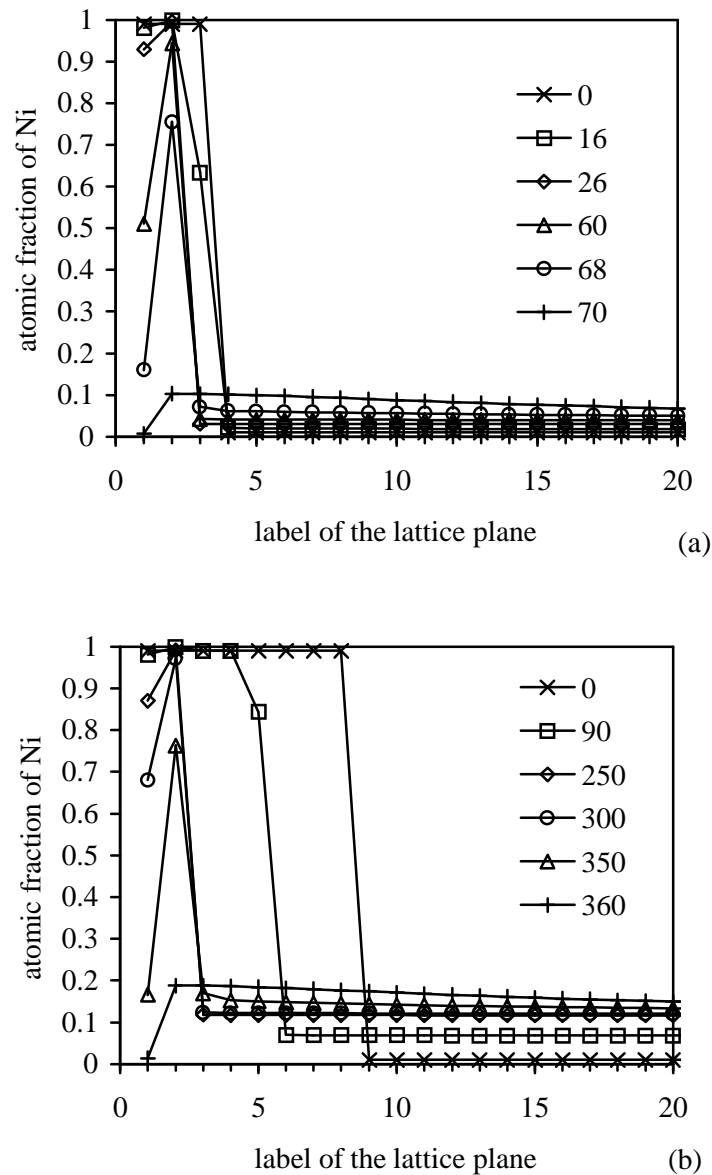


Figure III.15 Time evolution of concentration profiles in Ni/Cu(111) discrete lattices: (a) 3ML of nickel (I-system:) and (b) 8ML of nickel (II-system). (For the meaning of time units shown in the insert, see the text)

The time evolutions of the concentration profiles calculated from equation (I.41) are presented in Figure III.15. The time shown in the figures can be converted to "real" time by the relation $t_{real}/t = v^{-1} \exp\{E^0 - z(V_{AB} + V_{BB})/kT\}$. Note that, to reduce the computing time, a higher temperature was chosen in the computer simulation than the experimental annealing temperatures. This choice does not influence the characteristics of the dissolution kinetics, because it was supposed that the Cu-Ni system is ideal. It can be seen, in accordance with [36,37], that Cu segregates to the first surface layer. However, in case I (Figure III.15a), surface segregation of copper begins already after 26 time units, whereas in case II (Figure

III.15b) the surface segregation starts only after 250 time units. This is an obvious consequence of the different initial Ni thicknesses.

In Figure III.15 the most interesting feature is the step-wise character of the N dissolution. It can be especially well seen for case II that the dissolution starts at the interfacial layer, and until this is not consumed, the next layer remains complete (see in Figure III.15b the curve related to 90 times units: only the concentration of the 5th plane changes while the 4th and 6th planes remain almost pure Ni and Cu, respectively). Thus the interface shifts step by step. This layer -by-layer dissolution takes place until the moving “interface” reaches the Ni layer just before the last. Then, due to the driving force for surface segregation, the intermixing will be continued by the saturation of Cu in the top layer. Thus the change in the second layer will be retarded according to the segregation isotherm. Figure III.16 shows the concentration of the surface layer as a function of the concentration i the second layer (kinetic segregation isotherm) and the theoretical McLean isotherm (equilibrium segregation isotherm in monolayer limit; segregati energy: $\Delta H^{seg} = z_v(V_{BB} - V_{AA})/2$ [41]). This indeed corresponds, as it is expected, to a McLean isotherm and illustrates that the dissolution kinetics is linked to the segregation isotherm (“local equilibrium” [42, 43]), which is in good agreement with experiments [44,45,46] and other predictions obtained by a different model [37]. Finally, after the saturation of the surface layer by Cu, the final homogenisation takes place by the complete dissolution of the second layer.

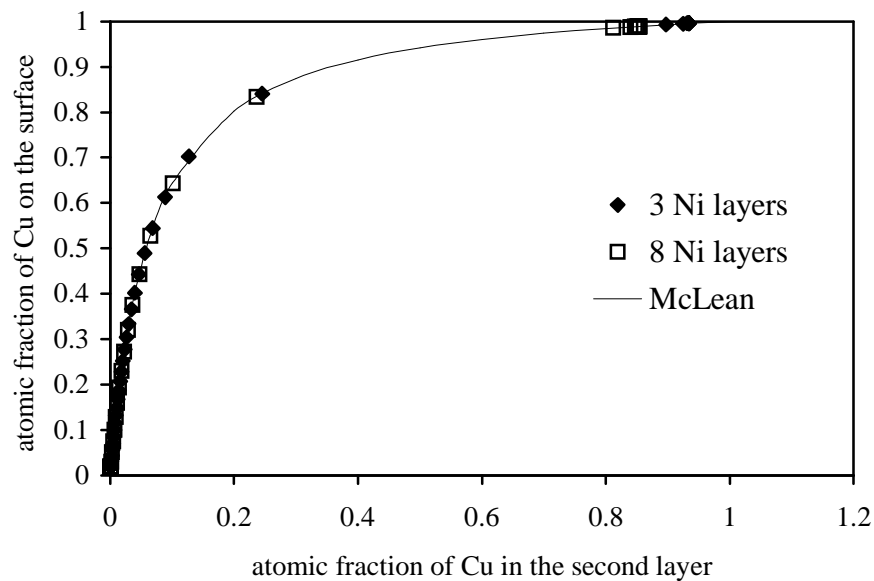


Figure III.16 Segregation isotherm of Ni/Cu system at 1000 K for cases I and II as well as the theoretical McLean isotherm.

In Figure III.15 we illustrated the case when the Cu substrate was finite (with 51 planes). However, as in many experiments, if a semi-infinite substrate is used then $c_1 = \dots c_{i-1} = 1$ (in the Ni) and $c_{i+1} = \dots = c_\infty = 0$, because the diffusion coefficient strongly depends on the concentration and has a very large value in Cu (*i.e.* $\Gamma_{i-1,i} \ll \Gamma_{i,i+1}$) and thus $J_{i-1,i} \ll J_{i,i+1}$. Consequently equation (I.41) can be reduced to:

$$\frac{dc_i}{dt} = -J_{i,i+1} = -z_v c_i \Gamma_{i,i+1}. \quad (\text{III.18})$$

On the other hand, the atomic flux from plane i to $(i+1)$, $j_{i,i+1}$ ($=J_{i,i+1}/A$ where A is the area of the specimen perpendicular to the direction of the diffusion), can also be given by (discrete Fick's first law):

$$j_{i,i+1} = -\frac{D}{\Omega} \frac{c_{i+1} - c_i}{d} \cong \frac{D}{\Omega} \frac{c_i}{d}, \quad (\text{III.19})$$

where Ω is the atomic volume ($\Omega=dA$ and d is the distance between the atomic planes in the direction of the diffusion). Note again that $c_{i+j} \cong 0$, since the substrate is semi-infinite. The speed of the interface shift, v , is related to j as

$$j = -v/\Omega \quad (\text{III.20})$$

and thus

$$D = -\frac{d}{c_i} v. \quad (\text{III.21})$$

{In the above equations D has the meaning of the *intrinsic* diffusion coefficient (composed as a product of the tracer diffusion coefficient and the Darken thermodynamic factor, Θ [47]) which, in the present case, is given by

$$D = z_v d^2 \Gamma_{i,i+1}. \quad (\text{III.22})$$

Since in an ideal system $\Theta = 1$, and if the jump frequencies are independent of c , i.e. $\Gamma_{i,i+1} = \Gamma_{i,i-1}$, $\Gamma = z_v(\Gamma_{i,i+1} + \Gamma_{i,i-1})$, and thus $\frac{1}{2}\Gamma = z_v \Gamma_{i,i+1}$ equation (III.22) equivalent to $D = \frac{1}{2}\Gamma d^2$ (see Eq. (1.11) in [48]).}

For the estimation of D from equation (III.21) the knowledge of v/c_i is needed. From equations (III.18) and (III.20), one can write

$$\frac{v}{d} = -z_v c_i \Gamma_{i,i+1} \left(= \frac{dc_i}{dt} \right). \quad (\text{III.23})$$

This result shows that v/d is in fact the decay rate of the concentration of the interface layer c_i .

Figure III.17a shows the v/d versus t function obtained from numerical solution of equation (III.18) for $c_i(t)$, taking also into account the concentration dependence of $\Gamma_{i,i+1}$ given by equations (I.43) and (I.44). Having $c_i(t)$ the $v(t)/d$ function was calculated using equation (III.23).

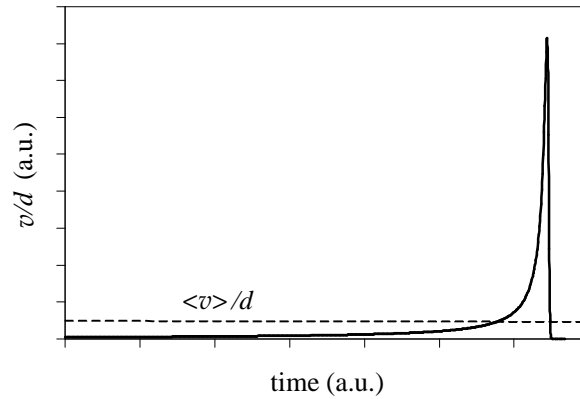


Figure III.17 One period of the interface shift speed versus time. The dashed line denotes its average.

We have seen that the dissolution of the $(i-1)$ -th plane begins only after the complete dissolution of the i -th plane. This means that this layer-by-layer dissolution results in a periodic behaviour as a function of time: each plane dissolves subsequently reproducing the same process. Therefore v/d (and thus D) is also a periodic function of time and the time evolution within one period characterizes the dissolution of one individual plane. In fact this is what is shown in Figure III.17 for v/d . Although, the value of v/d (and D) can change considerably, it is worthwhile to define an average value of v/d characterising the mean speed of the interface shift, $\langle v \rangle/d = (Td)^{-1} \int v dt$, where T is the time necessary for the consumption of one layer. *Due to the step-by-step character of the dissolution, this average speed of the interface shift should be constant, independent of time. This result is inherently related to the strong non-linearity of the problem: the strong concentration dependence of the diffusion coefficient (or $\Gamma_{i,i+1}$) shifts the validity limit of the continuum approach (from which a parabolic law i.e. $v \propto t^{1/2}$ would be expected) out of the range considered here. Of course, after the dissolution of more and more layers the supposition that $c_{i+1} \cong 0$ will be less and less valid and we will have a transition to the parabolic dissolution. Obviously, this transition will depend on the concentration dependence of the diffusivity. This is very similar to the results obtained in III.1, where the shift of the validity limit of the continuum approach to higher diffusion distances was obtained in multilayers with increasing non-linearity.*

Thus the time evolution of the thickness of Ni layer, containing originally n_0 atomic layers, can be given by:

$$n(t) = n_0 + \frac{\langle v \rangle}{d} t. \quad (\text{III.24})$$

In order to illustrate the validity of averaging leading to equation (III.24), Figure III.18 shows the position of the interface versus time, obtained from simulation for a semi-infinite Cu(111) substrate with 100 atomic layers of Ni. The position of the interface, y (in monolayers units), is defined as the place at which straight line interpolated between the two neighbouring planes, having compositions above and below $c = 0.5$, crosses the $c = 0.5$ value. Due to this the curve in Figure III.18 has periodic oscillations around the straight line fitted. Because of the log-log plot the first part of the curve (up to $y = 1$, i.e. $\log y = 0$)

clearly shows the time evolution illustrated already in Figure III.17. On the other hand, the slope of the straight line fitted is equal to $1 \pm 8 \times 10^{-4}$, i.e. the average shift is indeed linear.

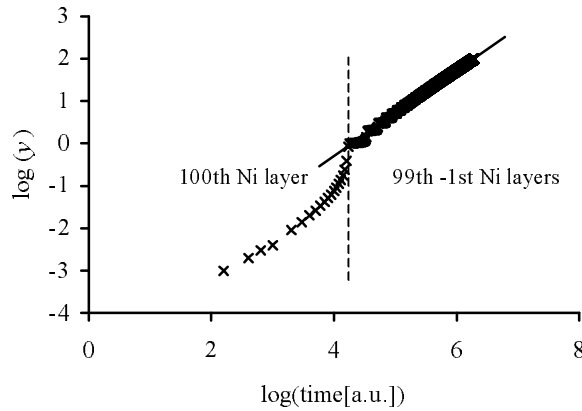


Figure III.18 Position of the interface versus time for the dissolution of 100 Ni layers into the semi - infinite Cu(111) substrate (see also the text).

III.3.1. DECAY OF THE AUGER CURVES

In the case of a homogeneous specimen containing n layers, the measured Auger intensity can be given by the following formula [49] :

$$I_n = I_1 + \alpha I_1 + \alpha^2 I_1 + \dots + \alpha^{n-1} I_1 = (1 + \alpha + \dots + \alpha^{n-1}) I_1 = \frac{1 - \alpha^n}{1 - \alpha} I_1 \quad (\text{III.25})$$

where I_1 is that part of the total intensity which would come from each layer without attenuation. The usual form of the attenuation coefficient is:

$$\alpha = \exp[-1/(\lambda \cos \vartheta)], \quad (\text{III.26})$$

where λ is the inelastic mean free path (IMFP) [in monolayer (ML) units], and ϑ is the emission angle of Auger electrons to the normal of the surface of the sample. I $n \rightarrow \infty$, i.e. for a bulk specimen, the Auger intensity is:

$$I_\infty = \lim_{n \rightarrow \infty} I_n = \frac{I_1}{1 - \alpha} \Rightarrow I_1 = (1 - \alpha) I_\infty. \quad (\text{III.27})$$

Since there are $(i-1)$ layers on the top of the i -th layer, the signal coming from layer i is attenuated by α^{i-1} ; hence the contribution of the i -th layer to the total measured intensity is:

$$I_i = (1 - \alpha) \alpha^{i-1} I_\infty. \quad (\text{III.28})$$

The atomic fraction of the i -th layer of an AB alloy can be determined using the following equation:

$$c_i = \frac{I(i)}{I_i} = \frac{I(i)}{(1-\alpha)\alpha^{i-1}I_\infty}, \quad (\text{III.29})$$

where $I(i)$ is the Auger intensity coming from the A atoms of the i -th layer. The total (measured) intensity can be expressed as the sum of the contributions of the layers:

$$I = \sum_{i=1}^n I(i) = (1-\alpha)I_\infty \sum_{i=1}^n c_i \alpha^{i-1}. \quad (\text{III.30})$$

The Auger curves corresponding to the above evolution of the concentration profiles, shown in Figure III.15, are calculated from (III.30) and reported in Figure III.19. In the present case, the values of λ [$\lambda(\text{Cu}_{920\text{eV}}) = 1.19$ nm, $\lambda(\text{Ni}_{848\text{eV}}) = 1.10$ nm] were calculated using Seah and Dench formalism [50], and $\vartheta = 42^\circ$. Moreover, a theoretical peak-to-peak height ratio, q , was calculated from the Auger curves:

$$q = \frac{I_{\text{Ni}848} / I_{\text{Ni}848}^0}{I_{\text{Cu}920} / I_{\text{Cu}920}^0} = \frac{I_{\text{Ni}848}}{I_{\text{Cu}920}} S, \quad (\text{III.31})$$

where the superscript zero denotes the pure element in the bulk form and S is the relative Auger sensitivity factor of both elements. This value can be estimated from the experimental bulk Ni and Cu Auger signals as $S = I_{\text{Cu}920}^0 / I_{\text{Ni}848}^0 = 1.13$. In order to show the influence of the segregation we have investigated the phenomenon with and without copper surface segregation. The results are presented in Figure III.19 for cases I and II, respectively. For the present curves without segregation, it was supposed that there was no free surface, *i.e.* the 1st, original surface, layer was covered by a 0th layer for which $c_0 = c_1$. It can be seen that at the beginning (region a in Figure III.19), no major differences can be observed between the curves with and without segregation. In the central part (region b) the curves diverge. Furthermore, curves without segregation change faster and show one extra step. Finally all curves approach equilibrium (region c).

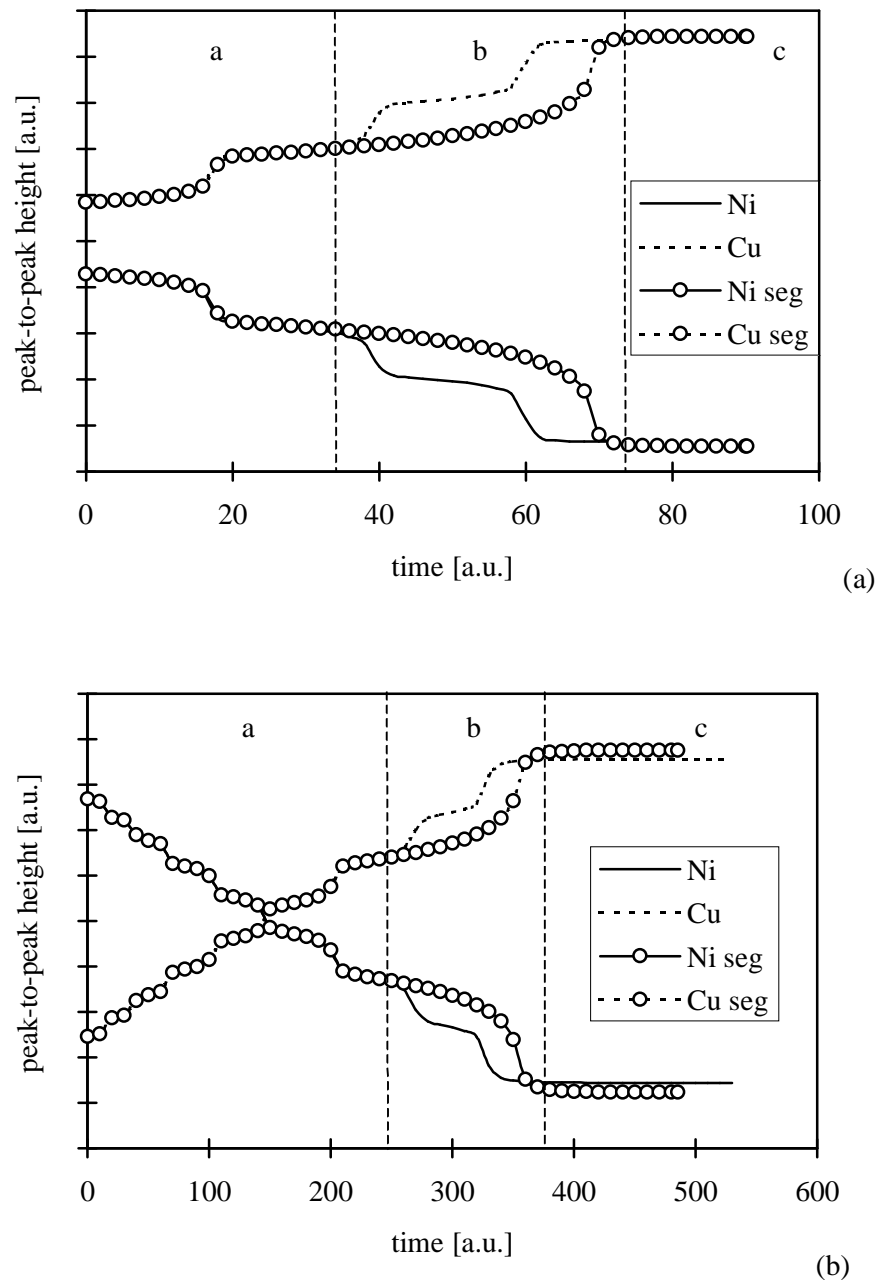


Figure III.19 Time evolution of Ni and Cu Auger signals (— and -----, respectively) for 3ML (a) and 8ML (b) Ni layers. (Curves with and without marks o refer to the case of with and without copper segregation.)

In the first stage, the process is completely *controlled by a concentration dependent diffusion on discrete lattice*. The steps are related to the step-wise character of the problem and each step corresponds to the end of the consumption of the atomic layer considered. Since the diffusion of Ni depends strongly on the nickel concentration c , the dissolution of the individual atomic layers will become faster as c falls. It is due to the fact that the diffusion of both elements in Cu is much faster than in Ni (practically there is no diffusion in Ni). Note that this follows not only from the choice of interaction energies entering into the activation energies of Γ [equations (I.44) and (I.75)] but also in accordance with the experimental self-diffusion coefficients in Ni and Cu [51] (they differ by a factor of about 10^{-4} at 1000 K). The appearance of an additional step in the stage b on the curve without

segregation is due to the lack of segregation; there is no enhanced saturation in the first layer and the remaining two layers dissolve “normally”.

III.3.1. DETERMINATION OF THE DIFFUSIVITY

This time evolution can be also determined from the dissolution kinetics measured by AES in the following way. Using the equations (III.25) and (III.27), the Auger intensity coming from the A atoms of a specimen containing n A atomic layers on a B substrate is:

$$I_{A,n} = (1 - \alpha_A^n) I_{A,\infty} \quad (III.32)$$

and the intensity coming from the B atoms of the bulk substrate is attenuated by the n A layers, *i.e.* the contribution of the substrate to the measured intensity is:

$$I_B = \alpha_B^n I_{B,\infty} \quad (III.33)$$

Thus the accumulation parameter:

$$q_n = \frac{I_{A,n}/I_{A,\infty}}{I_B/I_{B,\infty}} = \frac{1 - \alpha_A^n}{\alpha_B^n} \quad (III.34)$$

and supposing that $\alpha_A \cong \alpha_B$ (in Ni/Cu it is reasonable since $\lambda_{Ni} \approx \lambda_{Cu}$):

$$q_n \cong \alpha_B^{-n} - 1 \quad (III.35)$$

Thus one can determine n from this equation:

$$n(t) = -\frac{\ln(q_n + 1)}{\ln \alpha_B} \quad (III.36)$$

In general $n(t)$ should be (according to Figure III.19) a step-wise function. However, if it is approximated by a continuous curve (*e.g.* if the resolution of the measurement is not high enough) then plotting the right hand side of (III.36) versus time the linearity can be checked and then the slope will be just equal to $\langle v \rangle / d$ [see equation (III.24)] and the intercept will give an estimation of the original Ni thickness.

As we have seen, from the numerical solution of equation (III.18) $c_i(t)$ and $v(t)/d$ functions can be obtained. Obviously, if one defines an average value of v/d , as it has been done before, then a corresponding average value of c should also be introduced in equations (III.21) and (III.23). As it is illustrated in b, this average value corresponding to $\langle v \rangle / d$ can be obtained. We have calculated it at different temperatures for the interaction energies ($V_{NiNi} - V_{CuCu}$) used in the numerical solution of equation (III.23). It can be seen in Table 1 that it is practically independent of the temperature. Furthermore, the value of c is also not sensitive to the ($V_{NiNi} - V_{CuCu}$) difference: changing it by about 15% results in a change in c of less than 10%. Thus, in our temperature range, c is about 0.78. Substituting this value into equation (III.21) one can write approximately that in this system:

$$D \cong -1.28 d \langle v \rangle. \quad (\text{III.37})$$

The physical meaning of $c=0.78$ can also be enlightened by the following arguments. In contrast to diffusion with constant D (where the concentration gradient falls continuously with time, leading to parabolic law) in our case the linear shift of the interface with time is related to the constancy of the diffusion current [see equation (III.20)]. If we define a time independent average value of D , as we did, then the gradient of the concentration should be also constant *i.e.* $\langle \text{grad } c \rangle = \langle c_i \rangle / d (= 0.78/d \text{ in our case})$. Of course, in general, the numerical value of this average concentration will depend on the strengths of the concentration dependence of D .

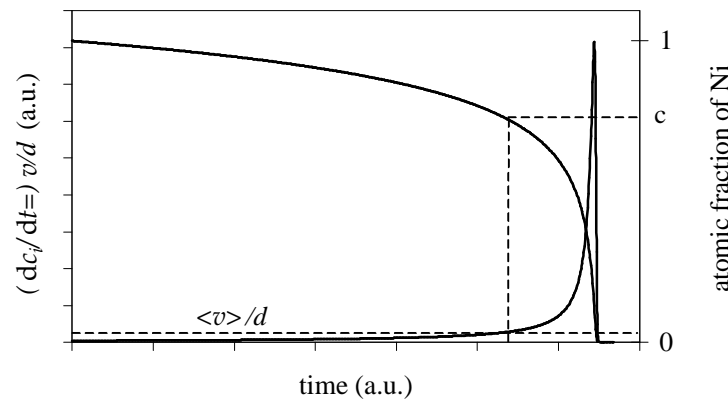


Figure III.20 Common plot of one period of the concentration of the dissolving plane and the speed of the interface shift versus time. Dashed lines indicate the average values of v/d and c corresponding to each other (see also the text)

Finally, it is worth to note that the evaluation procedure proposed here can be generally used in all cases when the dissolution takes place by a layer-by-layer mode into a semi-infinite substrate if the interface shifts linearly with time. [If $\alpha_A \cong \alpha_B$ in equation (III.34) cannot be assumed, then $n(t)$ can be determined from equation (III.34) instead of equation (III.36).] Obviously, if this linearity is not fulfilled the relation between the diffusivity and the interface speed will be different from equation (III.21). Furthermore, important to note that the determination of the $n(t)$ function from measurements of the time evolution of the Auger intensities can bring an important information on the character of the process controlling the interface shift. For example, as it was shown in [43] and [52] if there is an interplay between surface segregation and tendency for strong phase separation, but the non-linearity is negligible, the shift of the interface is proportional to $t^{1/2}$.

Table III.2 Temperature dependence of the corresponding c .

T [K]	1200	1000	800	700
c	0.71	0.73	0.76	0.78

III.3.2 Analysis of experimental data

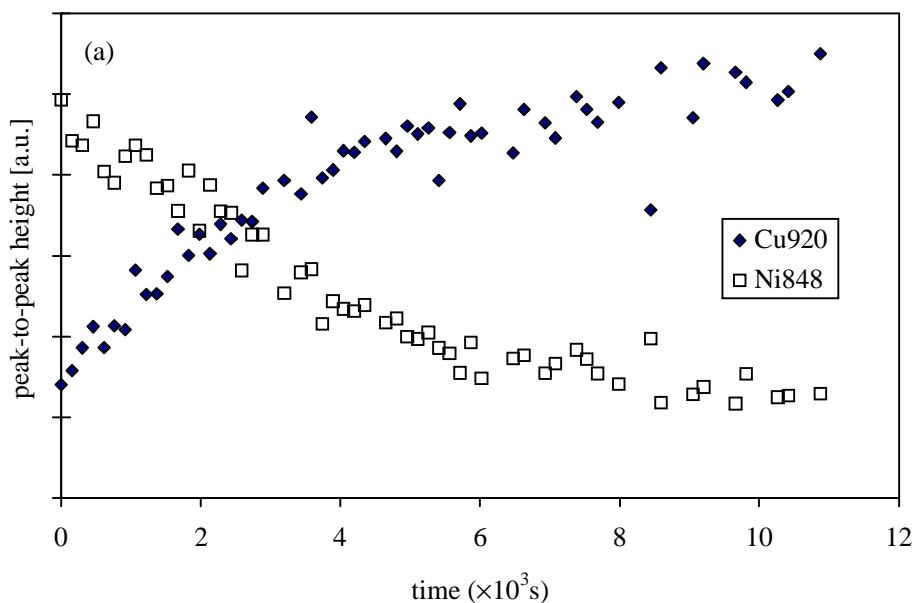
The general procedure applied for determination of kinetics is described in II.3.2.3. We just remark that prior to any nickel deposition, the Cu (111) sample was cleaned in situ b

repeated cycles of argon ion bombardment and thermal annealing at 400 °C until impurity could be detected (checked by AES) and that during this cleaning the monocrystalline structure of Cu(111) was conserved (checked by LEED). The pseudomorphic growth of 3-14 deposited nickel layers have also been checked by LEED.

The relative variation of the Auger signal is a smooth function of time, for 6 -14 eq-ML (Figure III.21a for 8 eq-ML and Figure III.21b for 14 eq-ML), whereas large fluctuations are observed for 3 eq-ML (Figure III.21c). In the latter case, it was not possible to use the proposed method because only a short initial sharp decrease of the Ni peak was observed. That is why the analysis of the experimental data, described above, can be carried out only for experiments made at: 721K, 713K, 701K and 679 K (in these cases the initial thickness of Ni was higher than about 6 eq-ML). As an illustration, Figure III.22 shows the thickness of Ni as a function of time calculated by equation (III.36) for 679 K. Note that usually, the first couple points fall above the straight line fitted to the first part of the $n(t)$ functions. Since the samples were prepared at room temperature the reason of this misfit can be recrystallisation and relaxation of the surface layers during heat treatment. Furthermore the change in the slope at the second layer (a $t \approx 4 \times 10^3$ s in Figure III.22) is a clear evidence of the effect of surface segregation. Nevertheless, from the slopes of the lines fitted to the first part of the curves, according to equations (III.24) and (III.37), the values of D have been calculated (with $d = 0.2032$ nm).

The Arrhenius plot of the diffusion coefficients is shown in Figure III.23 and the temperature dependence of the diffusivity can be given by:

$$D = 2.9 \exp\left(-\frac{297 \pm 62 \text{ kJ/mol}}{RT}\right) \text{m}^2/\text{s}. \quad (\text{III.38})$$



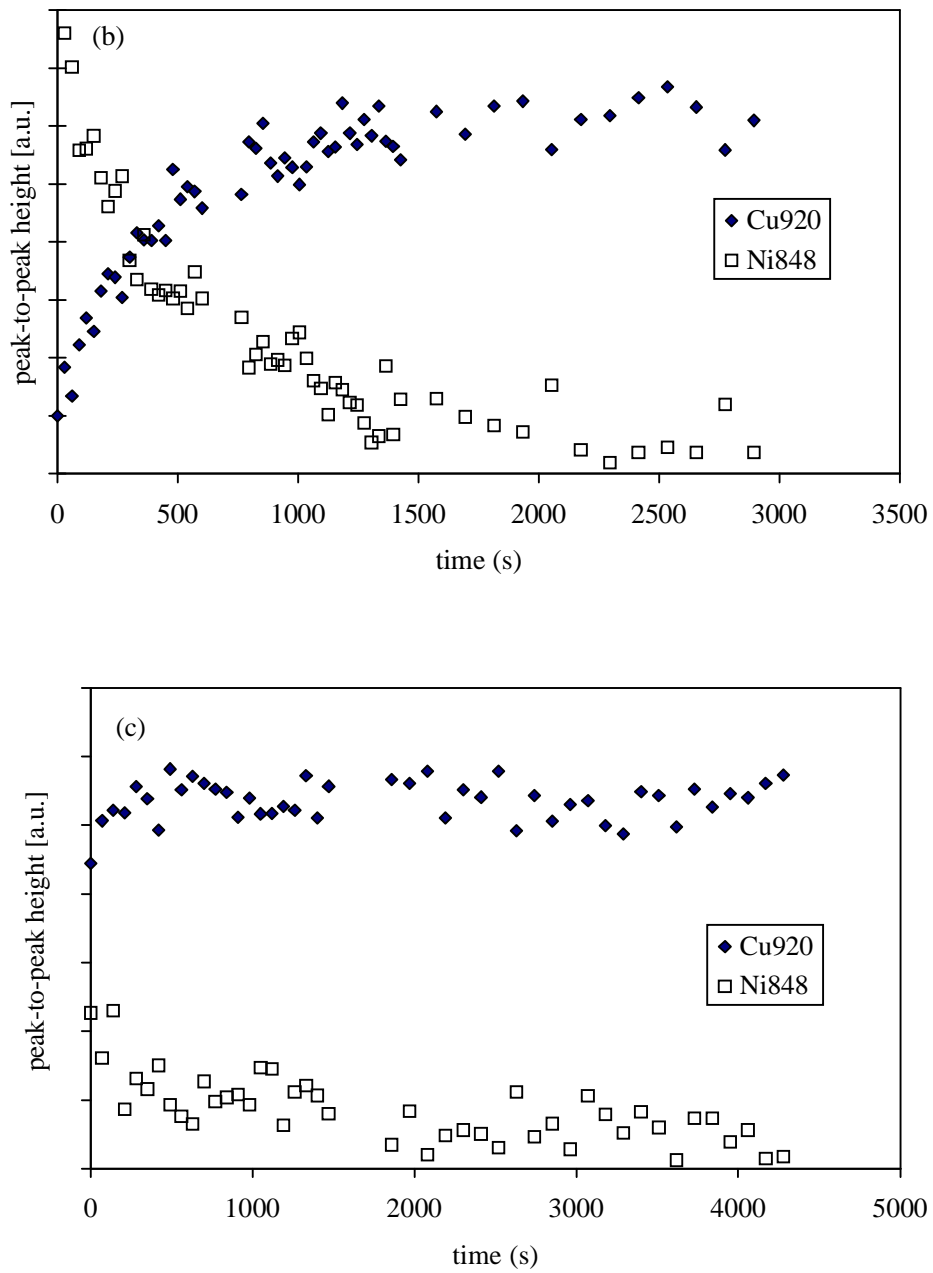


Figure III.21 Measured Auger kinetics of nickel dissolution in copper for a) 8 eq -ML at 701 K, b) 14 eq-ML at 721 K and c) 3 eq-ML at 639 K.

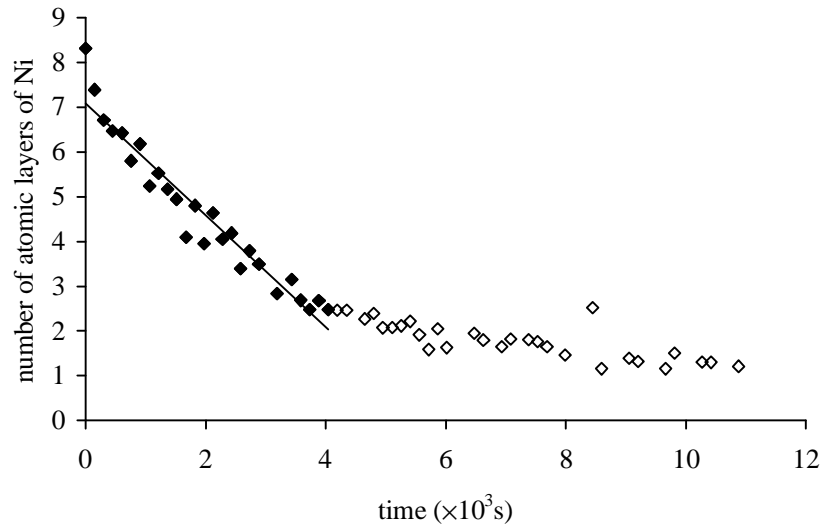


Figure III.22 Time evolution of the Ni thickness at 679 K. The first part of the curve fitted by a straight line corresponds to the part controlled by interdiffusion.

Figure III.23 Temperature dependence of the intrinsic diffusion coefficient.

III.3.3 Discussion

In our calculations, due to the direct exchange of atoms, it was assumed that the exchange jumps of Cu and Ni are equal (*i.e.* $\Gamma_{i,i+1}^{Cu \rightarrow Ni} = \Gamma_{i+1,i}^{Ni \rightarrow Cu}$). This means that the intrinsic diffusion coefficients of Ni and Cu [see equation (III.22)] are equal to each other; $D_{Ni}(c) = D_{Cu}(c)$, *i.e.* we are not able to distinguish the self- and impurity diffusion. We know that this is not the case in reality (see Figure III.24, where the Arrhenius plots for Cu self- and Ni heterodiffusion in Cu as well as for Ni self- and Cu heterodiffusion in Ni are different); this is an inherent limitation of the model. Nevertheless, the concentration dependence of the intrinsic diffusion coefficient is naturally included. That is why we could calculate an averaged intrinsic diffusion coefficient belonging to $c_{Ni} = 0.78$. This

result points out an important difference in the interpretation of the diffusion coefficients estimated in our work and the previous one [31]. In fact in [31], using the instantaneous source solution of the continuous Fick II equation, three main suppositions were made:

- i) there is no segregation
- ii) there is only a dissolution of Ni into the Cu (*i.e.* the diffusion of Cu into the Ni was neglected; only nickel heterodiffusion was considered)
- iii) the intrinsic diffusion coefficient of Ni is independent of concentration.
- iv) the process is controlled by a usual continuum diffusion behaviour (parabolic law)

In [31], the diffusion coefficient was interpreted as the Ni impurity diffusion in *pure* Cu (*i.e.* at $c_{Ni} = 0$), taking also into account that this system is ideal, and thus the intrinsic and tracer diffusivities are equal to each other (*i.e.* $\Theta = 1$). However, in our case, D is an intrinsic diffusion coefficient corresponding to $c_{Ni} = 0.78$. Thus its value should be located between the two hatched regions in Figure III.24. As one can see, this criterion is satisfied. Furthermore, since practically all Arrhenius curves in Figure III.24 are parallel, the activation energies should be close to each other, which is also reasonable (see also [51]).

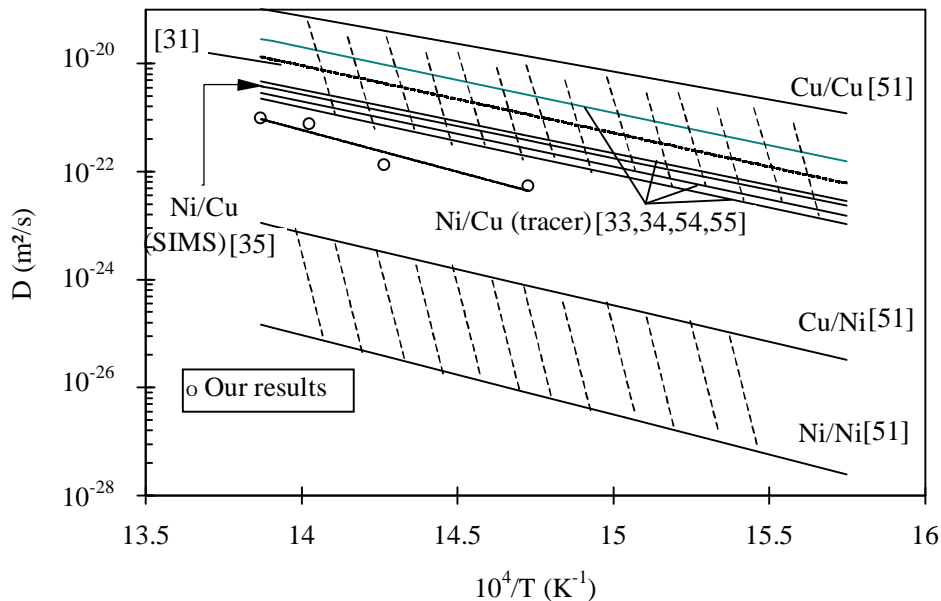


Figure III.24 Arrhenius plot of nickel lattice diffusion coefficients in copper (\circ our results) compared with the literature data.

It can be seen from our calculations that the first two suppositions can be accepted at least in the first stage of annealing. Indeed, the supposition ii) is generally valid and in fact it is a consequence of the strong concentration dependence of jump frequencies (diffusion coefficients). Furthermore the effect of surface segregation on the kinetics can be neglected until the time when the interface reaches the next-to-the-last layer.

There is obviously an important difference between our discrete model and the continuum one (which corresponds to the instantaneous or constant source solution of the continuous Fick II equation). As we have seen from our calculations, the shape of the concentration profile during dissolution is not an erfc-type function as it should be for constant source. Instead, a layer-by-layer dissolution mode can be observed (see Figure

III.15 and Figure III.19) and the $n \propto t$ relation indicates that the process cannot be described by the parabolic law.

It is worth noting that the behaviour shown in Figure III.15 is similar to that published by Saúl *et al.* [53]. However, in their case [Ag thin layer deposited on Cu(111)] the step-wise character is the result of the presence of the miscibility gap at the working temperature. A phase transition occurs in the interfacial layer during dissolution: the initially Ag-rich interfacial layer is transformed in a Cu-rich phase when its silver concentration reaches the bulk solubility limit. This transformation mechanism continues layer-by-layer.

Finally we note that, in this work we were not able to observe the step-wise behaviour because of technical limitations. However we believe that it can be measured by a high-resolution surface analysis technique. We also note that the method can be used only when the deposited element has a higher kinetic energy transition (in the case of Auger measurements, of course) in order to be possible to use about 8 atomic-layer thick deposit.

III.3.4 Conclusions

We have investigated the effect of segregation on the dissolution of a thin Ni layer (3-14 eq-ML) into a semi-infinite Cu substrate. Computer simulations have been also carried out to understand the details of the dissolution. On their basis we proposed a sophisticated method to analyse the experimental kinetics measured by AES.

The most important results are the following:

1) Our simulations indicated a step-wise character of dissolution and an interesting interference between the segregation and dissolution. Because of the strong concentration dependence of the diffusion coefficients of the diffusing species, the interface remains sharp and shifts until it reaches the next-to-the-last layer. In this part of the dissolution a *concentration dependent diffusion on discrete lattice* controls the process. Then, due to the driving force for segregation, the process continues by the saturation of Cu in the top layer. The change of the concentration of the second layer occurs according to the segregation isotherm. Finally, after the saturation of the surface layer by Cu, the final homogenisation takes place by complete dissolution of the second layer.

2) We have seen that the thickness of Ni decreases linearly with time, indicating the strong non-linearity and the deviation from the continuum description. An averaged intrinsic diffusion coefficient has been determined from the experimental AES kinetics of Ni dissolution into Cu substrate, obtained by the method developed in this paper. While the diffusion coefficient has a strong concentration dependence, this averaged diffusion coefficient belongs to a certain concentration which in our case is $c_{Ni} = 0.78$. At a given temperature this concentration corresponds to the mean speed of the shift of the interface. We have also determined the temperature dependence of D :

$$D = 2.9 \exp\left(-\frac{297 \pm 62 \text{ kJ/mol}}{RT}\right) \text{m}^3/\text{s},$$

which (the activation energy) agrees well with the values published in the literature for this system [33,34,54,55].

APPENDIX: GRADIENT ENERGY TERM IN THE STEPHENSON MODEL

As was mentioned in the paragraph I.1.3.4b), Stephenson [56,57] gave a set of general, coupled equations for the description of atomic currents, the resultant stress development and stress relaxation by Newtonian flow for interdiffusion. The most important difference of this description as compared to the treatment of the stress effects in multilayers by Cahn and Hilliard [58,59,60] is that the stress relaxation and a convective transport (Kirkendall - shift) are allowed. In the Cahn-Hilliard treatment, due to the suppositions $M_1 = M_2$ and $\Omega_1 = \Omega_2$ [see I.1.3.3a)], only the difference of the chemical potentials of the two components had to be determined. Thus, for the use of Stephenson's description, where the individual forms of the atomic currents are needed if the Kirkendall velocity is not zero, a generalisation is necessary if the gradient energy coefficient is not zero.

Since all effects taken into account are an additive term in the expression of atomic fluxes [e.g. equation (I.54) contains two, the first is related to the material transport and the second to the stress effect], it seems logical to join formally the gradient energy effect to the atomic flux as an additive term (j_i^{se}), i.e.:

$$j_i = -D_i \text{grad} \rho_i - L_i \rho_i \text{grad} p + j_i^{se}, \quad i = 1, 2 \quad (\text{III.39})$$

where j_i^{se} is proportional to the gradient energy coefficient κ , therefore for an ideal system $j_i^{se} = 0$. Note that from now on, our description is restricted to only one-dimensional case, but obviously it is possible to extend it to more dimensions.

For the determination of j_i^{se} , we use the results according to which the local free energy per volume unity of a non-uniform system for $\rho = \text{const}$ ($1/\rho = \Omega = \Omega_1 = \Omega_2$) and for $p = 0$ is given by equation (I.26) :

$$f = f_0(c) + \kappa \left(\frac{\partial c}{\partial x} \right)^2, \quad (\text{III.40})$$

and its variation by the atomic fraction c is:

$$\frac{\delta f}{\delta c} = f'_0 - 2\kappa \frac{\partial^2 c}{\partial x^2} = \mu_1 - \mu_2, \quad (\text{III.41})$$

where μ_i ($i=1,2$) is the chemical potential per volume unity. Moreover, according to Prigogine [61] for a system in mechanical equilibrium:

$$cX_1 + (1-c)X_2 = 0, \quad (\text{III.42})$$

where X_i denote the chemical driving forces, which for an isotherm system are related to μ_i as $X_i = -\text{grad} \mu_i$. Thus combining equations (III.41) and (III.42), one obtains:

$$X_1 = -\frac{1-c}{\rho} \text{grad} \left[f'_0 - 2\kappa \frac{\partial^2 c}{\partial x^2} \right] \quad (\text{III.43})$$

and

$$X_2 = \frac{c}{\rho} \text{grad} \left[f'_0 - 2\kappa \frac{\partial^2 c}{\partial x^2} \right]. \quad (\text{III.44})$$

According to the definition [56] $j_i = M_i \rho_i X_i$, where M_i is the mobility and assuming that κ does not depend on the spatial coordinate, one gets:

$$j_1 = -M_1 c(1-c) f'_0 \left(1 - \frac{2\kappa}{f''_0 \text{grad} c} \frac{\partial^3 c}{\partial x^3} \right) \text{grad} c = -D'_1 \rho \text{grad} c = -D'_1 \text{grad} \rho_1, \quad (\text{III.45})$$

where the last two expressions are the traditional form of the first Fick equation, but the diffusion coefficient is very complicated. For j_2 a similar expression can be written. Equation (III.45) give also the relation between the mobility (M_i) and the intrinsic diffusion coefficient (D_i'). Note that in equation (III.45), the last algebraic transformation is possible only if of $\rho = \text{const}$. From this correlation, it is clear that for $\kappa = 0$ it results the usual relation [see equation (I.57)], considering that f''_0 in a binary solid solution model is:

$$f''_0 = \rho RT \Theta / c(1-c), \quad (\text{III.46})$$

Where

$$\Theta = -\frac{2z_v Vc(1-c)}{RT} + 1. \quad (\text{III.47})$$

Comparing equations (III.39) and (III.45) if $p = 0$, we have:

$$j_1^{ge} = D_1 \rho \frac{2\kappa}{f''_0} \frac{\partial^3 c}{\partial x^3} = D_1 \frac{2\kappa}{f''_0} \frac{\partial^3 \rho_1}{\partial x^3}, \quad (\text{III.48})$$

where D_i is the intrinsic diffusion coefficient of the uniform system. We can determine similarly that:

$$j_2^{ge} = -D_2 \rho \frac{2\kappa}{f''_0} \frac{\partial^3 c}{\partial x^3} = -D_2 \frac{2\kappa}{f''_0} \frac{\partial^3 \rho_2}{\partial x^3}. \quad (\text{III.49})$$

Thus, a general expression of flux was obtained for the case when $1/\rho = \Omega = \Omega_1 = \Omega_2 = \text{const}$ but $M_1 \neq M_2$ ($D_1 \neq D_2$), which contains all the effects (gradient energy, Kirkendall, stress) mentioned before. If ρ is not constant, the situation is more complex and a general (variational) method is necessary for the general treatment.


REFERENCES

- 1 H.E. Cook and D. de Fontaine, *Acta Metall.*, **17**, 915 (1969)
- 2 H.E. Cook, D. de Fontaine and J.E. Hilliard, *Acta Metall.*, **17**, 765 (1969)
- 3 J. Philibert, *Atom Movements – Diffusion and Mass Transport in Solids, Les Editions de Physique* (1991)
- 4 G. Martin and P. Benoist *Scripta Metall.*, **11**, 503 (1977)
- 5 J.W. Cahn, *Acta metal.*, **9**, 795 (1961)
- 6 H. Yamauchi and J.E Hilliard, *Scripta metal.*, **6**, 909 (1972)
- 7 T. Tsakalakos, *Thin Sol. Films*, **86**, 79 (1981)
- 8 T. Tsakalakos, *Scripta Metall.*, **20**, 471 (1986)
- 9 E.S.K. Menon and D. de Fontaine, *Scripta Metall.*, **27**, 395 (1992)
- 10 H. Mehrer, *Diffusion in Solid Metals and Alloys*, Landolt-Börnstein, New Series, **III/26** (Berlin: Springer) (1990)
- 11 Z. Erdélyi, D.L. Beke, P. Nemes, G.A. Langer, *Phil.Mag. A*, **79**, No 8, 1757 (1999)
- 12 D.L. Beke, P. Nemes, Z. Erdélyi, I.A. Szabó, G.A. Langer, *Materials Reserach Society Symposium Proceedings: Diffusion Mechanisms in Crystalline Materials* Editors: Y. Mishin, G. Vogl, N. Ciwern, R. Catlow, D. Farkas MRS Warrendale, Pennsylvania, USA, **527**, 99 (1998)
- 13 D.L. Beke, A. Csik, G.A. Langer, Z. Erdélyi, Z. Papp, *Def. and Diff. Forum*, **194-199**, 1403-1416 (2001)
- 14 F.-L. Yang, R.E. Somekh, W.-C. Shih and A.L. Greer, *Proceedings of ISMANAM-94*, ed. A.R. Yavari (1994)
- 15 A. Csik, D.L. Beke, G.A. Langer, Z. Erdélyi, L. Daróczi, K. Kaptá, M. Kiss-Varga, *Vacuum*, **61**, No. 2-4, 297-301 (2001)
- 16 A. Simon, A. Csik, F. Pászti, Á.Z. Kiss, D.L. Beke, L. Daroczi, Z. Erdélyi, G.A. Langer, *Nuclear Instruments and Methods in Physics Research B*, 2000, **161-163**, 472-476
- 17 A. Csik, G.A. Langer, D.L Beke, Z. Erdélyi, M. Menyhárd, A. Sulyok, *Journal o Applied Physics*, **89**, No. 1, 804-806 (2001)
- 18 J. DuMond and J.P. Youtz, *J. Appl. Phys.*, **11**, 357 (1940)
- 19 F. Spaepen, *J. of Magn. Mat.*, **156**, 407 (1996)
- 20 O. Auciello and J. Engemann (Eds), *Multicomonnt and multilayerd Thin Films for Advanced Microtechnologies: hechniques, Fundamentals and Devices, NATO ASI Series*, **234** (1993)
- 21 E. Szilágyi, F. Pászti, G. Amsel, *Nucl. Instr. and Meth. B*, **100**, 103 (1995)
- 22 E. Szilágyi *Nucl. Instr. and Meth.*, **161-163**, 37 (2000)
- 23 E. Kótai, *Nucl. Instr. and Meth. B*, **85**, 588 (1994)
- 24 A.S. Witvrouw and F. Spaepen, *J. Appl. Phys.*, **74**, 7154 (1993)
- 25 T.B. Massalski, in *Binary Alloys Phase Diagrams, The materials Soc. Second Edition* (1992)
- 26 W. Frank, U. Gössele, H. Mehrer and S. Seeger, *Diffusion in Crystalline Solids*, Eds. G.E. Murch and A.S. Nowick, Academic, San Diego, 1984
- 27 N. Stolwijk and H. Bracht, *Diffusion in Semiconductors*, Ed. D.L. Beke (Landolt-Börnstein, New Series, III/33A), Springer, Berlin, 1998
- 28 S.M. Prokes, *PhD Thesis*, Harvard University: Cambridge, Massachusetts (1986)
- 29 S.M. Prokes and F. Spaepen, *J. of Appl. Phys. Lett.*, **47**, 234 (1985)
- 30 S.M. Prokes and F. Spaepen, *Mat. Res. Soc. Symp. Proc.*, **77**, 307 (1987)
- 31 Zs. Tôkei, D.L. Beke, J. Bernardini and A. Rolland, *Scripta Materialia*, **39**, 1127 (1998)

- 32 Zs. Tôkei, D.L. Beke, J. Bernardini and A. Rolland, *Def. Diff. Forum*, **156**, 129 (1998)
- 33 J. Bernardini and J. Cabané, *Acta Metall.*, **21**, 1571, (1973)
- 34 G. Neumann and V. Tölle, *Phil. Mag. A*, **57**, 621 (1988)
- 35 A. Almazouzi, M-P. Macht, V. Naudor , G. Neumann and V. Tölle, *Def. Diff. Forum*, **95-98**, 703 (1993)
- 36 G. Trégliã, B. Legrand and P. Maugain, *Surf. Sci.*, **225**, 319 (1990)
- 37 J. K. Strohl and T. King, *J. of Catalysis*, **118**, 53 (1989)
- 38 W. Wagner, R. Poerschke and A. Axmann, *Phys. Rev. B*, **21**, 3087 (1980)
- 39 G. Martin, *Phys. Rev. B*, **41**, 2279 (1990)
- 40 C. Kittel, *Introduction to solid state physics*, 5th ed. (Wiley, New York, 1976)
- 41 Cs. Cserhãti, H. Bakker, D.L. Beke, *Surf. Sci.*, **290**, 345 (1993)
- 42 M. Lagües and J.L. Domange, *Surf. Sci.*, **47**, 77 (1975)
- 43 S. Delage, B. Legrand, F. Soisson and A. Saül, *Phys. Rev.*, **B 58**, 15810 (1998)
- 44 H.H. Brongersma, M.J. Sparnaay and T.M. Buck, *Surf. Sci.*, **71**, 657 (1978)
- 45 H.H. Brongersma, P.A.J. Ackermans and A.D. van Langeveld, *Phys. Rev.*, **B 34**, 5974 (1986)
- 46 T. Sakurai, T. Hashizume, A. Kobayashi, A. Sakai, S. Hyodo, Y. Kuk and W.W. Pickering, *Phys. Rev.*, **B 34**, 8379 (1986)
- 47 J. Philibert, *Atom movements*, Les Editions de Physique (1991)
- 48 R. Ghez, *A Primer of Diffusion Problems* (John Wiley & Sons, New York 1988)
- 49 M.G. Barthèse and A. Rolland, *Thin Solid Films*, **76**, 45 (1981)
- 50 M. P. Seah and W. A. Dench, *Surface and Interface analysis*, **1**, No. 1, 2 (1979)
- 51 W.F. Egelhoff *J. Vac. Sci. Technol. A*, **7**, No. 3, 2060 (1989)
- 52 J-M. Roussel, A. Shaül, G. Trégliã and B. Legrand, *Phys. Rev.*, **B 60**, 13890 (1999)
- 53 A. Saül, B. Legrand and Guy Trégliã, *Suf. Sci.*, **331-333**, 805 (1995)
- 54 T. J. Renouf, *Phil. Mag.*, **22**, 359 (1970)
- 55 N. Aljeshin and S. I. Prokofjev, *Poverkhnost Fizika, Khimiya, Mechanika*, **9**, 131 (1986)
- 56 G.B. Stephenson, *Acta Metall.*, **36**, 2663 (1988)
- 57 G.B. Stephenson, *Defect and Diffusion Forum*, **95-98**, 507 (1993)
- 58 J.W. Cahn, *Acta Metall.*, **9**, 795 (1961)
- 59 J.W. Cahn, *Acta Metall.*, **10**, 179 (1962)
- 60 J.W. Cahn and J.E. Hilliard, *J. Chem. Phys.*, **28**, 258 (1958)
- 61 A.R. Allant and A.B. Lidiard, *Atomic Transport in Solid* (University Press, Cambridge), 170 (1993)

Chapter IV

Grain-Boundary Material Transport in Thin Films



In this chapter Ag grain-boundary diffusion in Cu will be determined by the Hwang-Balluffi method in C-kinetics regime from the Ag and Cu Auger signals measured on the surface of nanocrystalline Cu/Ag thin bilayers

Chapter I

GRAIN-BOUNDARY MATERIAL TRANSPORT IN THIN FILMS

From the Ag and Cu Auger signals measured on the surface of nanocrystalline Cu/Ag thin bilayers, the temperature dependence of the parameter ω' for Ag grain-boundary diffusion in Cu [$\omega' = \delta k_b D_b / \delta_s k_s$, where k_s is the surface segregation factor; $\omega' = \omega d^2/2$ due to the similar values of the grain size of the thickness, h , and the grain size, d , – see equation (I.78)] will be determined by the Hwang-Balluffi method in C-kinetics regime in the temperature range of 393-428 K. These values will be compared with triple products, $P = \delta k_b D_b$, determined in the temperature range of -804 K by Bernardini *et al.* [1] using radio tracer technique in B-kinetics regime. The temperature dependence of the surface segregation factor will be extracted as well [2,3,4].

IV.1 THEORY

Using the Hwang-Balluffi equation [equation (I.77)], in principle it is possible to calculate the grain-boundary diffusion coefficient, if the surface concentration of the segregated element is known.

Auger Electron Spectroscopy can be applied for grain-boundary diffusion studies by using the surface accumulation method based on the observation of surface accumulation of the diffusing atoms on the terminal surface of the sample [7,5]. However, this method can be affected by the presence of even small amounts of impurities, disturbing the velocity of the surface diffusion [6]. The quantitative analysis is not evident. This question will be detailed in this section.

IV.1.1 Surface accumulation parameter

If the surface accumulation is measured by Auger Electron Spectroscopy, in order to eliminate the possible fluctuation of the Auger current, it is useful to define a peak height ratio [7]:

$$q = \frac{I_A/I_{A,\infty}}{I_B/I_{B,\infty}}, \quad (\text{IV.1})$$

where I_A and I_B are the measured peak-to-peak heights coming from the A and B atoms of the specimen, respectively while $I_{A,\infty}$ and $I_{B,\infty}$ are the measured peak-to-peak heights coming from the bulk specimen containing only A and B atoms, respectively. This q parameter, representing the accumulation of the diffusant on the surface, is called the surface accumulation parameter. The value of q is sensitive to the details of the distribution of segregated atoms since the Auger electrons corresponding to the measured peaks can have widely different Inelastic Mean Free Path (IMFP).

Using equations (III.25) and (III.27), the Auger intensity coming from a homogeneous specimen containing n layers (or the part of the total intensity which comes from the n top layers of a homogeneous bulk specimen) is:

$$I_{i,n} = (1 - \alpha_i^n) I_{i,\infty} \quad i = A, B. \quad (IV.2)$$

The concentration of A atoms in an AB bulk alloy can be defined by the following way:

$$c = I_{AB,\infty}^A / I_{A,\infty}, \quad (IV.3)$$

where $I_{AB,\infty}^A$ and $I_{A,\infty}$ are the Auger intensity coming from the A atoms of the bulk alloy and the Auger intensity coming from the bulk specimen containing only A atoms, respectively. According to this definition, it is also possible to determine the concentration of A and B atoms in n AB homogeneous surface layers deposited on a pure B substrate:

$$c = I_{AB,n}^A / I_{A,n}. \quad (IV.4)$$

Since the substrate does not contain A atoms, $I_{AB,n}^A$ is equal to the I_A measured intensity coming from the A atoms of the whole specimen. Using equation (IV.2), the concentration of A atoms is:

$$c = \frac{I_A}{I_{A,n}} = \frac{I_A}{(1 - \alpha_A^n) I_{A,\infty}}. \quad (IV.5)$$

The concentration of B atoms is:

$$1 - c = I_{AB,n}^B / I_{B,n}. \quad (IV.6)$$

However, in the case of the B atoms, it is necessary to take into account the $I_{B,n+1\dots\infty}$ contribution of the substrate as well, thus $I_{AB,n}^B$ is not equal to the I_B measured intensity coming from the B atoms of the whole specimen:

$$1 - c = \frac{I_B - I_{B,n+1\dots\infty}}{I_{B,n}} = \frac{I_B - \alpha_B^n I_{B,\infty}}{(1 - \alpha_B^n) I_{B,\infty}} \quad (IV.7)$$

$$(I_{B,n+1\dots\infty} = I_{B,\infty} - I_{B,n} = I_{B,\infty} - (1 - \alpha_B^n) I_{B,\infty} = \alpha_B^n I_{B,\infty}).$$

Using the definition of q and equations (IV.5) and (IV.7), the surface accumulation parameter for n accumulated layers is:

$$q_n = \frac{I_A / I_{A,\infty}}{I_B / I_{B,\infty}} = \frac{c(1 - \alpha_A^n)}{1 - c(1 - \alpha_B^n)}. \quad (IV.8)$$

Using the usual form of the attenuation parameter [see equation (III.26)], the equation (IV.8), in two layers limit ($n = 2$), is the same as the one which was used by Hwang *et al.* in [1].

When there are monoatomic islands of A atoms on the B surface, introducing a surface coverage $f (< 1)$, equation (IV.2) can be rewritten as:

$$\begin{aligned} I_A &= f(1 - \alpha_A)I_{A,\infty} \\ I_B &= f\alpha_B I_{B,\infty} + (1 - f)I_{B,\infty}, \end{aligned} \quad (IV.9)$$

where the first and second terms in I_B correspond to the intensity attenuated by A islands and to the direct intensity from the free B surface, respectively. Thus q is given by

$$q = \frac{f(1 - \alpha_A)}{1 - f(1 - \alpha_B)}. \quad (IV.10)$$

Taking into account equation (IV.8) for $n = 1$, it can be seen that $f = c_s$, and thus from equation (I.77) ω can be also determined for the case when there is a discontinuous layer on the surface.

The surface accumulation parameter can be determined experimentally in the following form:

$$q = \frac{I_{356}/I_{356,\infty}}{I_{920}/I_{920,\infty}} = \frac{I_{356}}{I_{920}} S, \quad (IV.11)$$

where S is the so-called relative Auger sensitivity factor of both elements (for the present experiment $S = I_{920,\infty}/I_{356,\infty} = 0.26$).

IV.2 RESULTS

Twenty years ago, Gibson and Dobson [8] described that annealing of thin (10-20 nm) epitaxial films of nickel or copper grown on silver (111) at 300°C produced drastic changes in the morphology of the Ni or Cu layers. The flat deposits contracted into three-dimensional islands.

In our experiments, TEM was used to check the grain size of the nanocrystalline copper layer before and after heat treatment. It was shown that the grain size of the Cu deposited films corresponds to the thickness of the Cu deposited layer *i.e.* around 20 nm. The Ag/Cu couple was annealed at sufficiently low temperatures, so that the structure was frozen out [the copper grain size remained unchanged (around 20 nm) after annealing], and the diffusion occurred along the grain boundaries.

Due to silver grain-boundary diffusion onto the copper surface, typical evolution of the 356 eV silver Auger peak and the 60 and 920 eV copper peaks as a function of annealing time is plotted in Figure IV.1. Time evolution of c_s calculated from equation (IV.8) for $n = 2$ is shown in Figure IV.2. For calculation of c_s , we need to know the value of n , *i.e.* the thickness of the segregated layer. Hwang *et al.* [7] considered that, due to the carbon contamination of the surface, the accumulation takes place probably in more than one top layers. In their calculations of Ag grain-boundary diffusion in Au, for example, they supposed that this surface homogenisation sets in the top *two* monolayers. Barthès *et al.* [9] (Ag-Ni system) supposed that this value is one. Because of the choice is not evident, we computed for both cases and we found that the method is not too sensitive to this parameter. However, due to the surface “cleaning” by ion sputtering, the surface is surely not perfectly smooth, thus we think that probably the “two-layer supposition” is more close to the reality. This is why the results presented here are calculated for $n = 2$.

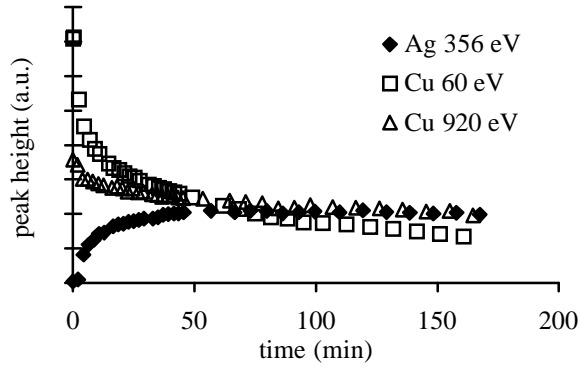


Figure IV.1 Evolution of the Ag(356) and Cu(60-920) Auger peak to peak heights with time at 428 K

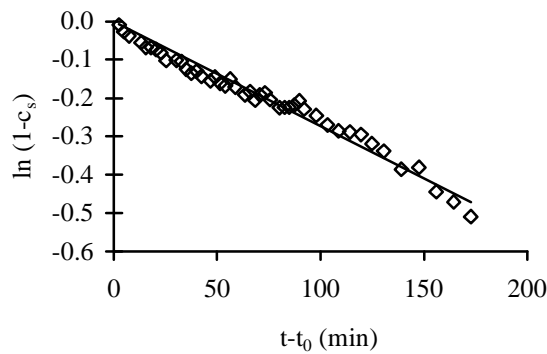


Figure IV.2 The time evolution of $\ln(1-c_s)$ at 403 K [c_s has been calculated by the equation (IV.8), with $n = 2$]

In our experiments, although $c_0 = 1$ can be assumed in equation (I.77), the surface saturation value of c_s was always smaller than 1, due for example to kinetics limitations [10] and/or carbon contamination, thermal stresses caused by the difference of thermal expansion coefficients of the films and the substrate [11,12]. The same effect arises because of the presence of k''/k' factor in the left hand side of this expression. Thus, taking into account that the value of $[1 - \exp(-\omega t')]$ should be normalised between 0 and 1, the calculated c_s concentrations were normalized by the saturation value measured.

Note that at 393 K and 403 K the surface concentrations never reached the saturation level, since at such low temperatures the diffusion was so slow that it was practically impossible to measure it. However, according to the tendency of the measured saturation kinetics, *i.e.* the c_s vs. time, we have estimated the saturation value by extrapolation.

Using the Hwang-Baluffi equation, under the conditions described above (and taking into account that [13] $\lambda_{356} = 5$, $\lambda_{920} = 7$, and $\vartheta = 42^\circ$, $d = 21$ nm) the $\delta k_b D_b / \delta_s k_s (= \omega')$ products have been calculated. Figure IV.3 shows the Arrhenius plot of this parameter, which can be given by

$$\omega' = \frac{\delta k_b D_b}{\delta_s k_s} = 1.49 \times 10^{-4} \exp\left[-\frac{(124 \pm 15) \text{ kJ/mol}}{RT}\right] \text{ m}^2/\text{s}, \quad (\text{IV.12})$$

where R , T are the molar Boltzmann's constant and the absolute temperature, respectively.

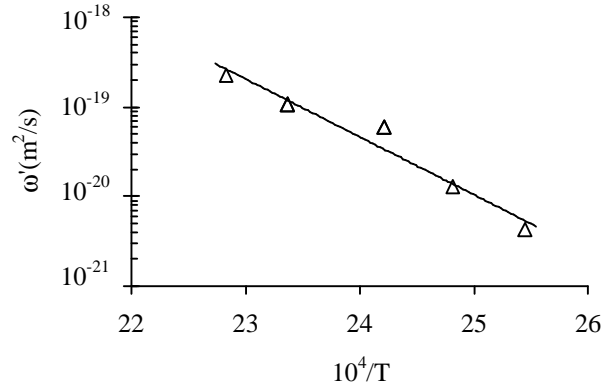


Figure IV.3 Arrhenius plot of the grain-boundary diffusion of Ag in Cu in C kinetic regime

IV.3 DISCUSSION

The determination of the *surface* segregation factors and the comparison of these values with the triple products ($P = \delta k_b D_b$) obtained from the grain-boundary tracer diffusion of Ag in Cu in B kinetics regime [1] will be discussed in this section.

Since in [1] the triple product P , was determined from tracer measurements and we measured the $\omega' = \delta k_b D_b / \delta_s k_s$ parameter, it is possible to estimate the *surface* segregation factor:

$$\frac{P}{\omega'} = \delta_s k_s, \quad (\text{IV.13})$$

In equation (IV.13), only δ_s is unknown, and either one or two monolayers are assumed, one can obtain a reasonable estimate for k_s (within a factor of two, which is independent of the temperature).

Before detailing this point, we emphasize the agreement between values obtained in 'classical' polycrystals at high temperatures in B kinetic regime and those concerning measurements performed at low temperatures by using nano-structured samples. This suggests a similar grain-boundary structure in both types of samples. This result confirms some results obtained recently for nanocrystals [14,15]. It invalidates the idea of particular structures of grain boundaries in this type of material for the applied temperature range and time of the heat treatment.

Furthermore in [1], using experimental data on Ag diffusion in Cu lattice published in [16], the triple products of Ag tracer diffusion in pure Cu as well as in a Cu-0.091at% Ag alloy were determined and the following Arrhenius equations were obtained:

$$P_{\text{pure}} = 3.7 \times 10^{-14} \exp\left(-\frac{90 \pm 6.2 \text{ kJ/mol}}{RT}\right) \text{ m}^3/\text{s}, \quad (\text{IV.14})$$

and

$$P_{\text{alloy}} = 2.1 \times 10^{-12} \exp\left(-\frac{119.4 \pm 6.6 \text{ kJ/mol}}{RT}\right) \text{ m}^3/\text{s}. \quad (\text{IV.15})$$

The activation energy corresponding to the heterodiffusion of silver in pure copper [see equation (IV.14)] contains the grain-boundary segregation energy. In an alloy, the radiotracer atoms have migrated in a grain-boundary for which $k = c_b^{sat}/c_v = \text{const}$ in so far as i) the grain boundaries are saturated by non active silver before the tracer diffusion and ii) the radiotracer concentration is negligible. Supposing to a first approximation that the concentration of silver saturating the grain boundaries is independent of the temperature in the range of the studied temperature, the activation energy of P_{alloy} (Q) corresponds to that of the grain-boundary diffusion coefficient of silver in copper. Therefore, these are the values characterising P_{pure} which have to be used to calculate k_s in equation (IV.13) and:

$$k_s = \frac{1}{\delta_s} 2.48 \times 10^{-10} \exp\left(\frac{34 \pm 16 \text{ kJ/mol}}{RT}\right). \quad (\text{IV.16})$$

The value of the activation energy agrees very well with other data previously published: 38.7 kJ/mol obtained from experimental surface segregation kinetics data by Eugène [17] and 37.6 kJ/mol by Bronner and Wynblatt [18], respectively.

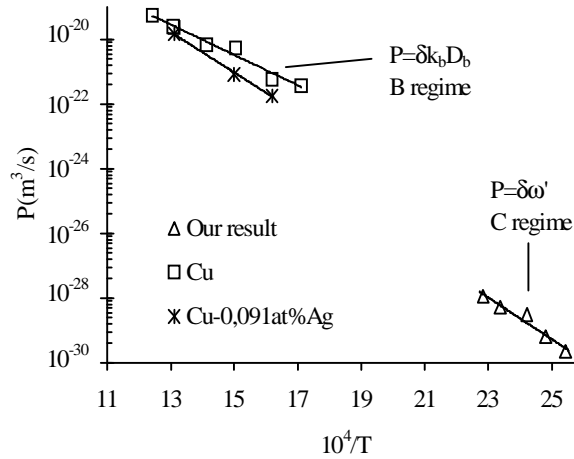


Figure IV.4 Arrhenius plots of the grain-boundary diffusion parameters (P , $\delta\omega'$) measured in B and C regimes

Figure IV.4 shows the Arrhenius plots obtained in the B and C -kinetics regime measurements and as it can be seen they are consistent with each other (taking $\delta = 0.5$ nm in both cases): *i.e.* the activation energy of ω' , which contains the surface segregation energy, is higher than that of P_{pure} and P_{alloy} . It is reasonable, since if one assumes Arrhenius-type temperature dependence for both $k' = k_s/k_b$ and D_b :

$$k' = k'_0 \exp\left(\frac{\Delta H'}{RT}\right) ; \quad D_b = D_0 \exp\left(-\frac{Q}{RT}\right) \quad (\text{IV.17})$$

and considering that $\omega' \propto D_b/k'$, the effective activation energy of ω' is $Q + \Delta H'$. Now, it is reasonable to assume that the difference of the segregation energies of k_s and k_b is positive, but less than the activation energy for grain-boundary segregation ΔH_b . Indeed in [1], from the difference of the activation energies given by equations (IV.14) and (IV.15),

$\Delta H_b = 29.4$ kJ/mol was given, which is less than our result for the surface segregation energy [see equation (IV.16)]. In fact a numerical estimate for $\Delta H'$ could be obtained either as the difference of the above energies or as the difference of the activation energies of ω' and P_{alloy} . Although the sign of $\Delta H'$ is correct, since unfortunately the errors are too high in both cases, it is meaningless to give these numbers.

IV.4 CONCLUSIONS

Using the Hwang-Balluffi method, the $\omega' = \delta k_b D_b / \delta_s k_s$ products for Ag grain-boundary diffusion in nanocrystalline Cu films have been determined at low temperatures where lattice diffusion was vanishingly small and type -C regime was prevalent. From the comparison of these data with triple products ($P = \delta k_b D_b$), previously determined by tracer technique in B regime under different segregation conditions, the activation energy of the *surface* segregation factor (k_s) was determined (34 ± 19 kJ/mol), which is in a good agreement with surface segregation energies of Ag in Cu(Ag) alloys published in the literature. These results as a whole show that there is no particular behaviour of the nanostructured substrate in relation to the grain-boundary material transport.

REFERENCES

- 1 J. Bernardini, Zs. Tôkei and D.L. Beke, *Phil. Mag. A*, **73**, 237 (1996)
- 2 Z. Erdélyi, Ch. Girardeaux, G.A. Langer, D.L. Beke, A. Rolland, J. Bernardini, *Journal of Applied Physics*, **89**, No. 7, 3971-3975 (2001)
- 3 Z. Erdélyi, Ch. Girardeaux, G.A.Langer, L. Daróczi, A. Rolland, D.L. Beke, *Applied Surface Science*, **162-163**, 213-218 (2000)
- 4 Z. Erdélyi, Ch. Girardeaux, J. Bernardini, D.L. Beke, A. Rolland, *Def. and Diff Forum*, **194-199**, 1161-1166 (2001)
- 5 A. Bukaluk, M. Rozwadowski R. Siuda, *Appl. Phys. A*, **34**, 193 (1984)
- 6 G. H. Gilmer and H. H. Farrell, *J. Appl. Phys.*, **47**, 3792 (1976)
- 7 J.C.M. Hwang, J.D. Pan and R.W. Balluffi, *J. Appl. Phys.*, **50**, No. 3, 1339 (1979)
- 8 M. J. Gibson and P. J. Dobson, *J. Phys. F: Metal Phys.*, **5**, 864 (1975)
- 9 M.G. Barthès and A. Rolland, *Thin Solid Film*, **76**, 45 (1981)
- 10 M.P. Seah, *Surf. Sci.* **32**, 703 (1972)
- 11 B. Bokstein and A. Ostrovsky *J. of -equilibrium Processing*, (2000) in press
- 12 A. Ostrovsky *Defect and Diffusion Forum*, **156**, 249 (1998)
- 13 M.P. Seah and W.A. Dench, *Surface and Interface analysis*, 1, No. 1 (1979)
- 14 R. Würschum, *Mat. Sc. Forum*, **363-365**, 35 (2001)
- 15 B. Fultz and H. N. Frase, *Hyperfine Interactions*, **130**, 81 (2000)
- 16 G. Barreau, G. Brunel, G. Cizeron and P. Lacombe, *C.R. Acad Sci.*, C **270**, 516 (1970)
- 17 J. Eugène, *Thesis*, Marseille 1989
- 18 S.W. Bronner and P. Wynblatt, *J. Matter. Res.*, **1**, No. 5, 646 (1986)

CONCLUSIONS

The aim of this study was to investigate diffusion, segregation and dissolution in multilayers and thin films, which present two particularities against classical bulk materials: diffusion distances, which are not infinite compared to the size of the sample and a sharp interface.

The first aspect of our work was to clarify the role of the ‘nano-effect’ on material transport. We have shown from simulations in multilayers A/B where the diffusion coefficients of A (B) atoms in B (A) are very different, which leads strongly (exponential concentration dependent diffusion coefficients during the homogenisation, that large asymmetry is observed in the evolution of the concentration profiles. We have seen that in multilayers a fast homogenisation takes place on the side where the diffusion is faster, and here the distribution is practically flat. Thus only the amplitude of the composition modulation decreases with time and the interface remains sharp and shifts. The Auger depth profiling technique provided direct evidence for this in amorphous Si-Ge system.

Furthermore, we found that there is a difference between the results obtained from the continuum and discrete models: the shape of the moving boundary changes with time in the discrete model and it shows a layer-by-layer dissolution kinetics, while in the continuum model the interface remains atomic sharp. Furthermore, the validity of the continuum model shifts as the function of the strength of the concentration dependence of the diffusion coefficients, and in many real multilayer systems with typical modulation length of few nanometers, it can break down.

Investigating the combined effects of stress and non-linearity due to the concentration dependence of the diffusion coefficients, it was shown that in the Si-Ge system not only the concentration but also the pressure distribution is also very asymmetrical. Furthermore, stress effects do not modify the behaviour of the composition profile and the time evolution of the intensity curve; only its ‘slope’, which is proportional to the diffusivity, has been changed. Consequently stress effects can slow down the homogenisation in multilayers.

We have investigated the effect of segregation on the dissolution of a thin Ni layer (3-14 eq-ML) into a semi-infinite Cu substrate. Our simulations indicated a step-wise character of dissolution and an interesting interference between the segregation and dissolution in accordance with the results obtained in multilayers. Because of the strong concentration dependence of the diffusion coefficients of the diffusing species, the interface remains sharp and shifts until it reaches the next-to-the-last layer. In this part of the dissolution a *concentration dependent diffusion on discrete lattice* controls the process. We have seen that the thickness of Ni decreases linearly with time, indicating the strong non-linearity, deviation from the continuum description and violation of the parabolic law. This was also experimentally confirmed from Auger measurements of dissolution of Ni into semi-infinite Cu substrate. In the final stage of the dissolution, due to the driving force for segregation, the process continues by the saturation of Cu in the top layer. The change of the concentration of the second layer (first underlayer) occurs according to the segregation isotherm. Finally, after the saturation of the surface layer by Cu, the final homogenisation takes place by complete dissolution of the second layer.

The second aspect of our study was to characterise the grain-boundary material transport in nanostructured thin films. Using the Hwang-Balluffi method and Auger electron spectroscopy, Ag grain-boundary diffusion in nanocrystalline Cu films have been

determined at low temperatures where lattice diffusion was vanishingly small and type -C regime was prevalent. From the comparison of these data with triple products, previously determined in polycrystalline samples by tracer technique in B regime, the activation energy of the *surface* segregation factor was also determined, which is in a good agreement with surface segregation energies of Ag in Cu(Ag) bulk alloys published in the literature. These results as a whole suggest that there is no difference between nanostructured and bulk polycrystals from the point of view of grain-boundary material transport.

Publications

1. D.L. Beke, G.A. Langer, M. Kiss-Varga, A. Dudas, P. Nemes, L. Daróczy, Gy. Kerekes, Z. Erdélyi, Thermal stability of amorphous and crystalline multilayers produced by magnetron sputtering, *Vacuum*, **50**, No. 3-4, 373-383 (1998)
2. D.L. Beke, P. Nemes, Z. Erdélyi, I.A. Szabó, G.A. Langer, Stress effects and nonlinearities in diffusional mixing of multilayers, *Materials Research Society Symposium Proceedings: Diffusion Mechanisms in Crystalline Materials* Editors: Y. Mishin, G. Vogl, N. Ciuern, R. Catlow, D. Farkas MRS Warrendale, Pennsylvania, USA, **527**, 99-110 (1998)
3. Z. Erdélyi, D.L. Beke, P. Nemes, G.A. Langer, On the range of validity of the continuum approach for nonlinear diffusional mixing of multilayers, *Phil.Mag. A*, **79**, No 8, 1757-1768 (1999)
4. Zs. Tôkei, Z. Erdélyi, Ch. Girardeaux, A. Rolland, Effect of sulphur content and pre annealing treatments on nickel grain -boundary diffusion in high-purity copper, *Phil.Mag. A*, **80**, No. 5, 1075-1083 (2000)
5. D.L. Beke, A. Dudas, A. Csik, G.A. Langer, M. Kis-Varga, L. Daróczy, Z. Erdélyi, On the thermal stability of multilayers, *Functional Materials*, **6**, No. 3, 539-544 (1999)
6. A. Dudás, G.A. Langer, D.L. Beke, M. Kis-Varga, L. Daróczy, Z. Erdélyi, Thermal stability of Mo-V epitaxial multilayers, *Journal of App. Phys.*, **86**, No. 4, 2008-2013 (1999)
7. D.L. Beke, Z. Erdélyi, P. Bakos, Cs. Cserháti, I.A. Szabó, Segregation Induced Phase Transformations in Nanostructures, *Proceedings of International Conference on Solid-Solid Phase Transformations '99 Kyoto*, 1999
8. Z. Erdélyi, Ch. Girardeaux, G.A.Langer, L. Daróczy, A. Rolland, D.L. Beke, Determination of grain -boundary diffusion coefficients by Auger Electron Spectroscopy, *Applied Surface Science*, **162-163**, 213-218 (2000)
9. A. Simon, A. Csik, F. Pászti, Á.Z. Kiss, D.L. Beke, L. Daróczy, Z. Erdélyi, G.A. Langer, Study of interdiffusion in amorphous Si/Ge multilayers by Rutherford backscattering spectrometry, *Nuclear Instruments and Methods in Physics Research B*, **161-163**, 472-476 (2000)
10. G.Erdélyi, Z. Erdélyi, D.L. Beke, J. Bernardini, C. Lexcellent, Pressure dependence of Ni self-diffusion in NiTi near equatomic alloy, *Phys. Rev. B*, **62**, No. 13, 1-4 (2000)
11. A. Csik, D.L. Beke, G.A. Langer, Z. Erdélyi, L. Daróczy, K. Kapta, M. Kiss-Varga, Non-linearity due to the strong concentration dependence of diffusion in amorphous Si-Ge multilayers, *Vacuum*, **61**, No. 2-4, 297-301 (2001)
12. Z. Erdélyi, Ch. Girardeaux, G.A. Langer, D.L. Beke, A. Rolland, J. Bernardini, Determination of grain -boundary diffusion of Ag in nanocrystalline Cu by Hwang-Balluffi method, *Journal of Applied Physics*, **89**, No. 7, 3971-3975 (2001)
13. A. Csik, G.A. Langer, D.L. Beke, Z. Erdélyi, M. Menyhárd, A. Sulyok, Investigation of interdiffusion in amorphous Si/Ge multilayers by Auger depth profiling technique, *Journal of Applied Physics*, **89**, No. 1, 804-806 (2001)
14. D.L. Beke, A. Csik, G.A. Langer, Z. Erdélyi, Z. Papp, Diffusion and thermal stability in multilayers, *Def. and Diff. Forum*, **194-199**, 1403-1416 (2001)
15. G. Erdélyi, Z. Erdélyi, D.L. Beke, Pressure dependence of self diffusion in B2 intermetallic phases, *Def. and Diff Forum*, **194-199**, 473-480 (2001)

16. Z. Erdélyi, Ch. Girardeaux, J. Bernardini, D.L. Beke, A. Rolland, Experimental and theoretical study of type C grain boundary and volume diffusion by AES in metal/metal structures, *Def. and Diff Forum*, **194-199**, 1161-1166 (2001)
17. J. Nyéki, Ch. Girardeaux, Z. Erdélyi, G.A. Langer, G. Erdélyi, D.L. Beke, A. Rolland, AES study of surface segregation of Ge in amorphous Si_{1-x} thin film alloys, *Surface Science*, in press (2001)
18. Z. Erdélyi, Ch. Girardeaux, Zs. Tôkei, D.L. Beke, Cs. Cserhádi, A. Rolland, Investigation of the interplay of nickel dissolution and copper segregation in Ni/Cu(111) system by Auger dissolution kinetics, *Surface Science*, in press (2001)